

---

Electronic Thesis and Dissertation Repository

---

8-26-2015 12:00 AM

## Investigating potential climatic cycles in glacially-influenced rhythmites of the upper Gowganda Formation using geochemical, sedimentological and spectral analyses

Timothy S. Howe, *The University of Western Ontario*

Supervisor: Dr. Patricia Corcoran, *The University of Western Ontario*

Co-Supervisor: Fred Longstaffe, *The University of Western Ontario*

Co-Supervisor: Elizabeth Webb, *The University of Western Ontario*

A thesis submitted in partial fulfillment of the requirements for the Master of Science degree in  
Geology

© Timothy S. Howe 2015

Follow this and additional works at: <https://ir.lib.uwo.ca/etd>



Part of the [Geology Commons](#)

---

### Recommended Citation

Howe, Timothy S., "Investigating potential climatic cycles in glacially-influenced rhythmites of the upper Gowganda Formation using geochemical, sedimentological and spectral analyses" (2015). *Electronic Thesis and Dissertation Repository*. 3264.

<https://ir.lib.uwo.ca/etd/3264>

This Dissertation/Thesis is brought to you for free and open access by Scholarship@Western. It has been accepted for inclusion in Electronic Thesis and Dissertation Repository by an authorized administrator of Scholarship@Western. For more information, please contact [wlsadmin@uwo.ca](mailto:wlsadmin@uwo.ca).

INVESTIGATING POTENTIAL CLIMATIC CYCLES IN GLACIALLY-  
INFLUENCED RHYTHMITES OF THE UPPER GOWGANDA FORMATION  
USING GEOCHEMICAL, SEDIMENTOLOGICAL AND SPECTRAL ANALYSES

by

Timothy Scott Howe

Graduate Program in Geology

A thesis submitted in partial fulfillment  
of the requirements for the degree of  
Master of Geology

The School of Graduate and Postdoctoral Studies  
The University of Western Ontario  
London, Ontario, Canada

© Timothy S. Howe, 2015

## Abstract

The upper Gowganda Formation of the Huronian Supergroup contains glacially-induced, varve-like rhythmites composed of turbiditic micro-laminae that potentially preserve a detailed record of climatic conditions during the Paleoproterozoic Era. A sedimentological analysis of upper Gowganda Formation deposits enabled identification of eight lithofacies comprising a glaciogenic depositional environment: 1) diamictite, 2) contorted argillite, 3) interlaminated siltstone and sandstone, 4) interbedded siltstone and claystone, 5) sandstone, 6) siltstone, 7) interbedded coarse-grained and fine-grained siltstone, and 8) wavy argillite. Major, trace, and rare earth element analyses indicate that the rhythmites have undergone limited recycling and chemical alteration. Whole-rock  $\delta^{18}\text{O}$  values are consistent with an Archean gneiss provenance and support that chemical weathering and diagenesis were insignificant. Spectral analysis of four rhythmic couplet thickness records using the MTM Toolkit of Mann and Lees (1996) supports the hypothesis of annual deposition for the rhythmites.

## Keywords

Paleoproterozoic, Huronian, Gowganda, glaciation, rhythmites, varves, micro-laminae, MTM Toolkit, red noise model

## Acknowledgments

Without the assistance of many people this thesis wouldn't have been possible. First and foremost I'd like to thank my supervisor, Dr. Patricia Corcoran, and co-supervisors Dr. Fred Longstaffe and Dr. Elizabeth Webb, for giving me the opportunity to work on such an interesting and challenging project, and for providing guidance and support along the way. Capable field assistance was provided by Mansour Al-Hashim, Alex Hockin and Bethany Dean. Anthony Pace provided access to the core logged in this thesis. Linux computer access to operate the spectral analysis program was provided by Dr. Kristy Tiampo. Assistance with the spectral analysis chapter was provided by Dr. Gerhard Pratt. Dr. Gary Hughes kindly provided me with his data so that I could compare his data with my data using the same software. Dr. Guy Plint helped me by suggesting that I reduce my project to a more manageable size, and along with Omar Al-Mufti, encouraged me to take a closer look at sedimentological depositional processes. Ryan Hladyniuk assisted with technical and administrative issues. And finally, I'd like to acknowledge all of the faculty, students, and administrative staff that make up the Department of Earth Sciences here at Western: I've never worked with such a consistently agreeable group of people in my life, and I can honestly say that it was always a pleasure to "show up to work". Warmest thanks to everyone for that.

# Table of Contents

Abstract.....	ii
Acknowledgments.....	iii
Table of Contents.....	iv
List of Tables.....	vii
List of Figures.....	viii
List of Appendices.....	xiii
1 Introduction.....	1
1.1 Varves.....	1
1.1.1 Varves in Glaciofluvial Lakes.....	2
1.1.2 Thermal Stratification in Glaciofluvial Lakes.....	2
1.1.3 Thermal Stratification and Varves.....	3
1.1.4 Non-glacial Varves.....	4
1.2 Varves in Precambrian Settings.....	4
1.3 Tidal Rhythmites.....	5
1.4 Tidal Rhythmites in Precambrian Settings.....	7
1.5 Turbidites.....	8
1.6 Glacially-influenced Turbidites in Precambrian Settings.....	9
2 Geological Setting.....	11
2.1 The Huronian Supergroup.....	11
2.1.1 Elliot Lake Group.....	15
2.1.2 Hough Lake Group.....	17
2.1.3 Quirke Lake Group.....	19
2.1.4 Cobalt Group.....	20
2.1.5 Flack Lake Group.....	21

2.2	Sudbury Igneous Complex.....	23
2.3	Penokean Orogeny .....	23
2.4	Thesis Focus: Gowganda Formation .....	24
2.4.1	General Description .....	24
2.4.2	Study Area .....	27
3	Sedimentology .....	29
3.1	Lower Gowganda Formation .....	29
3.2	Upper Gowganda Formation.....	30
3.2.1	Diamictite Lithofacies.....	31
3.2.2	Contorted Argillite Lithofacies .....	32
3.2.3	Interlaminated Siltstone and Sandstone Lithofacies .....	36
3.2.4	Interbedded Siltstone and Claystone Lithofacies.....	38
3.2.5	Sandstone Lithofacies .....	48
3.2.6	Siltstone Lithofacies.....	49
3.2.7	Interbedded Coarse-grained and Fine-grained Siltstone Lithofacies.....	49
3.2.8	Wavy Argillite Lithofacies .....	52
3.3	Depositional Model.....	53
3.4	Sedimentology Summary.....	56
4	Geochemistry .....	58
4.1	Sample Preparation .....	58
4.2	Major, Trace and Rare Earth Element Analysis .....	58
4.3	Powder X-ray Diffraction .....	65
4.4	Stable Isotopes .....	67
4.5	Geochemistry Discussion.....	69
5	Statistical Analysis of Rhythmites .....	73

5.1	Introduction.....	73
5.2	An Introduction to Spectral Analysis.....	73
5.3	Prior Study: Hughes et al. (2003) .....	74
5.4	The Present Study .....	77
5.4.1	Field Sampling and Data Plotting.....	77
5.4.2	The Multi-Taper Method of Spectral Analysis.....	79
5.4.3	Spectral Analysis Results.....	81
5.4.4	Spectral Analysis Interpretation.....	87
6	Discussion .....	91
6.1	Deltas and Fans in Glacially-Influenced Environments .....	91
6.1.1	Ice-contact Deltas.....	92
6.1.2	Ice-contact Subaqueous Fans .....	93
6.1.3	Glaciofluvial Deltas .....	93
6.2	Gowganda Formation Rhythmites: Varves, Turbidites or Both? .....	95
6.2.1	Grouping Varves by Fine-grained Layer Thickness.....	95
6.2.2	Group I Varves.....	95
6.2.3	Micro-laminae within Varve Layers.....	96
6.2.4	Micro-laminae in Turbidite Deposits.....	96
6.2.5	The Micro-laminae in this Study .....	97
6.2.6	Group II Varves .....	98
6.3	Spectral Analysis of the Rhythmite Measurement Data.....	98
6.3.1	Variations in the Depositional Environment.....	100
7	Conclusions.....	105
	References.....	107
	Appendices.....	127

## List of Tables

Table 4-1: Major and trace element compositions of the interlaminated siltstone and claystone lithofacies at Outcrop A of the Gowganda Formation.....	72
Table 4-2: Rare earth element compositions of the interlaminated siltstone and claystone lithofacies at Outcrop A of the Gowganda Formation.....	73
Table 4-3: pXRD and stable isotope results for 16 powdered samples of the interbedded siltstone and claystone lithofacies from Outcrop A.....	81
Table 5-1: Summary of spectral analysis results from this study, and the Hughes et al. (2003) study .....	101
Table 5-2: Comparison of this study with similar studies conducted near the Great Lakes region. ....	103

## List of Figures

- Figure 2-1: Distribution of the Huronian Supergroup in Ontario, Canada. The Huronian Supergroup comprises the eastern section of the Southern Province, and is divided into three regions: the Bruce Mines/Elliot Lake area, the Espanola/Whitefish Falls area and the Cobalt area. The Flack Lake fault and the Murray fault zone (dashed lines) indicate contemporaneous down-to-basin faulting. Map modified from Freeman (1978) and Young et al. (2001). ..... 12
- Figure 2-2: Generalized stratigraphic section of the Huronian Supergroup. Conglomerate is shown in grey, argillite/claystone in brown, sandstone in yellow and limestone in blue. Orange at the base of the section indicates volcanic rocks. Note the repeating conglomerate/ argillite or limestone/sandstone cycle in each of the Hough Lake, Quirke Lake and Cobalt groups (after Long, 2004). ..... 14
- Figure 2-3: Locations of studied outcrops and drill core locations in the Bruce Mines/Elliot Lake area. .... 28
- Figure 3-1: A (front view), B: Outcrop D, characterized by the interlaminated siltstone and sandstone lithofacies, the diamictite lithofacies and the contorted argillite lithofacies. C: Sandstone layers within the interlaminated siltstone and sandstone lithofacies locally display asymmetrical ripples. D: The contorted argillite lithofacies contains irregularly-shaped blobs of pink sandstone. .... 33
- Figure 3-2: The contorted argillite lithofacies at Outcrop A. A: folded rhythmite layers. B: Dropstones ranging from granule to boulder size are commonly scattered throughout the interbedded siltstone and claystone. Thin lenticular or wavy sandstone beds are found locally within the lithofacies (pink beds in stratigraphic section). .... 35
- Figure 3-3: Photomicrograph of rhythmites of the interlaminated siltstone and sandstone lithofacies at Outcrop D. Note the normal grading (G) and rippled tops (R). .... 37

Figure 3-4: The interbedded siltstone and claystone lithofacies at Outcrop C is characterized by thinly laminated siltstone layers (dark grey in photo) and claystone layers (light grey in photo) that contain dropstones ranging from granule to boulder in size. The rhythmites are overlain by a 2-3 m thick bed of the pink sandstone lithofacies. Green tape for scale measures 2.4 cm thick vertically..... 39

Figure 3-5: A: Pinched sandstone ripples that are locally connected to form thin lenticular or wavy sandstone beds are interbedded with the rhythmites of the interbedded siltstone and claystone lithofacies at Outcrop A. B: A thin bed of conglomerate within the interbedded siltstone and claystone lithofacies..... 40

Figure 3-6: A: The sandstone lithofacies (Sst) at Outcrop A is interbedded with thin beds of claystone (Clst). Scale card: 7 cm. B: The upper section of the interbedded siltstone and claystone lithofacies at Outcrop A is characterized by an increase in lenticular and wavy sandstone beds, and in grain size. .... 42

Figure 3-7: A: Irregular bedding and an increase in the amount of siltstone upsection in the interbedded siltstone and claystone lithofacies at Outcrop A. A 5-7 cm thick bed of claystone shows a rippled erosional surface (arrow in A) at the contact with the overlying sandstone lithofacies. B: Above the sandstone lithofacies, the interbedded siltstone and claystone lithofacies resumes. The layer marked with an arrow in B indicates the brecciated lamination shown in thin section (C). Scale in A is in cm, marker in B is 13 cm long. .... 43

Figure 3-8: A: Micro-laminae in claystone (clst) layers in the lower section of the interbedded siltstone and claystone lithofacies at Outcrop A are defined by thin layers of siltstone (slst) that separate individual lamina. Siltstone micro-laminae are separated by thin claystone layers. B: Micro-laminae in the fine-grained siltstone (f-slst) layers of the interbedded coarse-grained and fine-grained siltstone lithofacies at Outcrop B are defined by thin layers of coarse siltstone (c-slst) that separate individual fine-grained siltstone lamina. C, D: Micro-laminae in claystone layers in the lower section of the interbedded siltstone and claystone lithofacies at Outcrop C (C) and Outcrop A (D) are defined by thin layers of siltstone that separate individual laminae. Thicker siltstone laminae

dividing claystone layers were observed locally. Siltstone micro-laminae are separated by thin claystone or fine-grained siltstone layers. .... 44

Figure 3-9: A: Flame (flm) structures in fine-grained siltstone (f-slst) laminae, irregular bedding and an increase in the prevalence of coarse-grained siltstone (c-slst) laminae upsection in the interbedded coarse-grained siltstone and fine-grained siltstone lithofacies. B, C: Flame, ball-and-pillow (bap) structures in thin sections from the upper section of the interbedded siltstone and claystone lithofacies at Outcrop A. Thicker and coarser grained siltstone laminae are also displayed upsection. Claystone (clst) laminae grade to fine-grained siltstone laminae upsection (C). D: Photomicrograph of the upper section of the interbedded siltstone and claystone lithofacies at Outcrop C displays slump (slp) structures..... 46

Figure 3-10: The siltstone lithofacies at Outcrop A is characterized by siltstone beds measuring 15 – 25 cm thick interbedded with thin beds of rhythmically layered siltstone and claystone that combine to form beds up to 10 cm thick..... 50

Figure 3-11: The rhythmic laminations that compose the interbedded coarse-grained siltstone and fine-grained siltstone lithofacies are evident at Outcrop B. Dropstones were not found in this lithofacies..... 51

Figure 3-12: Depositional model of the upper Gowganda Formation based on lithofacies found in the study area. .... 57

Figure 4-1: Trace element discrimination diagrams for the claystone and siltstone layers in rhythmites of Outcrop A. (A) Plot of Ti vs Zr showing the claystone layers to be enriched in Ti relative to the siltstone layers, and siltstone layers to be enriched in Zr relative to the claystone layers. (B) Plot of Th/Sc vs Zr/Sc shows little Zr enrichment (low Zr/Sc ratio), indicating that both layers underwent little recycling. Sediment recycling leads to zircon enrichment (upper trend line), whereas samples from active margins display a simple correlation between Th/Sc and Zr/Sc (compositional variations trend line). After McLennan et al. (1993)..... 62

Figure 4-2: Tectonic discrimination diagram of samples from the interbedded siltstone and claystone lithofacies at Outcrop A, with the average of all samples shown in red. The average composition point plots just outside the continental island arc (CIA) field. Other fields shown are: passive margin (PM), active continental margin (ACM) and ocean island arc (OIA). After Bhatia and Crook (1986). ..... 64

Figure 4-3: REE diagram of samples from the interbedded siltstone and claystone lithofacies at Outcrop A. NASC normalizing values are from Haskin et al. (1968) except for Dy, which is taken from Gromet et al. (1984). ..... 66

Figure 4-4: Relative abundance of chlorite + mica versus oxygen-isotope compositions of samples from the interbedded siltstone and claystone lithofacies at Outcrop A. .... 70

Figure 5-1: Plot showing the thickness of the 229 couplets that compose the lower set of measurements from Outcrop A. .... 78

Figure 5-2: Plot showing the thickness of the 585 couplets that compose the upper set of measurements from Outcrop A. .... 78

Figure 5-3: Plot showing the thickness of the 216 couplets that compose the lower set of measurements from Outcrop B. .... 80

Figure 5-4: Plot showing the thickness of the 119 couplets that compose the upper set of measurements from Outcrop B. .... 80

Figure 5-5: Spectral analysis results using the method of Mann and Lees (1996) for the rhythmite measurements of Hughes et al. (2003)(G Hughes 2014, pers. comm., 5 July). Quasi-periodic cycles with periods ranging from 2.3 to 13.3 couplets are shown. A harmonic cycle of period 2.7 couplets is indicated by the open black rectangle. The default frequency resolution of 2 and 3 tapers was used under the assumption of background red noise. .... 82

Figure 5-6: Spectral analysis results using the method of Mann and Lees (1996) for the lower rhythmite measurements from Outcrop A. Quasi-periodic cycles with periods

ranging from 2.2 to 9.2 couplets are shown. The default frequency resolution of 2 and 3  
tapers was used under the assumption of background red noise. .... 83

Figure 5-7: Spectral analysis results using the method of Mann and Lees (1996) for the  
upper rhythmite measurements from Outcrop A. Quasi-periodic cycles with periods  
ranging from 2.3 to 56.9 couplets are shown. A harmonic cycle of about 2.5 couplets is  
indicated in black by an open black rectangle. The default frequency resolution of 2 and 3  
tapers was used under the assumption of background red noise. .... 84

Figure 5-8: Spectral analysis results using the method of Mann and Lees (1996) for the  
lower rhythmite measurements from Outcrop B. Quasi-periodic cycles with periods  
ranging from 2.3 to 30.1 couplets are shown. A harmonic cycle with a period of about 2.8  
couplets is indicated by the open black rectangle. The frequency resolution of 2 and 3  
tapers was used under the assumption of background red noise. .... 85

Figure 5-9: Spectral analysis results using the method of Mann and Lees (1996) for the  
upper rhythmite measurements from Outcrop B. Quasi-periodic cycles with a period  
ranging from 2.9 to 6.9 couplets are shown. The default frequency resolution of 2 and 3  
tapers was used under the assumption of background red noise. .... 86

Figure 6-1: Centimetre-scale rhythmic deposits found in the upper section of the  
interbedded siltstone and claystone lithofacies at Outcrop A (A) bear a strong  
resemblance to Subgroup IIb varves (B) formed by turbidity currents 3 km from shore in  
26 m of water in glacial Lake Hitchcock (Ashley, 1975). Scale in A is in cm..... 99

## List of Appendices

Appendix A: Core Logs, Gowganda Formation .....	127
---	-----

# 1 Introduction

Rhythmites are subaqueous sediment couplets that are deposited in horizontal layers on a periodic basis (Bramlette, 1946; Reineck and Singh, 1972). The couplets generally consist of a coarse-grained lower layer, predominantly composed of fine sand or coarse silt, and a fine-grained upper layer, which is generally composed of fine silt or clay (Williams, 2000). The three classifications of rhythmites are tidalites, turbidites, and varves, divisions that are based on the depositional processes from which they form. In addition, rhythmite development may be influenced by climatic conditions at the time of deposition, particularly if they are formed in association with deglaciation. The rhythmite sequences in the Paleoproterozoic upper Gowganda Formation of the Huronian Supergroup, Canada have previously been identified as glacial varves (Lindsey, 1969; Hughes et al., 2003), and therefore may represent some of the oldest deglaciation deposits on Earth. However, tidal rhythmites and turbidites can also present facies that are strikingly similar to varves. This thesis examines the rhythmites and associated sedimentary deposits of the upper Gowganda Formation northwest and northeast of Wharncliffe, Ontario in order to determine: 1) the depositional processes that formed the strata, 2) the provenance of the deposits, and 3) any paleoclimatic information that can be inferred from the depositional processes. If the rhythmic deposits can be confirmed as varves, each rhythmite will represent an annual depositional event, and will thus collectively provide a high-resolution record of Paleoproterozoic deglacial activity.

The geological age of the Gowganda Formation is constrained to 2.45-2.2 Ga (Krogh et al., 1984; Corfu and Andrews, 1986), a timeframe that encompasses the period when Earth was becoming oxygenated. This study seeks a greater understanding of climatic conditions during this important time in Earth evolution.

## 1.1 Varves

The term varve, coined by De Geer (1912), was originally used to describe a laminated couplet composed of two distinct layers, a claystone layer and a siltstone/sandstone layer. Recurring couplets formed a series of rhythmites that De Geer interpreted as annual sediment layers that formed in a glaciomarine environment. De Geer (1912) postulated

that the repeating couplets represented the annual deposition of sediments released by glacial melt. Antevs (1925) noted that the summer, coarse-grained layers in his study were substantially thicker than the winter, fine-grained deposits. The varve study of Agterberg and Banerjee (1969) subdivided the winter layer into a lower turbidite deposit overlain by a clay layer that rained out from suspension. More recently, varves have been defined to be composed of two or more laminal layers that cyclically repeat annually (Ojala et al., 2012). Ultimately, the thickness of individual varves in glacially-influenced environments is related to the annual influx of sediment to a regional basin, which is influenced by the annual rate of glacial meltwater discharge, which in turn is influenced by climate (Delaney, 2005). Glacially-influenced varves can be characterized by dropstones, which are clasts transported by icebergs, that drop into the sediment as the iceberg melts (Benn and Evans, 2010).

### 1.1.1 Varves in Glaciofluvial Lakes

One of the depositional environments associated with glacial melt is that of the glaciofluvial lake. Glaciofluvial lakes are primarily fed by the outwash stream(s) of a glacier that is not in direct contact with the lake (Smith and Ashley, 1985; Ashley, 2002). Coarse-grained outwash sediment is predominantly deposited on the sandur (outwash plain) that separates the glacier from the lake, resulting in lake deposits that are fine-grained and well sorted (Ashley, 2002). As a glacier recedes, the density of the meltwater stream can be reduced by warming and by the influx of sediment-poor rainwater, leading to a reduction in the sediment load delivered to the lake over time (Ashley, 2002). Reduced sediment delivery and stream warming contribute to the establishment of thermal stratification in the distal glaciofluvial lake environment (Ashley, 2002).

### 1.1.2 Thermal Stratification in Glaciofluvial Lakes

In glaciofluvial systems, varve formation is associated with thermal stratification within a lake (Smith and Ashley, 1985). Thermal stratification occurs because water temperature in a lake varies with depth, and the density of water varies with temperature, which leads to stratification in deep lakes in temperate zones (cf. Dake and Harleman, 1969). The maximum density of water, which is a non-linear function of temperature, is

approximately  $1000 \text{ kg m}^{-3}$  and occurs at  $4^\circ\text{C}$  (Benn and Evans, 2010). As the surficial water in a lake heats up in the spring, it becomes less dense, forming an upper layer called the epilimnion (Smith and Ashley, 1985; Ashley, 2002). A layer of cold, deep, dense and quiescent water occupies the bottom of the lake, a layer called the hypolimnion. A transitional layer sandwiched between the epilimnion and the hypolimnion is characterized by a rapid temperature change in the water, and is known as the metalimnion. Within the metalimnion is the thermocline, the depth at which the water temperature decreases at the greatest rate (Ashley, 2002). Stability of thermal stratification peaks in mid-summer (Smith and Ashley, 1985). With cooling temperatures in the autumn, the epilimnion and thermocline cool to a temperature approximating that of the hypolimnion which, combined with strong winds, leads to mixing between the layers, a process known as overturning. Overturning occurs once a year in monomictic lakes, twice a year (spring and autumn) in dimictic lakes and at irregular intervals in polymictic lakes, which are lakes that lack persistent thermal stratification (Smith and Ashley, 1985). Thermal stratification influences glaciofluvial sedimentation – rhythmic deposits are generally found beneath the thermocline (Ashley, 2002). In lakes without thermal stratification, or if topography places the lake bottom above the thermocline, sedimentation consists of homogeneous muds (Ashley, 2002).

### 1.1.3 Thermal Stratification and Varves

Coarse-grained laminations are deposited during the summer melting season by underflows, bottom hugging currents that plunge beneath the hypolimnion due to heavy sediment loads and perhaps colder temperatures (Smith and Ashley, 1985). Underflows are similar to turbidity currents, but underflows are continuously fed by high-density currents generated by river flow, whereas turbidity currents are generated by episodic sediment gravity flows (Smith and Ashley, 1985).

Fine-grained summer laminations are laterally dispersed by interflows, flows that remain above the hypolimnion, and by lower density underflows that breach the thermocline, but have enough buoyancy to remain above the lake bed (Smith and Ashley, 1985; Ashley, 2002). When inflow initiated by summer melting ceases, clay in suspension settles to form a fining-upward layer (Ashley, 2002). Seasonal rhythmicity is denoted by this thick

layer of fining-upward clay that marks the winter freeze season, with the termination of the freeze season marked by a sharp contact with the overlying silt layer (Smith and Ashley, 1985).

#### 1.1.4 Non-glacial Varves

The formation of varves need not be associated with glaciation. Variations in couplet thickness have been interpreted to result from flooding during spring nival (snow) melting, which results in greater catchment erosion and clastic input, whereas the thinner winter varves are associated with reduced precipitation and quiet deposition (Hambley and Lamoureux, 2006). In addition to varve thickness, colour has been used to identify periods of high sediment input, as controlled by mineral and organic components, as well as the chemistry of alternating layers (e.g. Landmann et al., 1996). Although early work on varves focused on clastic deposits, the definition of a varve has since been extended to include a broader range of sediment types. Zolitschka (2007) classified lacustrine varves as clastic, biogenic or evaporitic, although more than one type of varve may form in extended time periods (Ojala et al., 2012). Varves may also contain more than two texturally distinct layers (Hambley and Lamoureux, 2006; Ojala et al., 2012).

## 1.2 Varves in Precambrian Settings

Varves are difficult to identify in the Precambrian rock record because there is a lack of time indicators, such as the summertime deposition of fossils or pollen, that allow for interpretations of annual control. In addition, radiometric age dating can only be conducted on detrital minerals, giving maximum ages for deposition. Nonetheless, several investigations have attempted to consider rhythmites as varves, thereby enabling interpretations of ancient climatic variations. Lacustrine couplets of the Mesoproterozoic Poll a'Mhuilt Member of the Stoer Group, northern Scotland, contain silt-clay laminations of variable thickness separated by very thin organic laminations (Andrews et al., 2010). These couplets have been interpreted as varves due to their similarity to Middle Devonian varves of the Orcadian Basin in Scotland (Andrews et al., 2010). Attempts to identify solar forcing in the inferred Mesoproterozoic varves were made by applying spectral analysis to measured couplet thickness. Andrews et al. (2010) identified

periods of 9.2 and 10.6 years that they associated with the Schwabe cycle, which has a modern mean period of 11 years. Schwabe cycles are periods of intense magnetic flux observable from Earth as peaks in sunspot activity, and have a range of 8 – 17 years (Weedon, 2003). Significant increases in solar UV radiation associated with sunspot peaks may influence climate patterns; however this correlation has not been conclusively demonstrated (Weedon, 2003).

Micro-banded deposits in the Paleoproterozoic banded-iron formation of the Hamersley basin, Australia, have been interpreted as chemical varves (Trendall, 2002; Klein, 2005). Iron layers are interpreted to have precipitated from biogenic activity while silica layers formed during abiotic periods. In this model, oxygen produced annually by algae in a water basin combined with ferrous iron, which precipitated to form ferric iron deposits. Annual control was inferred from the lateral and vertical extent of the rhythmic deposits, and the assumption that biogenic activity was suspended on an annual basis (Trendall, 1983). Krapež et al. (2003), however, disagreed and interpreted the deposits as the products of density currents.

A third putative example of Precambrian varves is found in the Mesoproterozoic McArthur Basin, northern Australia (Jackson, 1985; Donnelly and Jackson, 1988). The deposits contain laminations composed of alternating layers of organic-rich claystone (shale) and carbonate (dolostone). In this rhythmic sequence, annual control is inferred from the appearance of multiple layers of alternating biogenic and chemical laminations, with the assumption that biogenic activity is suspended annually.

### 1.3 Tidal Rhythmites

The gravitational force exerted by the Moon on the Earth's oceans results in the formation of a tidal bulge (Nichols, 2009). This tidal bulge is most prominent in the water that is closest to the moon. A secondary bulge, which forms on the opposite side of the Earth, forms due to the property of inertia: water opposite the tidal bulge resists being set in motion. The rise and fall of the tidal bulge manifests itself at a shoreline as the tidal cycle: a surge in water landward as the tidal bulge is proximal, and a recession of the water seaward as the bulge passes with the rotation of the Earth away from the moon.

Most areas record a second and slightly weaker high tide about twelve hours later as the tidal bulge created by inertia passes. These twice-daily tides are called semidiurnal tides (Nichols, 2009). In some environments the reach of the secondary tide is insufficient to flood the local landmass, in which case only one tidal cycle (a diurnal cycle) is observed (Archer and Johnson, 1997).

The Sun also exerts a gravitational pull on Earth's oceans, which has been measured to be a little less than half that exerted by the Moon. The strongest (spring) tides are recorded when the Sun, Moon and Earth are in alignment, and the weakest (neap) tides occur when Earth is most out of alignment with the Sun and the Moon (Archer and Johnson, 1997). The modern semidiurnal neap/spring cycle (synodic half-month) lasts about 14.7 days, with the traction current progressing from being weak during neap tide to strong during spring tide. This cycle can be observed in the rock record as a gradual increase in bed thickness from neap tide to spring tide (Nio and Yang, 1991; Chan et al., 1994). The declination of the moon also influences tidal heights, to a lesser degree (Archer et al., 1990). The modern tropical half-month, which is the time that it takes for the lunar declination to range from a maximum northerly declination to maximum southerly declination, is 13.7 days (Archer et al., 1990). The distance between the Earth and the Moon also impacts tidal height, with the perigee (lunar distance closest to Earth) and apogee (lunar distance farthest from Earth) and back to perigee cycle occurring over a period of 27.6 days (Archer et al., 1990). Although solar and lunar gravitational forces are the driving mechanisms behind tides, it is ultimately the geographical shape of the shore region that dictates the height differential between the flood (inflow) and ebb (outflow) tides (Nichols, 2009).

Rhythmically laminated sediments deposited from tidal activity are called tidal rhythmites, although they are also referred to as tidalites (Klein, 1971; Chan et al., 1994). Tidal rhythmites are composed of alternating sandstone/siltstone and claystone laminations that reflect the flood and ebb stages of diurnal or semidiurnal tides. Traction currents operating during the flood and ebb stages of a tidal cycle deposit coarse-grained (silty) sediment, whereas fine-grained (muddy) material is deposited during the slackwater period when the flow direction alternates (Klein, 1971). Typically, the planar-

laminated silty layers are normally graded and much thicker than the thin clay drapes that overlie them (Archer et al., 1995). Although tidal rhythmites may resemble varves in the rock record, changes in the lunar and solar cycles influence the strength of tidal flow, resulting in periodic variations in bed thickness (Williams, 1989). Maximum rhythmite thickness occurs at the peak of the spring tide, with rhythmite thickness decreasing as the tide cycle progresses to the neap tide (Archer et al., 1990). Thin beds associated with a neap tide may be difficult to discern in the rock record, leading to rhythmite counts that have a lower sum than expected, which may confound efforts to identify tidal periodicities (Archer and Johnson, 1997). Sedimentary structures such as mud cracks, raindrop imprints, rill marks or falling water marks may be found in tidal environments, and indicate subaerial exposure or very shallow water (Archer and Johnson, 1997). Tidal rhythmites commonly form in inner estuaries, delta fronts, and tidal channels (Tessier, 1993; Greb and Archer, 1998; Tessier, 1998).

## 1.4 Tidal Rhythmites in Precambrian Settings

Williams (1989) was one of the early researchers to recognize tidal rhythmites in the Precambrian rock record. In this study conducted on the ~ 680 Ma Elatina Formation at Pichi Richi Pass in South Australia, laminated couplets composed of a lower fine-grained sandstone layer and an upper claystone/siltstone layer were originally interpreted to be annually deposited glacial varves, based on the periglacial nature of the deposit and apparent solar periods of about 11 and 22 years (Williams, 1981; Williams, 1985). Closer examination of the rhythmic couplets revealed cyclic groups containing an average of 12 laminations, with the end members of each group indicated by a series of thin, muddy laminations. Re-interpretation of the data revealed alternating high and low amplitude cycles that closely resembled the fortnightly tidal cycle of Townsville, Queensland. Under this interpretation, the late Precambrian year consisted of approximately 400 days, made up of 13.1 lunar months containing approximately 30.5 days (Williams, 1989; Williams, 1991).

A study of tidal rhythmites located in the Chaibasa Formation, India indicated a semidiurnal tidal system and suggested that the late Paleoproterozoic lunar month consisted of about 32 days (Mazumder, 2004). Chan et al. (1994) identified tidal

rhythmites in the Neoproterozoic Big Cottonwood Formation, Utah, USA based on an interpretation of rhythmites that cyclically thicken and thin on average 7-9 times over the course of a neap-spring cycle. Although the cyclicity was typically less than the 14 couplets expected in a lunar event, the authors suggest that the cycle was truncated, perhaps due to low traction current activity during neap cycles, or by an elevated depositional environment that is out of reach of tidal flow during neap cycles. Chan et al. (1994) also identified monthly, semi-annual and annual tidal periods. One of the oldest tidal records is located in the Barberton Greenstone Belt, South Africa where Eriksson and Simpson (2000) identified tidal rhythmites that display a neap-spring-neap cycle of around 13 days, although this study also yielded results that could be interpreted to imply an 18 to 20 day lunar cycle.

## 1.5 Turbidites

The term turbidite was introduced to describe sedimentary layers that are deposited by turbidity currents (Kuenen, 1957). Subaqueous landslides generate the debris that combines with water to form a turbidity current (Hampton, 1972). A turbidity current can result from: 1) a debris flow initiated by sediment overload in an upslope location, which collapses when it can no longer support itself (loss of shear strength), or 2) a debris flow set in motion by an external de-stabilizing force such as an earthquake (Stow et al., 1996). Regardless of how the flow is initiated, a turbidity current is driven by gravitational instability, a condition that may be exacerbated in environments with high sedimentation rates, where fine-grained sediment is more unstable than coarse-grained sediment (Hampton, 1972, Stow et al., 1996).

Bouma (1962) identified five divisions of turbidite deposits, which from top to bottom include:

T<sub>e</sub> – massive to laminated mudstone

T<sub>d</sub> –parallel-laminated siltstone

T<sub>c</sub> –rippled, wavy or convolute laminated, fine-grained sandstone

T<sub>b</sub> –planar laminated, fine- to coarse-grained sandstone

T<sub>a</sub> –massive or normally graded fine- to coarse-grained sandstone

Turbidite deposits exhibit a general fining-upward trend; however each division is not always found in any single turbidite deposit. For example, Lowe (1982) suggests that only the T<sub>b</sub>, T<sub>c</sub>, and T<sub>d</sub> layers are present if the material composing the turbidity current is of low density. Mulder and Alexander (2001) state that the nature of a turbidity flow is based on the concentration, cohesivity and support mechanism of the sediment particles, and the duration of the flow. Turbidity currents displaying a mostly steady-state flow result in the deposition of massive to cross-bedded sandstone overlain by mudstone. Surging turbidity flows deposit rhythmic layers of sandstone and mudstone, and hybrid surge-like turbidity currents deposit the classic Bouma sequence as described above (Mulder and Alexander, 2001). Although turbidite deposits form as a result of sediment reworking resulting from gravitational processes, sedimentary units that resemble turbidite deposits may result from other re-sedimentation processes. For example, Shanmugam (1997) attributes the presence of T<sub>b</sub>, T<sub>c</sub>, and T<sub>d</sub> layers to bottom current reworking. Laminated and graded rhythmites can also be formed as a result of storm activity (Reineck and Singh, 1972).

## 1.6 Glacially-influenced Turbidites in Precambrian Settings

In contrast to varves, turbidite deposits are quite common in the Precambrian rock record and have often been found associated with glacial deposits. For example, Eyles and Eyles (1989) described Neoproterozoic glacially-influenced turbidite deposits of the Conception Group located on the Avalon Peninsula, southeast Newfoundland, Canada. The turbidite succession is 4 km thick, and contains partial and complete Bouma sequences. Locally, tabular beds of diamictite are interbedded with the turbidite deposits (Eyles and Eyles, 1989). Evidence of slumping was also observed. The upper Bouma divisions, T<sub>d</sub> (planar laminated silt) and T<sub>e</sub> (massive or planar laminated mud) locally resemble varves, and thus caution needs to be employed when identifying these types of deposits in a glaciogenic environment. de Alvarenga and Trompette (1992) described Neoproterozoic glaciogenic and turbiditic marine sediments of the Cuiabá Region, west-

central Brazil. Dropstones were found in rhythmites ranging from silty mudstone to very fine-grained sandstone in proximal platform deposits. Distal platform deposits interpreted to be turbidites were found to be composed of re-sedimented diamictite and laminated, fine-grained sedimentary rocks. Normal and reverse grading of sandstone-to-conglomeratic material was also observed (de Alvarenga and Trompette, 1992). Martins-Neto et al. (2001) described non-glacial Proterozoic rhythmic couplets composed of interlaminated very fine-grained wacke and mudstone in the Macaúbas-Salinas Basin of eastern Brazil. These deposits are interbedded with massive and normally graded wacke beds, with local parallel lamination and climbing ripples comprising a complete Bouma sequence. The authors interpret the deposits as forming in a deep marine environment along a passive margin, resulting from recurring, very low density turbidity currents sourced from a continental shelf.

## 2 Geological Setting

### 2.1 The Huronian Supergroup

The Huronian Supergroup, which comprises the majority of the geological Southern Province, is a Paleoproterozoic, sedimentary-dominated succession that unconformably overlies Archean rocks of the Superior Province to the north of Lake Huron in Ontario, Canada (Figure 2-1). The succession forms an approximately 325 km long belt that extends from Noranda, Quebec in the northeast to the Sault Ste. Marie area in the west (Willingham et al., 1985). The Huronian Supergroup is up to 12 km thick at its southern boundary where it underlies Paleozoic rocks of the Michigan Basin (Young et al., 2001), and thins toward the north and west of the Southern Province. The southeastern boundary of the Huronian Supergroup is characterized by the Grenville Front, which separates rocks of the Southern and Grenville Provinces. The Grenville Province contains the remnants of a mountain building event that terminated at ca. 1.0 Ga (Young and Nesbitt, 1985; Young et al., 2001). Rocks in the Bruce Mines-Elliot Lake area and the Cobalt area have been metamorphosed to greenschist grade, and rocks in the Espanola area have been metamorphosed to amphibolite grade (Lindsey, 1969), but the prefix “meta” to describe the rock types (e.g. meta-sandstone, meta-siltstone) is herein omitted for simplicity.

The maximum age of the Huronian Supergroup is  $2450 \pm 25/-10$  Ma, based on U-Pb zircon analysis of the Thessalon Formation (Fig.2-2; Krogh et al., 1984). The minimum age of the Huronian Supergroup was determined to be  $2217.0 \pm 6.0$  Ma based on U-Pb analysis of primary baddeleyite from the Nipissing diabase dikes that intrude the succession (Corfu and Andrews, 1986). Tang and Chen (2013) have suggested that the duration of the Huronian glaciation events could be constrained to 2.29-2.25 Ga, given their similarity to diamictite deposits in the Turee Creek Group, Hammersley Basin, Western Australia; Makganyene Formation, Griqualand West Basin, South Africa; Boshhoek Formation and Duitschland Formation, Transvaal Basin, South Africa; Sariolian Group, Karelian Supergroup, Eastern Baltic Shield, Russia; Chocolay Group, Marquette

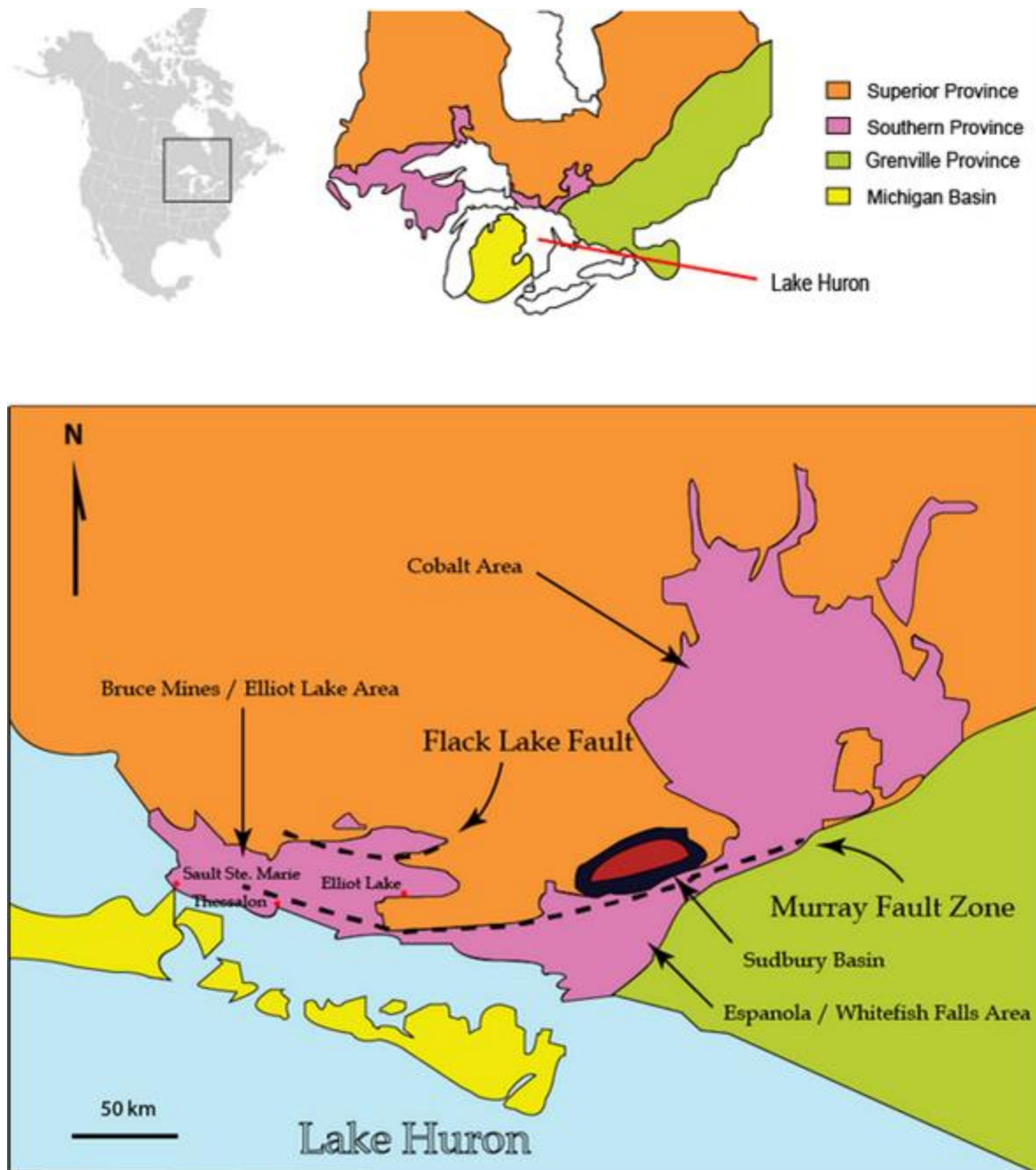


**Figure 2-1:** Distribution of the Huronian Supergroup in Ontario, Canada. The Huronian Supergroup comprises the eastern section of the Southern Province, and is divided into three regions: the Bruce Mines/Elliot Lake area, the Espanola/Whitefish Falls area and the Cobalt area. The Flack Lake fault and the Murray fault zone (dashed lines) indicate contemporaneous down-to-basin faulting. Map modified from Freeman (1978) and Young et al. (2001).

Range Supergroup, Michigan/Wisconsin USA; and Snowy Pass Supergroup, Wyoming, USA. In an American Geophysical Union abstract, however, Bekker et al. (2010) reports a ca. 2.31 Ga U-Pb age from a tuff in the Gordon Lake Formation, upper Huronian Supergroup, suggesting that most of the Huronian formations are older than 2.31 Ga.

The lower Huronian units (pre-Gowganda Formation) are interpreted to have been deposited in transtensional to extensional (synrift) basins whereas the upper Huronian Supergroup represents passive margin deposits (Young and Nesbitt, 1985; Mustard and Donaldson, 1987; Holm et al., 2005; Eyles, 2008; Young, 2013). Although most workers separate the Huronian Supergroup into four groups, Wood (1973) and Long (2009) have suggested that five groups comprise the succession, based mainly on disconformable relationships (Figure 2-2): the basal Elliot Lake Group, overlain in ascending order by the Hough Lake, Quirke Lake, Cobalt and Flack Lake groups. Volcanic rocks and conglomerate comprise the basal units of the Elliot Lake Group, which are sequentially followed upsection by sandstones and claystones/wackes. The overlying three groups represent tripartite cycles, with each containing glacial diamictite (poorly sorted, matrix-supported conglomerate) at their bases, followed upsection by thinly laminated siltstone and claystone that are, in turn, overlain by arenaceous sandstone (Young et al., 2001). This complex period of glaciation has been identified in the literature as the 'Huronian Glacial Event'. Striations and grooves in rock surfaces underlying the diamictite, striated and faceted clasts within the diamictite, and the presence of lonestones/dropstones in the fine-grained laminated deposits all support a glacial interpretation for the basal units of the middle three Huronian groups (Lindsey, 1969; Young, 1970). The argillites (meta-mudstones) and claystone/siltstone rhythmites that dominate the middle sections of each formation have been interpreted as post-glacial deltaic deposits (Lindsey, 1969; Young et al., 2001). The third stage of each glacial cycle is represented by cross-bedded, medium- to coarse-grained sandstones that have been interpreted as having been deposited in shallow marine, fluvial-deltaic or fluvial environments (Palonen, 1973; Long, 1978; Young et al., 2001).

# Huronian Supergroup

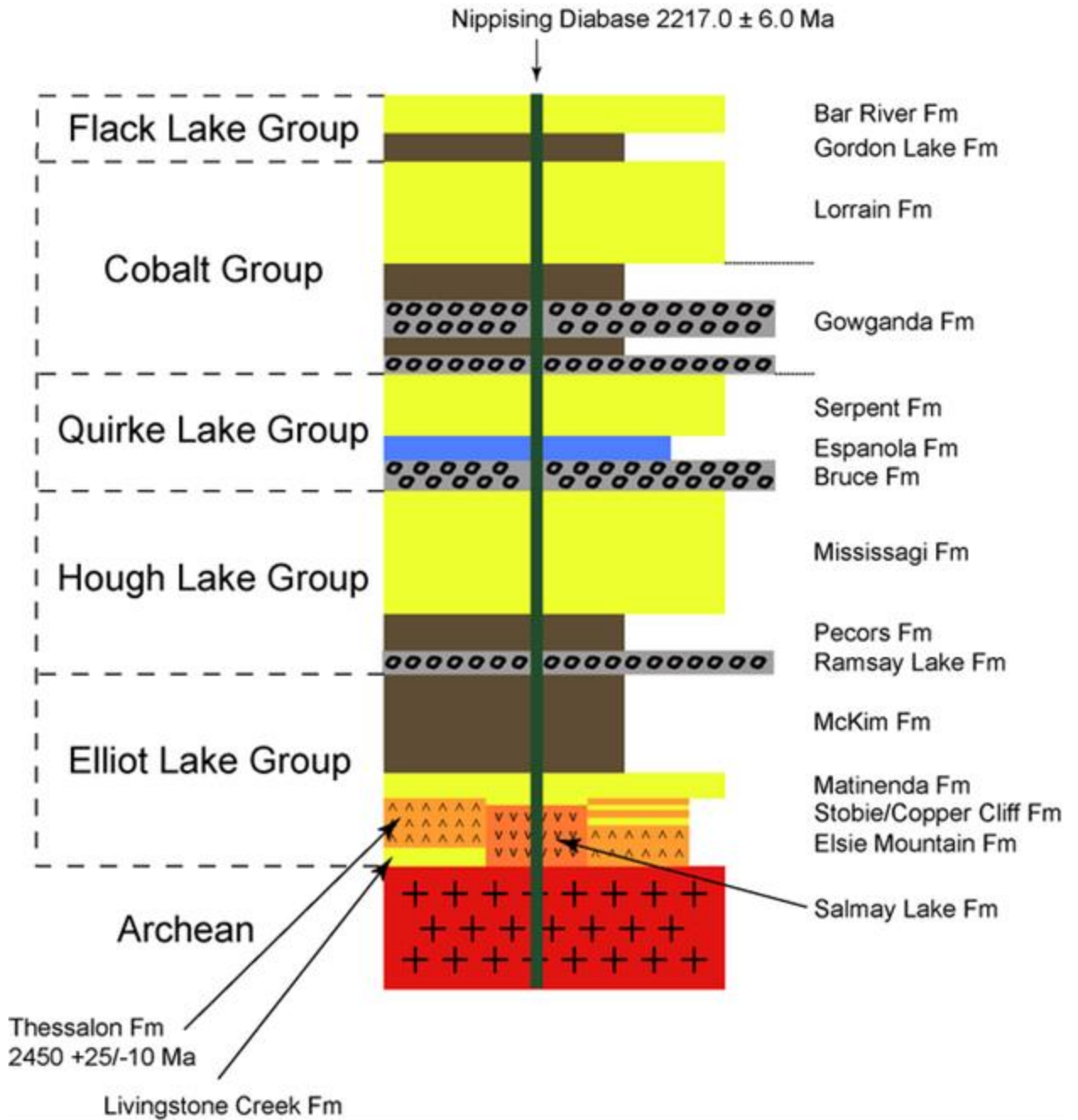


**Figure 2-2:** Generalized stratigraphic section of the Huronian Supergroup. Conglomerate is shown in grey, argillite/claystone in brown, sandstone in yellow and limestone in blue. Orange at the base of the section indicates volcanic rocks. Note the repeating conglomerate/ argillite or limestone/sandstone cycle in each of the Hough Lake, Quirke Lake and Cobalt groups (after Long, 2004).

## 2.1.1 Elliot Lake Group

The Elliot Lake Group is the only group in the Huronian Supergroup that contains significant uranium deposits and volcanic rocks (Bennett et al., 1991). It is composed of the Livingstone Creek, Thessalon, Matinenda and McKim formations in the western part of the Huronian belt, whereas the Elsie Mountain, Stobie, Copper Cliff, Matinenda and McKim formations constitute the group in the east.

### 2.1.1.1 Livingstone Creek Formation

The Livingstone Creek Formation is approximately 400 m thick in the Sault Ste. Marie area and approximately 300 m thick northeast of Thessalon, although outcrops as thin as 100 m have been measured (Frarey, 1977; Bennett et al., 1991). Medium- to fine-grained trough cross-bedded sandstones of fluvial origin dominate the formation; however, thin polymictic conglomerates thought to be alluvial fan deposits have been identified locally. The composition of the sandstones ranges from arenite to wacke (Bennett et al., 1991). Chemical weathering of the conglomerate in the lower Livingstone Creek Formation was probably minimal, based on the presence of a significant amount of feldspar within the clasts and matrix, and a complete lack of quartz clasts (Young, 2001).

### 2.1.1.2 Thessalon Formation

The Thessalon Formation is 650-820 m thick in the Sault Ste. Marie area and ranges from 330 m to 1200 m in the east (Frarey, 1977). The formation is composed of bimodal volcanic flows, minor volcanic breccia and felsic to intermediate tuffs (Bennett et al., 1991) intercalated with uraniumiferous conglomerate towards the top. The deposits are interpreted to have been associated with rifting, which supports the existence of a tectonically active environment during this time frame (Koglin et al., 2010).

### 2.1.1.3 Elsie Mountain Formation

The <1000 m thick Elsie Mountain Formation is predominantly composed of marine basalts, many of which are pillowed (Card, 1978). Intercalated argillites and sandstones are prominent in the upper part of the formation.

#### 2.1.1.4 Stobie Formation

The  $\leq 1500$  m thick Stobie Formation conformably overlies and is lithologically similar to the Elsie Mountain Formation, but contains more sedimentary units, with increasing proportions of interbedded wacke, siltstone and arenite up-section (Card, 1978).

#### 2.1.1.5 Copper Cliff Formation

Conformably overlying the Stobie Formation is the  $\leq 760$  m thick Copper Cliff Formation, which is predominantly composed of felsic flows and felsic pyroclastic rocks with minor arkosic sandstones (Card, 1978; Bennett et al., 1991). Zircons from rhyolite in the Copper Cliff Formation were dated using U-Pb geochronology at  $2450 \pm 25$  Ma (Krogh et al., 1984) and  $2452 \pm 6.2$  Ma (Ketchum et al., 2013).

#### 2.1.1.6 Salmay Lake Formation

The  $\leq 1500$  m thick Salmay Lake Formation is described by Card (1978) as possibly correlative with the Elsie Mountain and Stobie formations. Volcanic rocks ranging from basalt to rhyodacite, which are interbedded with quartz-pebble conglomerate and wacke, dominate the Salmay Lake Formation (Card, 1978; Bennett et al., 1991). Card (1978) observed a lithological similarity between lower Salmay Lake Formation sedimentary rocks and those of the Matinenda Formation.

#### 2.1.1.7 Matinenda Formation

The Matinenda Formation, which is up to 600 m thick (Bennett et al., 1991), is mainly composed of medium- to coarse-grained arkose, with beds of quartz-pebble conglomerate, some containing uranium-bearing minerals and pyrite (Roscoe, 1969; Card, 1978). Up-section the arkose becomes finer grained, and the conglomerate becomes more polymictic, which locally grades back into uraniferous conglomerate and coarse-grained arkose (Roscoe, 1969; Roscoe, 1981). Locally, the Matinenda Formation is intercalated with basalts, wackes and argillites of the Stobie Formation and argillites of the McKim Formation (Card, 1978). The presence of ripple marks, scour-and-fill structures and cross-bedding in the sandstones allowed for paleocurrent analysis, which indicated a southeasterly flow direction and support an interpretation of a shallow braided

channel system associated with a braid delta (Fralick and Miall, 1989; Bennett et al., 1991).

#### 2.1.1.8 McKim Formation

The uppermost unit of the Elliot Lake Group is the McKim Formation, which conformably overlies and is intercalated with the Stobie, Copper Cliff, Salmay Lake and Matinenda formations (Card, 1978). Alternating facies of wacke, laminated argillite-siltstone and quartz-feldspar sandstone comprise the McKim Formation, which measures up to 2400 m thick in the Sudbury area (Bennett et al., 1991). A transition from laminated siltstones in the western part of the McKim Formation to thickly bedded wackes, some containing partial Bouma cycles, in the east suggests an eastern source area for the sedimentary rocks (Card, 1978). The depositional environment for the McKim Formation is interpreted to be deep marine, below wave base (Card, 1978).

#### 2.1.2 Hough Lake Group

Three formations comprise the Hough Lake Group, which in ascending order are the Ramsay Lake, Pecors and Mississagi formations. The contact between the McKim Formation and the overlying Ramsay Lake Formation varies from erosional to disconformable (Robertson, 1976). Locally, the McKim Formation is absent and the Ramsay Lake Formation unconformably overlies the Matinenda Formation or the Archean basement (Bennett et al., 1991).

##### 2.1.2.1 Ramsay Lake Formation

The  $\leq 550$  m thick Ramsay Lake Formation is predominantly composed of massive diamictite, consisting of pebble- to boulder-size clasts of quartz, granite and volcanic rocks in a medium- to coarse-grained sandstone matrix (Bennett et al., 1991). The diamictite is broadly interstratified with argillaceous mudstone. Sandstone and siltstone interbeds are locally intercalated with Matinenda Formation conglomerates, suggesting that the Matinenda Formation was not lithified at the time of deposition of the Ramsay Lake Formation (Bennett et al., 1991). The Ramsay Lake Formation is the first of three Huronian formations that are interpreted and widely accepted as being of glacial origin

(Young, 1970; Robertson, 1976; Miall, 1985). As such, the basal contact of the Ramsay Lake Formation is widely accepted to be erosional, but not significantly disconformable (Bennett et al., 1991). Fralick and Miall (1989) interpret the tillites of the Ramsay Lake Formation to be the result of three processes associated with glaciers: ice-proximal melting, subaqueous deposits resulting from ice-rafted debris, and gravity flows and outwash deposits due to fluvial activity.

### 2.1.2.2 Pecors Formation

The up to 900 m thick Pecors Formation conformably overlies the Ramsay Lake Formation. The thickest deposits are found in the Sudbury area, and thin to the west with no observed preservation west of Thessalon (Bennett et al., 1991). Laminated and bedded wacke, argillite and sandstone comprise the Pecors Formation, and basal deposits are locally composed of claystone and siltstone rhythmites, which locally contain dropstones (Roscoe, 1969; Bennett et al., 1991). Additional sedimentary structures include slumps, ripple marks, clastic dykes and ball-and-pillow structures. Partial Bouma sequences are common and indicate deposition by turbidity currents in a deep water environment (Card, 1978). However, local mud cracks suggest deposition in shallower water (Bennett et al., 1991).

### 2.1.2.3 Mississagi Formation

The Mississagi Formation is found throughout the Huronian belt, and exceeds 3000 m in thickness in some locations (Bennett et al., 1991). Moderate to well-sorted, medium- to coarse-grained subarkose to arkose with planar and trough cross-beds dominate the Mississagi Formation. Quartz arenite to wacke have been found locally (Bennett et al., 1991; Long, 1976). Basal thin beds of pyritiferous conglomerates are in contact with Archean basement locally, as are pebble conglomerates, units of which measure up to 60 m thick (Long, 1986; Long et al., 2011). Numerous paleocurrent studies of the Mississagi Formation have been conducted, but with conflicting interpretations. Bimodal distributions in the Espanola area indicate strong westerly and southerly modes, whereas in the Elliot Lake area, a south-easterly unimodal distribution was determined (Palonen, 1973). Palonen (1973) proposed a marine shelf depositional environment, whereas Long

(1976) suggested that two large braided-stream systems led to deposition of the Mississagi Formation.

### 2.1.3 Quirke Lake Group

The three formations that comprise the Quirke Lake Group, from the base to the top, are the Bruce, Espanola and Serpent formations. The contact between the Mississagi Formation and the overlying Bruce Formation is generally interpreted to be unconformable (Bennett et al., 1991).

#### 2.1.3.1 Bruce Formation

The Bruce Formation is estimated to be up to 760 m thick, and is dominated by diamictite comprised of subangular to rounded clasts of granite and quartzite set in a medium- to coarse-grained wacke matrix (Bennett et al., 1991; Long, 2009). The clasts are derived from Archean basement and older Huronian formations that predate the Bruce Formation. Intercalations of orthoconglomerate, arkose, wacke and siltstone, some of which are calcareous, have also been identified (Card, 1978; Bennett et al., 1991). The Bruce Formation is widely interpreted to be composed of glacially-derived sediments deposited in a terrestrial environment (Casshyap, 1969; Bernstein and Young, 1990).

#### 2.1.3.2 Espanola Formation

The Espanola Formation extends from Sault Ste. Marie to an area about 70 km northeast of Sudbury, reaching a maximum thickness of approximately 600 m in the Espanola-Lake Panache area (Bennett et al., 1991). It is the only formation that contains significant carbonate deposits, locally containing stromatolites (Hofmann et al., 1980; Bennett et al., 1991). In some locations, the stratigraphy of the Espanola Formation can be divided into three units: a basal unit composed of limestone, a middle unit composed of carbonate-rich siltstone-wacke-arenite, and a top unit composed of dolomite (Card, 1978; Bernstein and Young, 1990). Each of these units is generally laminated or thinly bedded, and grade vertically into one another. The presence of carbonates and stromatolites in the Espanola Formation suggests a shallow marine depositional environment in association with a moderate to warm climate (Bennett et al., 1991; Bernstein and Young, 1990; Fedo et al.,

1997b). Lacustrine (Veizer et al., 1992), tidal (Card and Jackson, 1995) and deltaic environments (Junnala and Young, 1995) have also been proposed for the Espanola Formation. The contact between the upper dolomite unit and the overlying Serpent Formation has been found to be both gradational and disconformable in some locations (Frarey, 1977; Bennett et al., 1991).

### 2.1.3.3 Serpent Formation

The Serpent Formation extends from Sault Ste. Marie to an area approximately 70 km northeast of Sudbury, and ranges from 150-250 m thick at Bruce Mines to a maximum thickness of 1500 m in the Sudbury-Espanola and Falconbridge Township areas (Bennett et al., 1991). Glacial erosion by the unconformably overlying Gowganda Formation may account for the significant variation in thickness of the Serpent Formation (Bennett et al., 1991). Isolated lenses and interbeds of polymictic para- and ortho-conglomerate are common at the base of the formation. Fine- to medium-grained feldspathic arenite and arkose are predominant, and are finely laminated, planar or festoon cross-bedded. Additional structures include ripple marks and mud cracks. Sedimentary structures in the Serpent Formation are suggestive of an overall subaerial depositional environment (Young, 1982), and more specifically, distal alluvial braided-stream environment (Long, 1976; Fedo et al., 1997a).

### 2.1.4 Cobalt Group

The two formations comprising the Cobalt Group are the basal Gowganda Formation and the conformably overlying Lorrain Formation (Rousell and Long, 1998; Long, 2009). Cobalt Group strata are present throughout the Huronian belt, and reach a maximum thickness of 5800 m southwest of Sudbury near Lake Panache (Bennett et al., 1991). Paleomagnetic evidence suggests a low paleolatitude during deposition of the Cobalt Group (Williams and Schmidt, 1997).

#### 2.1.4.1 Gowganda Formation

In the Cobalt area, the Gowganda Formation unconformably overlies Archean basement (Lindsey, 1969), whereas in the south it is erosionally conformable with the underlying

Serpent Formation (Young and Nesbitt, 1985). The thickness of the Gowganda Formation is approximately 1070 m near Sault Ste. Marie, ranges from 970 - 1150 m around Whitefish Falls, ranges from 950 - 2700 m in the Sudbury area, is 1500 m in the Maple Mountain area, and 700 m in the area of Temagami (Bennett et al., 1991). Diamictite and laminated siltstone and argillite containing abundant dropstones comprise the lower Gowganda Formation, which is interpreted to have been deposited by a continental ice sheet (Young and Nesbitt, 1985). Interbedded sandstone and argillite characterize the upper part of the formation and are inferred to represent a prodeltaic succession that was deposited as the continental ice sheet retreated (Rainbird, 1985; Young et al., 2001; Long, 2009).

#### 2.1.4.2 Lorrain Formation

The Lorrain Formation conformably overlies the Gowganda Formation, and ranges from 1500 - 2300 m thick in the Maple Mountain area, 2400 - 2500 m thick near Sault Ste. Marie, and 2300 - 3300 m thick north of Sudbury (Bennett et al., 1991). The Lorrain Formation is predominantly composed of arkose, which matures up-section to quartz arenite. However, intervals of massive to crudely cross-stratified jasper and quartz pebble conglomerate, as well as laminated shale, have been identified locally (Lowey, 1985). Sedimentary structures include ripple marks, planar and trough cross-bedding, ball-and-pillow structures, convolute bedding, gravel lags, low-angle scours and mud intraclasts (Bennett et al., 1991). Both a fluvial (Wood, 1973; Frarey, 1977; Chandler, 1986) and transitional marine (Lowey, 1985; Young et al., 2001) environment have been proposed for the Lorrain Formation, which is commensurate with the increasing sedimentological maturity of the deposits from the base to the top of the formation.

#### 2.1.5 Flack Lake Group

The Flack Lake Group is composed of two units, the lower Gordon Lake Formation and the upper Bar River Formation (Wood, 1973; Rousell and Long, 1998; Long, 2009). Some workers include the Gordon Lake Formation and the Bar River Formation in the Cobalt Group (Roscoe, 1969; Card, 1978; Eyles, 2008), and Lowey (1985) notes that the Flack Lake Group has not been formally defined and is not widely accepted. This thesis

includes this division based two main observations: 1) drill core records indicate that the contact between the Gordon Lake Formation and the underlying Lorrain Formation is disconformable (Wood, 1973), and 2) the Lorrain Formation represents the third sandstone unit of the third and final Huronian glacial cycle. Although the Flack Lake deposits are similar to the upper units of the glacially influenced groups, the absence of a glacial tillite (diamictite) overlying the Lorrain Formation suggests that glaciation did not play a role in deposition of the Flack Lake Group (Rousell and Long, 1998).

#### 2.1.5.1 Gordon Lake Formation

Outcrops of the Gordon Lake Formation are located near Sault Ste. Marie, where the formation is approximately 300 m thick, in the Blind River area where it measures 300 - 360 m thick, in the Sudbury-Espanola area where it is approximately 700 m thick, and east of Cobalt where it measures 540 - 600 m thick (Bennett et al., 1991). The base of the Gordon Lake Formation contains red, fine-grained sandstone, interpreted to have been deposited in a coastal sabkha (Wood, 1973; Chandler, 1986). The middle section of the Gordon Lake Formation contains small-scale sedimentary cycles resembling Bouma sequences (Card, 1978). The presence of symmetrical wave ripples within this unit, however, has led Chandler (1986) to interpret the depositional environment as shallow marine, suggesting that the gradational bedding resulted from storm activity. The upper part of the Gordon Lake Formation is composed of upward coarsening, predominantly cross-bedded sandstone that conformably grades into the overlying Bar River Formation (Card, 1978; Chandler, 1986). U-Pb dating of zircons found in thin tuff beds in the lower Gordon Lake Formation yielded an age of approximately 2310 Ma (Bekker et al., 2010); however a significant spread of older and younger ages was noted (Rasmussen et al., 2013), and if the zircons are detrital, the Gordon Lake Formation could conceivably be much younger (Young, 2014).

#### 2.1.5.2 Bar River Formation

The Bar River Formation is approximately 300 m thick in the Sault Ste. Marie - Elliot Lake area, 900 m thick in the Sudbury-Espanola area, and 400 - 600 m thick in the Maple Mountain area northeast of Cobalt (Bennett et al., 1991). Massive and cross-bedded

quartz arenite containing symmetrical ripple marks dominates the Bar River Formation, suggesting a beach or aeolian depositional environment (Wright and Rust, 1985). However, minor exposures of fine-grained deposits, containing mud cracks and desiccation features, have led to a meso- to macro-tidal (shallow marine) environmental interpretation (Robertson, 1986).

## 2.2 Sudbury Igneous Complex

Rocks of the Huronian Supergroup were affected by a meteorite impact at ca. 1.85 Ga (Dietz, 1964; Krogh et al., 1984). The remnant elliptically-shaped structure is known as the Sudbury Basin (Rousell et al., 1997; Young et al., 2001) and is approximately 58 km x 28 km in size. The basin forms a boundary with Archean basement rocks to the north and Huronian Supergroup deposits to the south. The Sudbury Igneous Complex (SIC), interpreted as an impact melt sheet, forms part of the Sudbury basin and underlies sedimentary strata of the Whitewater group. These sedimentary rocks postdate those of the Huronian Supergroup, and are found only within the Sudbury basin (Rousell et al., 1997). Evidence of a meteorite impact in the Huronian Supergroup rocks includes shatter cones, planar deformation features, shocked quartz and pseudotachylitic breccia (Dressler, 1984). The latter deposits are termed Sudbury breccia, which is composed of irregular pods of brecciated country rock consisting of fine-grained subrounded fragments (Rousell et al., 1997).

## 2.3 Penokean Orogeny

The Penokean Orogeny is a mountain-building event that occurred following deposition of the Huronian Supergroup, during closure of a passive margin that existed on the southern margin of the Archean Superior craton (Young et al., 2001). Occurring at ca. 1875 – 1835 Ma (Holm et al., 2005), the Penokean Orogeny is identified by evidence of past metamorphic, structural and igneous activity in Minnesota, Wisconsin, Michigan and within strata of the Huronian Supergroup in Ontario, extending as far east as the Grenville Orogen (Van Schmus, 1976; Sims et al., 1989). Contemporaneous with the Penokean Orogeny was reverse faulting associated with the Murray Fault Zone, a pre-existing down-to-basin normal fault that trends roughly east-west as a southward bulging

convex arc through the Southern Province (Zolnai et al., 1984). North of the Murray Fault Zone, rocks show either modest evidence of deformation, with a northwest dip of  $15^\circ$ , and subgreenschist facies metamorphism, or show no evidence of metamorphism at all (Zolnai et al., 1984). South of the Murray Fault Zone, the rocks have become highly strained (garnet amphibolite facies), and dip to the south in a manner that is almost vertical (Zolnai et al., 1984).

## 2.4 Thesis Focus: Gowganda Formation

### 2.4.1 General Description

Investigations of the rocks that comprise the Gowganda Formation date back to the 1840s, and were initiated by the Geological Survey of Canada (Young and Nesbitt, 1985). Coleman (1907) identified striated clasts in Gowganda tillite in the Cobalt region, becoming the first to suggest that the Gowganda Formation was of glacial origin. Collins (1925) supported this interpretation with the identification of laminated argillites containing dropstones. Rocks of the Gowganda Formation are typically described using three geographic regions: the Bruce Mines/Elliot Lake area, the Espanola/Whitefish Falls area and the Cobalt area (e.g. Lindsey, 1969; Young et al., 2001). In most of the Cobalt area, the Gowganda Formation unconformably overlies Archean basement. At Whitefish Falls, the Gowganda Formation conformably overlies the Serpent Formation, whereas in the Bruce Mines/Elliot Lake area the contact between the Gowganda Formation and various underlying lower Huronian deposits is unconformable.

In the area of Whitefish Falls, the Gowganda Formation is approximately 968 m thick, (Lindsey, 1969). The lower Gowganda Formation is composed of basal diamictites, with a middle argillite unit that is capped by a mixed unit of diamictite, orthoconglomerate, sandstone and argillite (Young and Nesbitt, 1985). The upper Gowganda Formation is composed of argillite, sandstone and siltstone, and locally contains minor carbonate (Lindsey, 1969). Although some authors have named the lower Gowganda Formation in this area the Coleman Member, and the upper Gowganda in this region the La Cloche Member (Lindsey, 1969; Young and Nesbitt, 1985), these names are not widely recognized. Throughout the central Whitefish Falls/Espanola area, the Gowganda

Formation is composed of approximately 40% conglomerate and is 900 - 1680 m thick (Card, 1978). Near the Grenville Province, in the eastern section of the Whitefish Falls/Espanola area, the Gowganda Formation thins to 180 - 500 m, and the proportion of conglomerate is approximately 5%. The southern part of the Whitefish Falls/Espanola area is composed of 15-25% conglomerate, and is 850 - 160 m thick (Card, 1978). In the central and southern areas, Card (1978) divided the Gowganda Formation into seven units:

- 1) A lower, 90 - 300 m thick conglomerate member that is generally massive or poorly stratified with local bedded and cross-bedded units. The sorting ranges from poorly to well sorted, with local normal grading. Sandstone lenses and other irregular structures were identified.
- 2) A lower, 60 - 240 m thick argillite member consisting of rhythmically laminated argillite and siltstone with interbedded, irregularly laminated siltstone and sandstone up-section. The upper sandstone/siltstone units contain graded beds, parallel laminations and climbing ripples, indicating a partial Bouma sequence. Starved ripples, ball-and-pillow structures, contorted and slumped beds were also identified.
- 3) A middle member, 150 - 300 m thick, consisting of sandstone, conglomerate and siltstone. Southern exposures are dominated by sandstone and siltstone, most of which is irregularly laminated. Flame, and ball-and-pillow structures, load casts and contorted bedding commonly underlie thin conglomerate units, which are composed of polymictic paraconglomerate and orthoconglomerate. Siltstone units are composed of partial Bouma sequences, with the laminated beds locally deformed by dropstones. Central exposures of this member are dominated by polymictic conglomerate, which contains lenses of sandstone, siltstone and orthoconglomerate.
- 4) An upper, 60 - 90 m thick conglomerate member composed of polymictic paraconglomerate with lenses of sandstone and orthoconglomerate.

5) A 105 - 180 m thick slumped member composed of contorted argillite and siltstone lower in the unit, and interbedded siltstone and sandstone up-section. Up to 10% carbonate was observed in the lower section.

6) A 300 - 600 m thick sandstone member composed of interbedded siltstone and sandstone. Near the base of the member, lenticular bedded siltstone with minor interbedded sandstone is predominant, whereas the middle contains approximately equal proportions of sandstone and siltstone, and the top of the member is mainly characterized by planar to trough cross-bedded sandstone. Siltstone beds contain parallel-, cross-, and convolute laminations, in addition to ball-and-pillow structures. Sandstone beds also contain ball-and-pillow structures.

7) An upper argillite member, 60 - 137 m thick, composed of argillite and siltstone at its base, coarsening upward and forming a gradational contact with the overlying sandstones of the Lorrain Formation. Structures within this member include planar and irregular beds, ripples, cross-laminations, and ball-and-pillow structures.

In the Cobalt area, the Gowganda Formation is described as being composed of two conformable members: the lower Coleman Member and the upper Firstbrook Member (Thomson, 1957). The Coleman Member is dominated by paraconglomerate, with local truncated beds of sandstone, laminated siltstone and claystone, and minor orthoconglomerate and the Firstbrook Member is dominated by laminated argillite and siltstone. The contact between the Coleman Member and the Firstbrook Member is regionally conformable. At locations where the contact is gradational, the base of the Firstbrook member is indicated by an absence of dropstones in argillite laminates that are common in the upper Coleman member (Rainbird and Donaldson, 1988). Rainbird and Donaldson (1988) defined the Firstbrook Member in the Cobalt area as being composed of three distinct lithological units, proposed to sequentially represent prodelta, delta slope and delta foreslope environments respectively:

1) A lower argillite-dominated unit, up to 365 m thick, consisting of rhythmically laminated argillite and fine-grained siltstone, with increasing siltstone content and lamination thickness toward the upper part of the unit. Siltstone layers are graded.

Interspersed within these laminations are irregular beds of lenticular starved ripples that display internal cross-lamination.

2) A middle siltstone-dominated unit, up to 300 m thick, consisting of thickly laminated argillite and siltstone that grades up-section into rhythmically bedded siltstone and sandstone. Normal grading is common throughout the unit, with flute marks, load structures and flame structures commonly marking the base of each bed. Irregular beds composed of lenticular starved ripples contain internal cross-lamination that becomes more prevalent up-section.

3) An upper sandstone-dominated unit, up to 140 m thick, consisting of sandstone interbedded with siltstone and minor argillite. Up-section grain size and bedding thickness increases, and lenticular bedding gives way to more laterally continuous wavy bedding. Straight- to moderately sinuous-crested ripples are common, with local asymmetric ripples, interference ripples and herringbone cross-lamination. Scours resembling flute rills or meandering grooves are preserved up-section, as are ball-and-pillow and flame structures, load casts, soft-sediment folds and convolute laminations.

#### 2.4.2 Study Area

This thesis focuses on the deposits of the Gowganda Formation in the Bruce Mines/Elliot Lake area. Three of the outcrops studied are adjacent to Highway 129, which runs north of Lake Huron's North Channel at Thessalon, Ontario from an intersection with Highway 17 approximately 90 km east of Sault Ste. Marie (Figure 2-3). Outcrop A is located approximately 25 km north of Thessalon, and Outcrop C and Outcrop D are located 7 km north of Outcrop A. Outcrop B is located approximately 4 km east of Outcrop A on County Road 554, which meets Highway 129 just north of Outcrop A.



**Figure 2-3:** Locations of studied outcrops and drill core locations in the Bruce Mines/Elliot Lake area.

## 3 Sedimentology

The lithological units composing the Gowganda Formation in the study area were determined based on the rock exposures at outcrops A, B, C and D, and from two drill cores (Figure 2-3). Core 150-4 was drilled just south of Dunlop Shores Road about 10 km northwest of Elliot Lake and approximately 95 km east of outcrop A. Core 150-1 was drilled just east of Stanrock Road approximately 12 km northeast of Elliot Lake and 105 km east of Outcrop A.

### 3.1 Lower Gowganda Formation

The lower Gowganda Formation was examined only in drill core, as the rocks exposed in the study area are all interpreted to be part of the upper Gowganda Formation. Drill core 150-1 contains only the lower Gowganda Formation, whereas drill core 150-4 penetrates the entire Gowganda Formation (Appendix A). The latter drill core is described herein. In Core 150-4, the pink (Munsell Colour 5YR 8/6) sandstone of the Serpent Formation rapidly grades upsection into a 234 cm thick dark grey (Munsell Colour 5GY 3/N), mudstone-containing sandstone bed, which marks the base of the lower Gowganda Formation. The top of the lower Gowganda Formation is defined in this study as the uppermost bed of diamictite. In core 150-4, the lower Gowganda Formation is approximately 400 m thick, and is composed of diamictite, mixed units, sandstone and argillite.

Two types of diamictite units were observed within the lower Gowganda Formation. The first type is a massive, matrix-supported conglomerate containing clasts that range in size from pebble to boulder, with cobble size dominating. The clasts in this type of diamictite are generally composed of the granitic bedrock, although sedimentary clasts were also observed. The roundness of the clasts ranges from angular to well-rounded, with subrounded to rounded clasts dominating. The second type of diamictite is also a massive, matrix-supported conglomerate, but contains only pebble-sized and smaller clasts. The majority of the pebbles are angular to subangular and are composed of granitic bedrock. The matrix material in both types of diamictite is dark grey argillite

(Munsell Colour 5GY 5/N). The thickness of the diamictite units ranges from a few centimetres to >50 m.

The sandstone units vary in colour from pink (Munsell Colour 5YR 8/6) to brown (Munsell Colour 5YR 2/2) to black (Munsell Colour 5YR 1/N). Grain sizes found in different units range from very fine to very coarse, with grading observed locally. Some sandstone units contain cross-bedding whereas others contain no visible sedimentary structures. The sandstone beds range from a few centimetres to approximately 13 m thick. The mixed units contain beds composed of various combinations of diamictite, argillite, sandstone and granulestone. Mixed units range in thickness from 40 cm to approximately 5.5 m. The argillite units are composed of grey (Munsell Colour 5YR 3/N) claystone and siltstone that appear massive, laminated, cross-bedded or contorted. The contorted beds contain argillaceous swirls that are pink (Munsell Colour 5YR 7/6) or beige (Munsell Colour 5Y 6/6). Argillite beds range in thickness from a few centimetres to approximately 11 m.

## 3.2 Upper Gowganda Formation

The upper Gowganda Formation in drill core is composed of sandstone, argillite and mixed units containing interbeds of argillite, sandstone and/or granulestone. In Core 150-4, the Upper Gowganda Formation measures 107.5 m thick (Appendix A). Sandstone beds that range from 0.35 -12 m thick dominate the lower half of the core whereas the upper half is dominated by 0.2 – 6.5 m thick argillite beds. The sandstone is massive and cross-bedded. Argillite beds are either massive, planar laminated or cross-bedded, with cross-bedding becoming more prevalent upsection near the contact with the overlying Lorrain Formation. The argillite beds are locally contorted. Granulestone beds, measuring 9-23 cm thick locally display normal grading.

Four outcrops also comprise the upper Gowganda Formation in this study (Figure 2-3). Outcrop A forms an exposure that is approximately 900 m long and 50 m high. The base of the exposure was determined to be 288 m above sea level (asl). The beds in the outcrop strike 248 - 309° and dip 2 - 4° to the north. The exposure at Outcrop B is 82 m long and has a maximum height of 6.5 m from a base that was measured to be 245 m asl.

Folding is evident in the outcrop, leading to a dip that varies between 20 and 30° in the middle section, with a lower dip of 12° at the eastern and western ends of the outcrop. Strike was measured at 337 - 354°. Outcrop C extends for a length of 82 m and has a maximum height of 5.4 m from its base at 298 m asl. The beds strike 353 - 358° and dip 9 - 12°. The base of the exposure at Outcrop D lies at 296 m asl. The length of the outcrop is 27.5 m, and the maximum height of the exposure is 2.5 m. In planar laminated sections, the beds strike 322° and dip 10°.

The upper Gowganda Formation in this study is divided into eight lithofacies: 1) diamictite, 2) contorted argillite, 3) interlaminated siltstone and sandstone, 4) interbedded siltstone and claystone, 5) sandstone, 6) siltstone, 7) interbedded coarse-grained and fine-grained siltstone, and 8) wavy argillite. The interbedded siltstone and claystone lithofacies, and the interbedded coarse-grained and fine-grained siltstone lithofacies, contain rhythmites that resemble varves, and are of particular interest in this thesis.

Mineralogically, based on observational (petrographic) estimates, the dominant minerals in the lithofacies comprising this study are quartz (50-65%), feldspar (30-35%) and chlorite (10-15%), with muscovite flakes and opaques typically making up 5% of the rock. Granule-sized dropstones composed of gneiss, granite, or rip-up siltstone/claystone clasts are common in dropstone-containing units.

### 3.2.1 Diamictite Lithofacies

The diamictite lithofacies is a massive paraconglomerate composed of granule- to boulder-sized clasts set in an argillaceous matrix. This lithofacies is found only at Outcrop D (Figure 3-1), where it is in a basal, discontinuous bed, in contorted “blobs” within the overlying argillite. In thin section, the argillaceous matrix is composed of rock flour, fragmented rock that is dominantly composed of silt- and sand-sized grains. About 65% of the grains are quartz, with 20% of the grains composed of potassium feldspar displaying chlorite alteration, 10% displaying unaltered plagioclase and 2% composed of mica.

### 3.2.1.1 Diamictite Lithofacies Interpretation

Diamictite is the term used to describe glacial diamict (till) that has been lithified (Brodzikowski and van Loon, 1991). Diamict is deposited during the melting of glacial ice, and is commonly associated with supraglacial and terminoglacial subenvironments although diamict facies are also associated with subglacial and englacial subenvironments (Brodzikowski and van Loon, 1991). Eskers and moraines are two common morphological features associated with glacial retreat that are composed of diamict. Eskers are elongate, sinuous ridges of diamict that form when ice-walled river channels or tunnels within a glacier fill with glacial debris (Benn and Evans, 2010). Moraines are ridges of glacial debris that form at the front and along the sides of a glacier (Brodzikowski and van Loon, 1991).

The contact between the diamictite lithofacies and the contorted argillite lithofacies in this study is abrupt and irregular, suggesting that deposition was a result of gravitational flow (slumping), an interpretation that is supported by the contorted blobs of diamictite in the overlying contorted argillite lithofacies (Benn and Evans, 2010). The sides of eskers or moraines are known to collapse leading to slides or thaw slumps (Flint, 1971; Dowdeswell et al., 2015; Lacelle et al., 2015), which may account for the presence of the contorted diamictite in this unit. The presence of diamictite at Outcrop D suggests that the outcrop is the lowest stratigraphically of the studied outcrops.

### 3.2.2 Contorted Argillite Lithofacies

The contorted argillite lithofacies was identified at two exposures. At Outcrop D (Figure 3-1-D), the diamictite lithofacies is locally overlain by grey argillite containing contorted fine- to very fine-grained pink sandstone beds and irregularly shaped blobs of pink sandstone. Lower and upper contacts with the underlying and overlying lithofacies at Outcrop D are abrupt and irregular. In thin section, cross-lamination was observed in the sandstone. Most of the grains are angular to subangular, with a 5% population of subrounded grains. Quartz makes up about 68% of the grains, whereas 15% of the grains are feldspar, 15% chlorite, and 2% mica. The argillite ranges from a siltstone to clayey

## Outcrop D

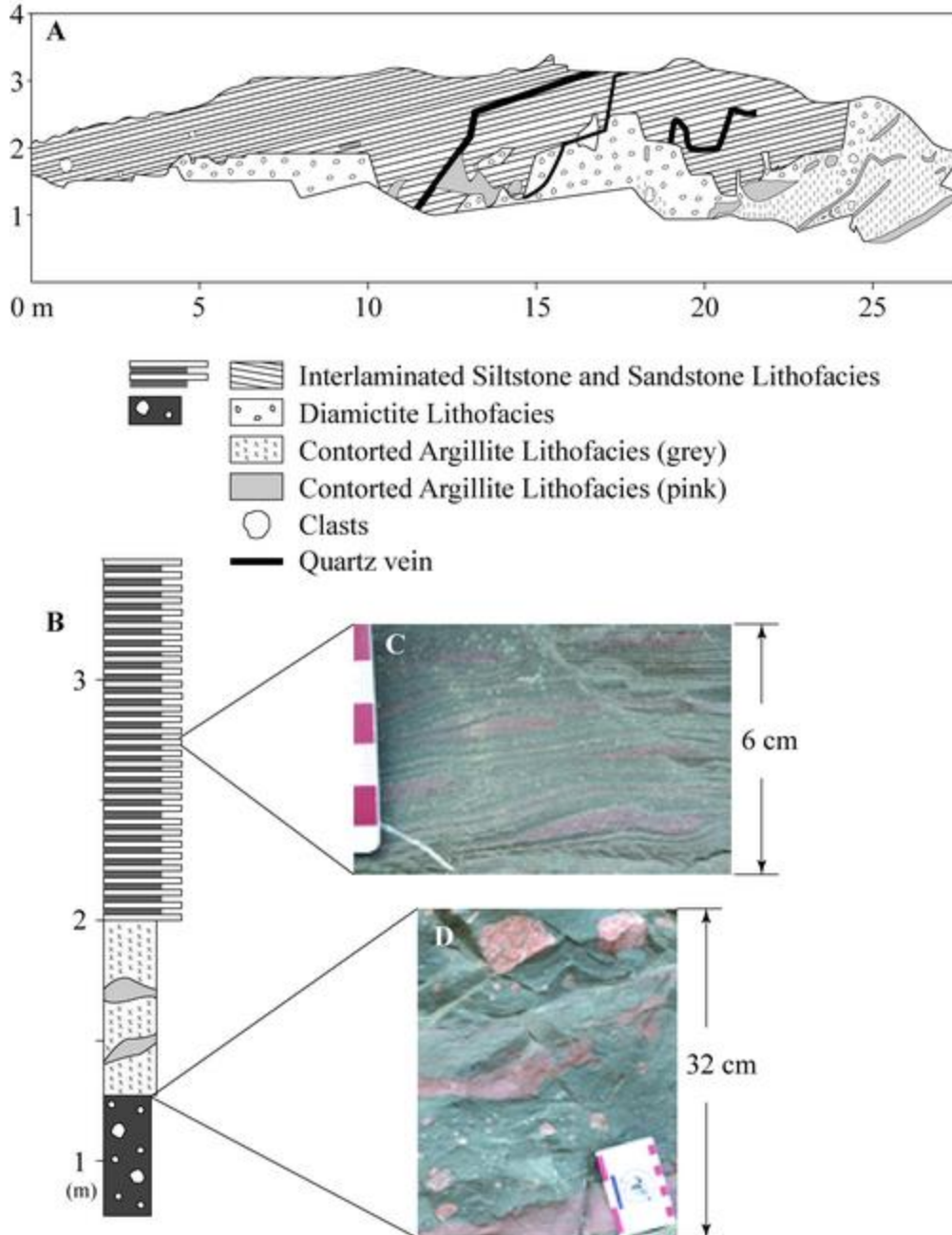


**Figure 3-1:** A (front view), B: Outcrop D, characterized by the interlaminated siltstone and sandstone lithofacies, the diamictite lithofacies and the contorted argillite lithofacies. C: Sandstone layers within the interlaminated siltstone and sandstone lithofacies locally display asymmetrical ripples. D: The contorted argillite lithofacies contains irregularly-shaped blobs of pink sandstone.

siltstone according to the Udden-Wentworth (Udden, 1914; Wentworth, 1922) grain size classification.

At Outcrop A, contorted argillaceous beds measuring up to 109 cm thick are interbedded with sequences of rhythmic couplets (Figure 3-2-A). Locally, the argillite beds contain groups of thinly laminated rhythmites that are overturned. Rhythmites within the contorted units measure approximately the same thickness as the rhythmites that form the planar beds overlying and underlying the contortions. Dropstones ranging from pebble to cobble size, and composed of gneiss or granite, were observed in both units.

### 3.2.2.1 Contorted Argillite Lithofacies Interpretation

At Outcrop D, the irregular upper contact and the contorted pink sandstone beds contained within the argillite suggest that deposition was a result of slumping (e.g. Brodzikowski and van Loon, 1991). Slumping can be defined as the downslope transport of sediment on a subaqueous slope, and is initiated by the failure of shear planes within sediment, with the risk of shear plane failure increasing with increasing sediment load (Nemec, 1990). This can occur in depositional environments such as river deltas and submarine fans that have steep slopes and that experience high depositional rates (Benn and Evans, 2010). At Outcrop A, contorted beds display evidence of rhythmic laminations locally, but the laminations are not always visible, which again suggests that the deposits were deformed, a characteristic of slumping (Benn and Evans, 2010). Thus, the contorted argillite lithofacies probably resulted from gravitational failure resulting from sediment overloading (e.g. Benn and Evans, 2010). Given the close spatial relationship with glacial diamictite, the contorted argillite lithofacies is interpreted to have formed from the melting of marginal glacial ice and fluvial flow, which delivers significant amounts of glacial material to the margins of glacial lakes. Gravitational instability in this debris would have led to slumping and sliding (Smith and Ashley, 1985; Siegenthaler and Sturm, 1991; Benn and Evans, 2010). Contorted bedding underlain and overlain by parallel strata in the lower unit of the Conne River, Newfoundland deposits was interpreted to result from low angle slumping (Morgenstern, 1967; Leckie and McCann, 1982). Gilbert (1975) also found evidence for infrequent sediment slumping associated with glacially-influenced varves in Lillooet Lake, British Columbia.

## Outcrop A (0-6 m)

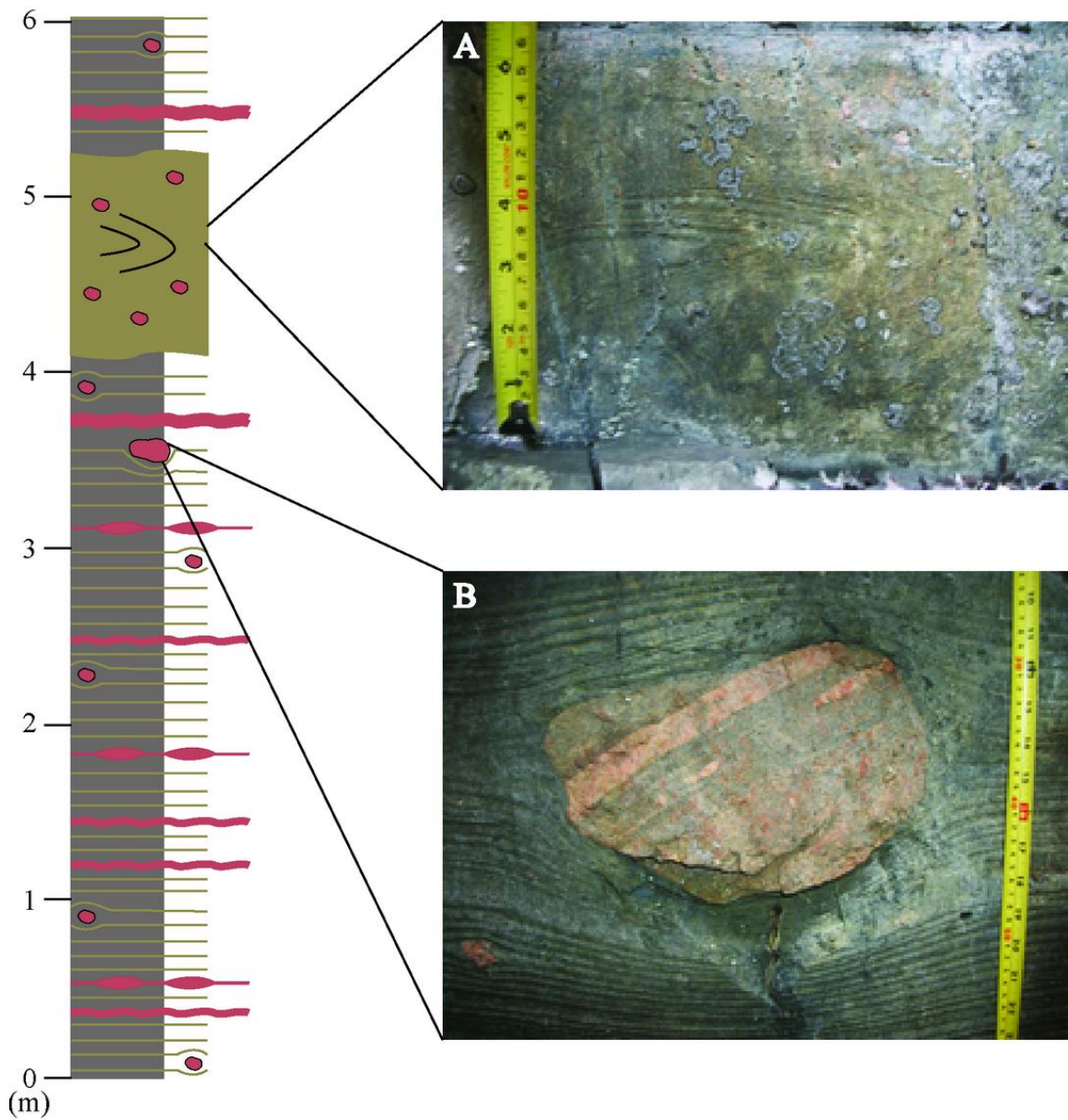


**Figure 3-2:** The contorted argillite lithofacies at Outcrop A. A: folded rhythmite layers. B: Dropstones ranging from granule to boulder size are commonly scattered throughout the interbedded siltstone and claystone. Thin lenticular or wavy sandstone beds are found locally within the lithofacies (pink beds in stratigraphic section).

### 3.2.3 Interlaminated Siltstone and Sandstone Lithofacies

The diamictite and contorted argillite lithofacies are abruptly, but conformably overlain by the interlaminated siltstone and sandstone lithofacies. The latter lithofacies at Outcrop D is composed of thin, rhythmic laminations of pink, fine- to very fine-grained sandstone and dark grey siltstone. Where planar, the couplets are a few mm thick; however the sandstone layers are locally composed of asymmetrical ripples or thin lenses that are 4–5 cm long and can exceed 1 cm thick before they pinch out (Figure 3-1-C). Rhythmic laminations that overlie the contorted argillite and diamictite lithofacies are also contorted, whereas adjacent rhythmic laminations that overlie rubble (unknown base) are parallel laminated and undistorted. Local clasts interpreted to be dropstones were observed in the rhythmic laminations.

In thin section, the rhythmites at Outcrop D commonly display normal graded sandstone layers, with erosional tops separating the underlying siltstone layer from the overlying sandstone layer (Figure 3-3). Upper surfaces of siltstone layers are planar to wavy. Sandstone grains are predominantly angular, although they range from angular to subrounded. The grains are mainly composed of quartz (68%) with the remainder composed of plagioclase (17%), chlorite (11%), mica (3%) and potassium feldspar (1%).

#### 3.2.3.1 Interlaminated Siltstone and Sandstone Lithofacies Interpretation

Asymmetrical ripples that form lenticular bedding can be found in tidal settings, and in marine and lacustrine delta front or submarine fan environments (Coleman, 1966; Reineck and Wunderlich, 1968; Mutti, 1977). The asymmetrical ripples found in the interlaminated siltstone and sandstone lithofacies appear locally adjacent to, and within, the area of slumping at Outcrop D, which implies that deposition was not a result of tidal action because lateral continuity would be expected. In addition, a finer grain size in the “slack water” layer is expected if the setting is tidal, which was not observed in this lithofacies. Therefore, it is inferred that the interlaminated siltstone and sandstone lithofacies does not represent a tidal setting deposit.

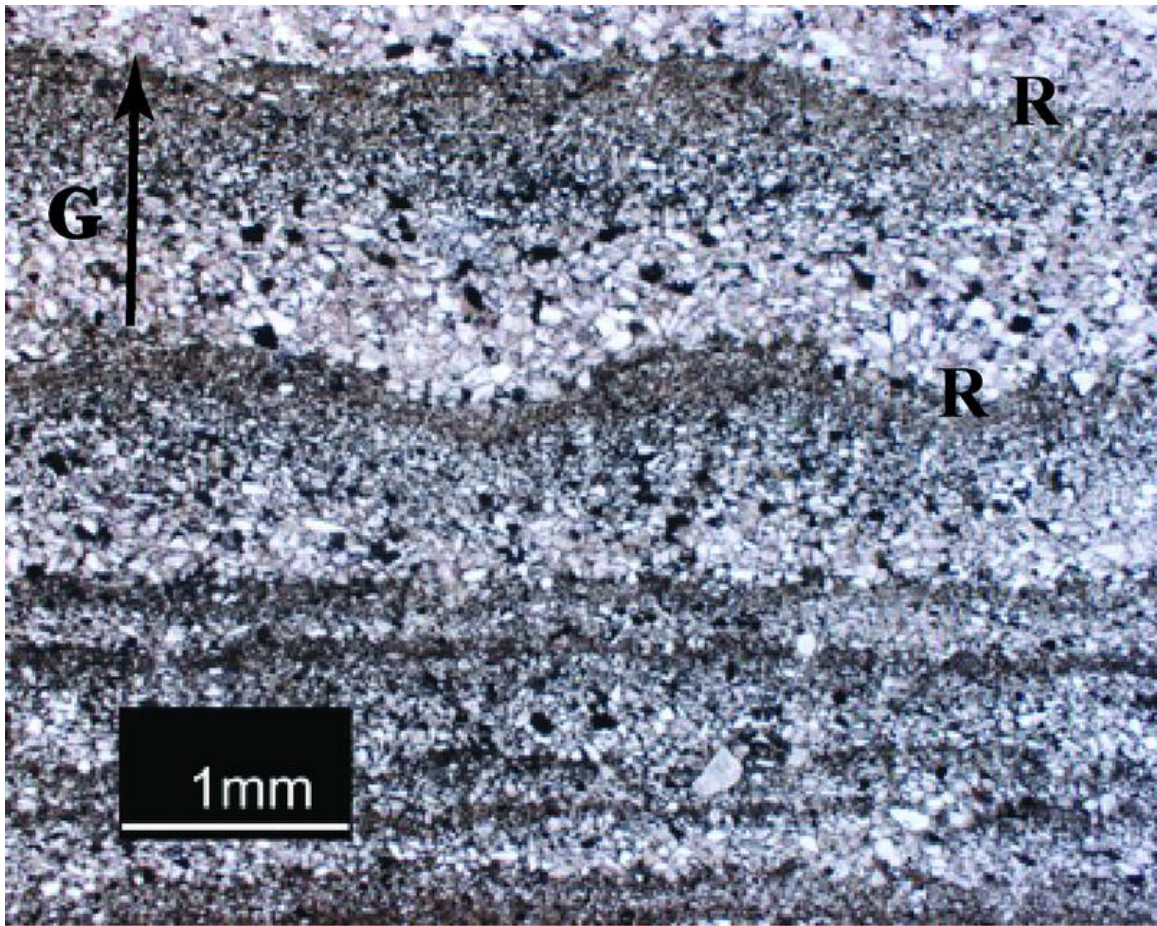


**Figure 3-3:** Photomicrograph of rhythmites of the interlaminated siltstone and sandstone lithofacies at Outcrop D. Note the normal grading (G) and rippled tops (R).

The interlaminated siltstone and sandstone lithofacies was probably associated with an active river channel-mouth. Mutti (1977) reported laterally discontinuous lensoid sandstone beds in submarine fan channel mouth bar deposits, which were described as “paradoxically” resembling lenticular bedding commonly associated with a tidal setting. These lenticular-like channel mouth deposits were described as forming when external turbidity currents rapidly decelerate upon intersecting the mouth of an active channel (Mutti, 1977). The lithofacies may represent a distal (minor mouth) bar deposit (Elliott, 1974; Prothero and Schwab, 1996). Mouth bars form when fluvial velocity is rapidly reduced upon entering a large body of water (Nichols, 2009). Distal mouth bar couplets are composed of sandy, graded layers draped with finer grained sediment that displays rippled upper bedding surfaces, with the ripples becoming asymmetrical upsection as water levels fall (Elliott, 1974). These features are present within the lithofacies local to the area of slumping.

### 3.2.4 Interbedded Siltstone and Claystone Lithofacies

The interbedded siltstone and claystone lithofacies, which contains the rhythmites that resemble varves, was identified in the basal parts of both Outcrop C (Figure 3-4) and Outcrop A (Figure 3-5). In Outcrop C, the lithofacies is 8.5 m thick and is abruptly overlain by a pink sandstone bed. The rhythmites are composed of <3 mm thick planar couplets with variations in thickness resulting mainly from differences in the thickness of the claystone layer. On fresh surfaces the rock is typically medium to dark grey, with the siltstone layers displaying a darker grey colour than the thicker claystone layers.

Dropstones ranging from pebble- to boulder-size are common throughout the lithofacies. Ripples and lenses were not observed in the rhythmites of Outcrop C; however these features are quite common in the morphologically similar basal unit of Outcrop A.

At Outcrop A, the lithofacies is approximately 15 m thick. From the base of the exposure, the siltstone layer of each couplet consistently measures about 1-2 mm thick, and increases to 3–4 mm thick toward the top of the unit. The claystone layers range from 1–2 mm thick to 29–30 mm thick, with thickness varying throughout, although generally increasing upsection. Thus, variations in the thickness of each couplet result mainly from

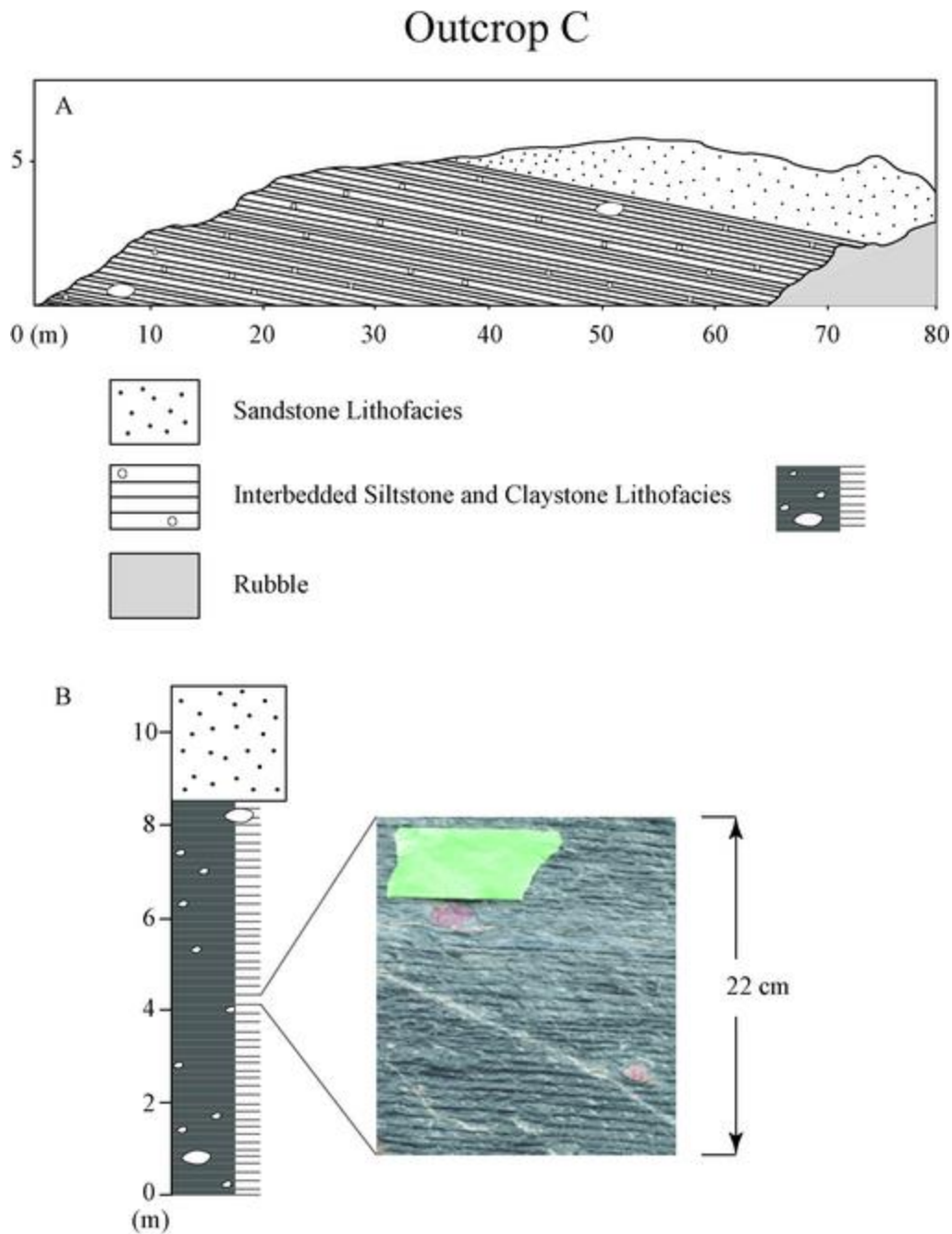


**Figure 3-4:** The interbedded siltstone and claystone lithofacies at Outcrop C is characterized by thinly laminated siltstone layers (dark grey in photo) and claystone layers (light grey in photo) that contain dropstones ranging from granule to boulder in size. The rhythmites are overlain by a 2-3 m thick bed of the pink sandstone lithofacies. Green tape for scale measures 2.4 cm thick vertically.

## Outcrop A (5-11 m)

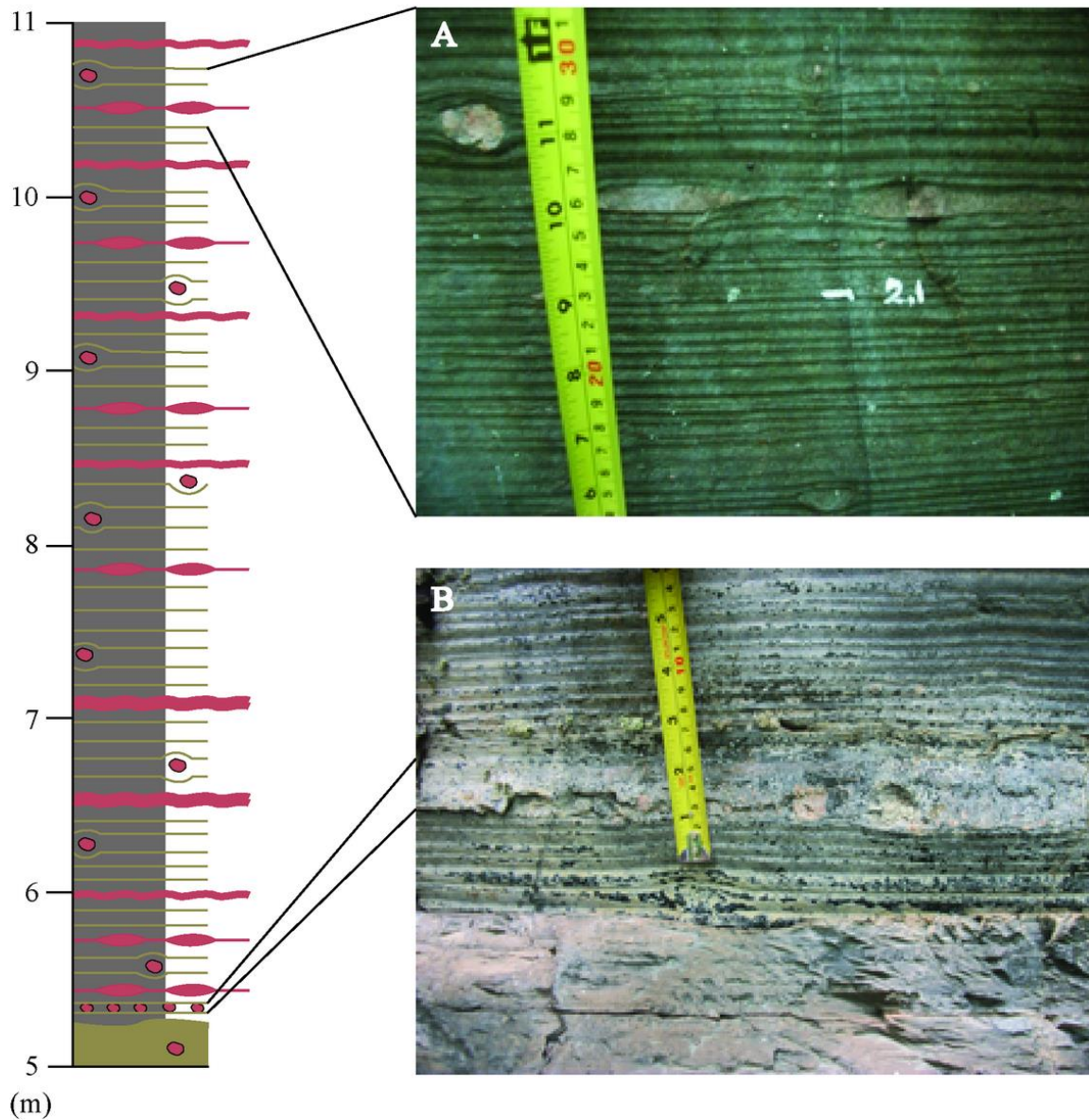


**Figure 3-5:** A: Pinched sandstone ripples that are locally connected to form thin lenticular or wavy sandstone beds are interbedded with the rhythmites of the interbedded siltstone and claystone lithofacies at Outcrop A. B: A thin bed of conglomerate within the interbedded siltstone and claystone lithofacies.

variations in the thickness of the claystone layer. The dropstones, which become less abundant upsection, range from pebble- to boulder-size (Figure 3-2-B), with the majority having granitic/gneissic compositions. Rip-up sandstone granules were also observed, particularly in thin section. On fresh surfaces the rock is dark green to dark grey. Single, pink, fine- to very fine-grained wavy sandstone beds of starved ripples are irregularly interbedded within the lithofacies at Outcrop A, as are local beds of orthoconglomerate (Figure 3-5-B). Increasing grain size and irregular, non-rhythmic lamination of bedding was observed upsection (Figure 3-6) where grey-green to grey-black siltstone layers of variable thickness are interlaminated and interbedded with moderately rippled to lenticular pink sandstone layers. The pattern of irregular lamination ceases about 1 m from the top of the interbedded siltstone and claystone lithofacies, which is overlain by a 4 cm thick, micro-laminated bed of claystone that displays a rippled upper surface (Figure 3-7-A). A 10 cm thick pink sandstone bed with a rippled upper surface, overlies the claystone. The sandstone bed is overlain by a 3 cm thick claystone layer, above which irregularly bedded siltstones interbedded with rippled to wavy sandstone beds and laminations continue to the top of the lithofacies.

In thin section, the claystone layers are characterized by multiple planar laminae, which are locally separated by razor-thin siltstone layers (Figure 3-8-A, -C, -D). Although the micro-laminae can be difficult to discern, the number present in any individual claystone layer appears to range from 14 to more than 60, with no readily apparent pattern in the number of micro-laminae found. The colour of the laminae range from light to dark grey, and individual grains of silt, and rarely, sand, were observed. Reverse grading was rarely identified in the claystone micro-laminae.

Siltstone layers are composed of multiple laminae; however grain size varies considerably both between and within individual laminae. The micro-laminae comprising a siltstone layer are rippled to wavy, and are mainly interlayered with claystone micro-laminae. Contacts between the micro-laminae are not clearly defined, and are generally irregularly rippled to mildly contorted, although planar laminae occur locally. Thick, normally graded laminae were also identified. Load and flame structures become more prevalent upsection, in conjunction with increasing grain size (Figure 3-9-B, -C, -D) and

## Outcrop A (10-16 m)

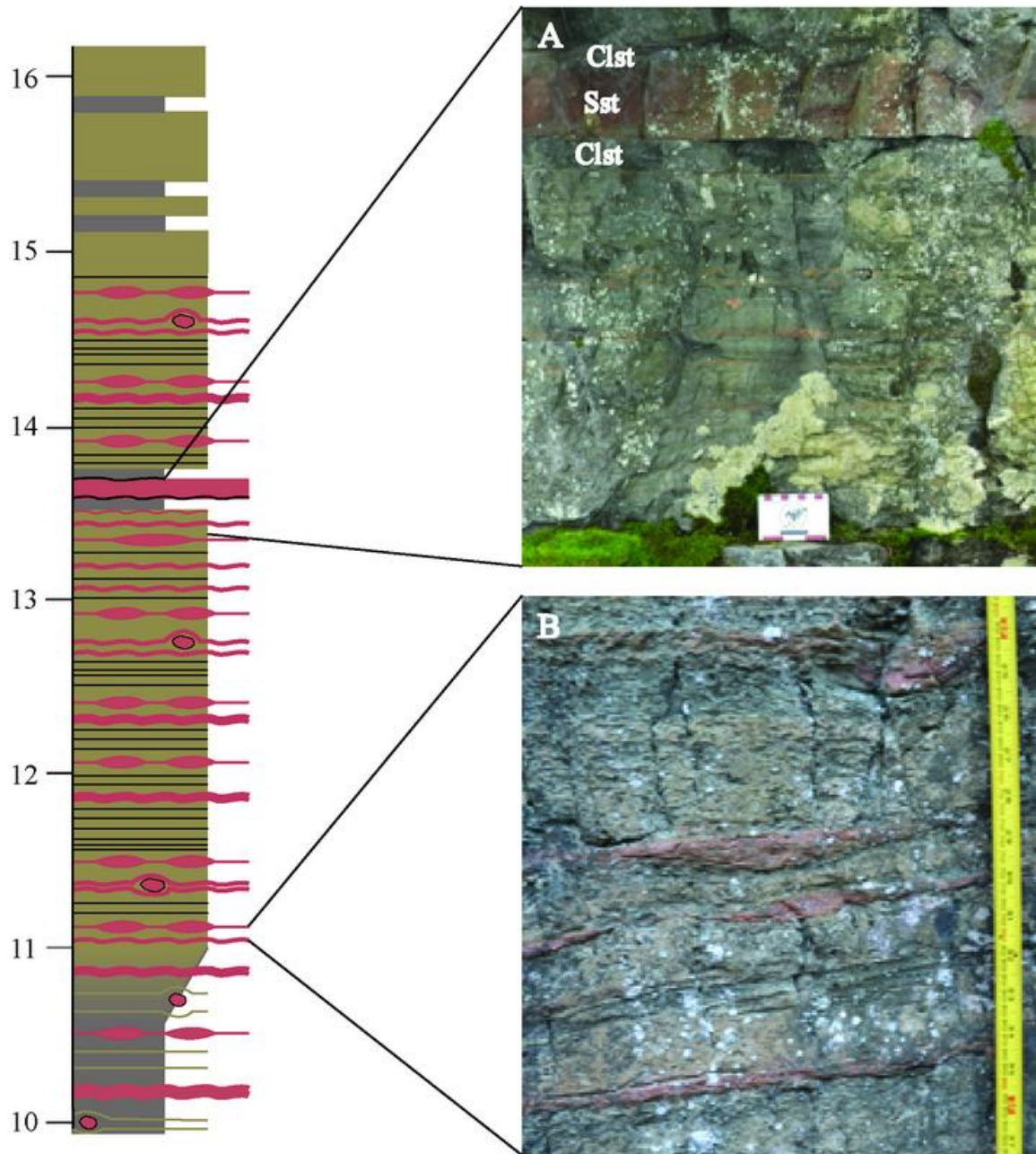


**Figure 3-6:** A: The sandstone lithofacies (Sst) at Outcrop A is interbedded with thin beds of claystone (Clst). Scale card: 7 cm. B: The upper section of the interbedded siltstone and claystone lithofacies at Outcrop A is characterized by an increase in lenticular and wavy sandstone beds, and in grain size.

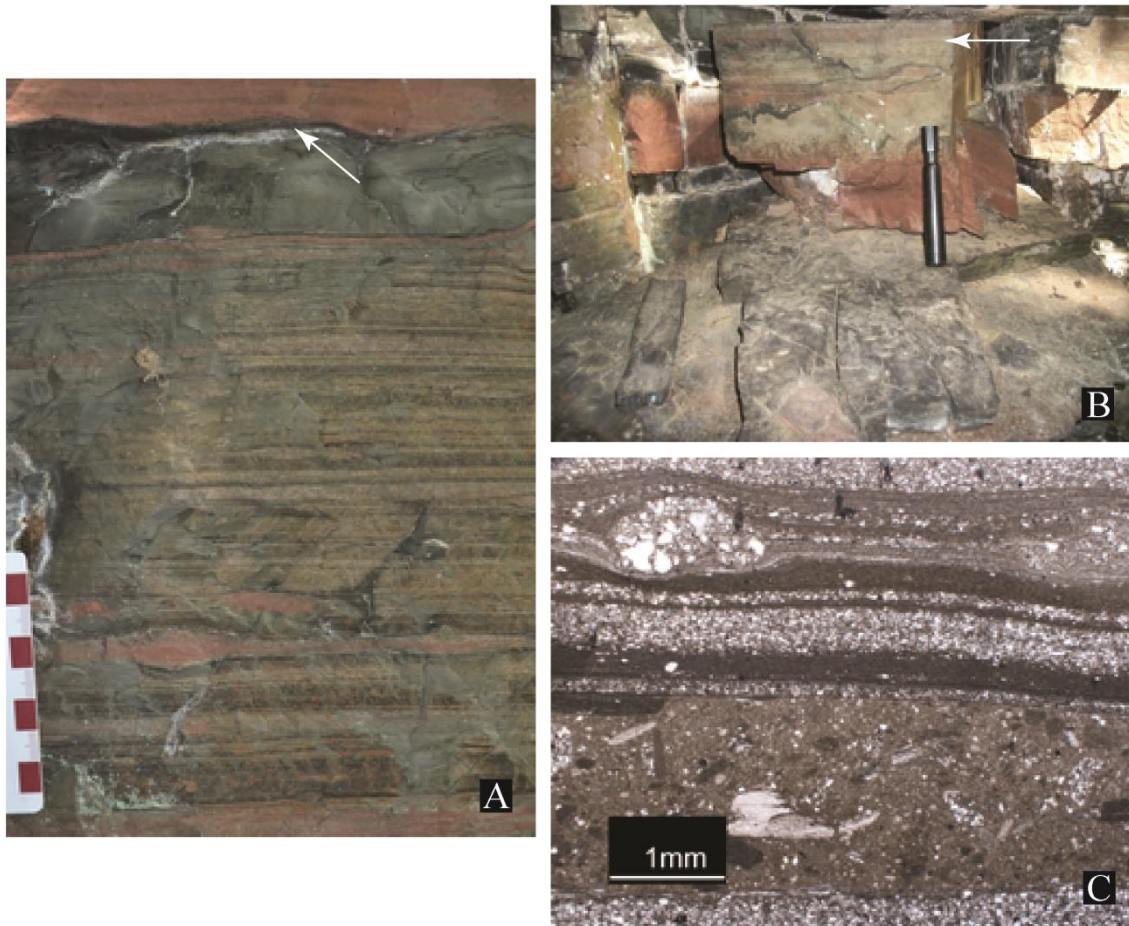


**Figure 3-7:** A: Irregular bedding and an increase in the amount of siltstone upsection in the interbedded siltstone and claystone lithofacies at Outcrop A. A 5-7 cm thick bed of claystone shows a rippled erosional surface (arrow in A) at the contact with the overlying sandstone lithofacies. B: Above the sandstone lithofacies, the interbedded siltstone and claystone lithofacies resumes. The layer marked with an arrow in B indicates the brecciated lamination shown in thin section (C). Scale in A is in cm, marker in B is 13 cm long.

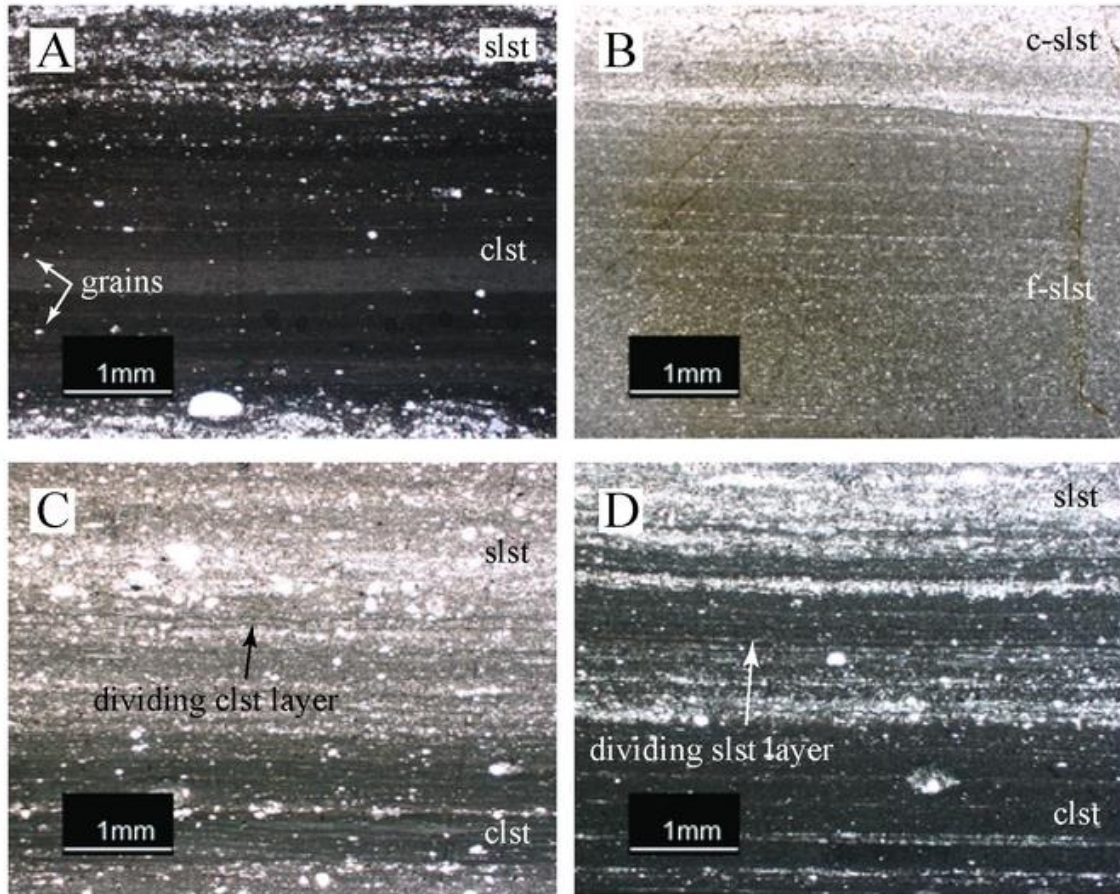


**Figure 3-8:** A: Micro-laminae in claystone (clst) layers in the lower section of the interbedded siltstone and claystone lithofacies at Outcrop A are defined by thin layers of siltstone (slst) that separate individual lamina. Siltstone micro-laminae are separated by thin claystone layers. B: Micro-laminae in the fine-grained siltstone (f-slst) layers of the interbedded coarse-grained and fine-grained siltstone lithofacies at Outcrop B are defined by thin layers of coarse siltstone (c-slst) that separate individual fine-grained siltstone lamina. C, D: Micro-laminae in claystone layers in the lower section of the interbedded siltstone and claystone lithofacies at Outcrop C (C) and Outcrop A (D) are defined by thin layers of siltstone that separate individual laminae. Thicker siltstone laminae dividing claystone layers were observed locally. Siltstone micro-laminae are separated by thin claystone or fine-grained siltstone layers.

increasing contortion. Sorting is generally poor in the irregularly rippled laminae, improving to moderate in the planar laminae. Individual grains in the siltstone layers are subangular to subrounded. Quartz is the predominant mineral, estimated to be 50-65% of the lithofacies. Plagioclase accounts for about 30-35% of the mineralogy, with chlorite and mica accounting for up to 15%, but generally in the range of 5-10%.

#### 3.2.4.1 Interbedded Siltstone and Claystone Lithofacies Interpretation

The interbedded siltstone and claystone lithofacies represents a recurring flux in transport energy: periods of lower energy result in the deposition of claystone layers, whereas periods of higher energy result in the deposition of siltstone layers (Reineck and Singh, 1980). Clasts disrupting the layers are interpreted as ice-rafted debris (IRD) resulting from the calving and transport of proximal glacial ice (Brodzikowski and van Loon, 1991). Periods of much higher fluvial transport energy initiated perhaps by distal jökulhlaups (glacial lake outburst floods) or periods of intense precipitation could have led to channel washout that resulted in the deposition of cross-bedded, lenticular sandstone beds within the rhythmite sequences (Benn and Evans, 2010; Huang et al., 2014).

Rhythmic sequences in the upper section of Outcrop A typically consist of three layers: a coarse-grained argillite to fine-grained siltstone layer, a coarse-grained siltstone layer typically consisting of micro-interlaminated siltstone and argillite, and a moderately rippled to lenticular sandstone layer that locally contains cross-lamination. Triumvirate rhythmic sequences composed of a winter clay rainout layer, a spring nival (snow) melt layer, and a post nival melt layer attributed to continental sediment transported by meteoric water have been interpreted by Hambley and Lamoureux (2006) as non-glacial, temperate lake varves in northern Canada. If a similar process formed the triumvirate layers found in this study, the coarse-grained argillite to fine-grained siltstone layer may represent winter deposition fed by reduced winter glacial melt flows, the coarse-grained-siltstone layer may represent deposits resulting from increased spring/summer flow, and the moderately rippled to lenticular sandstone layers may represent sediment derived

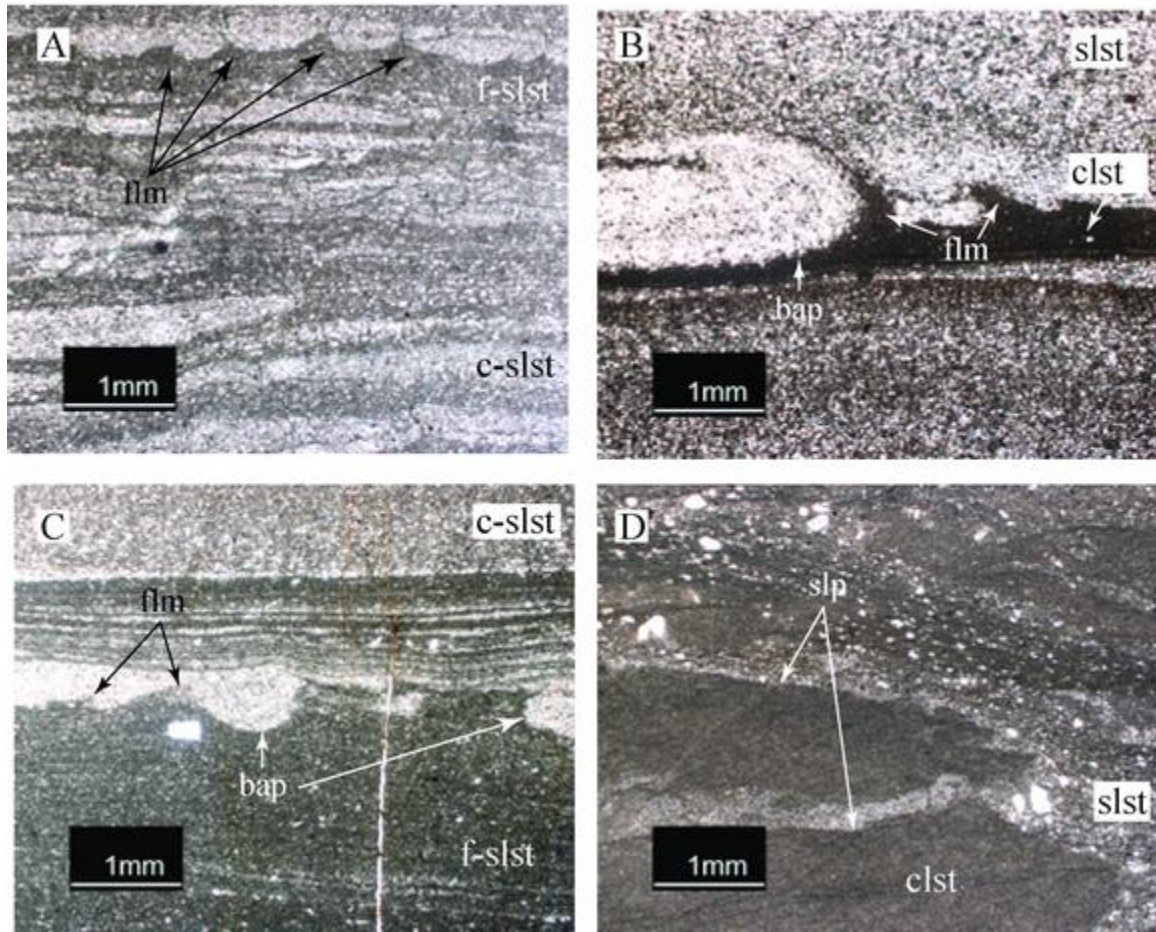


**Figure 3-9:** A: Flame (flm) structures in fine-grained siltstone (f-slst) laminae, irregular bedding and an increase in the prevalence of coarse-grained siltstone (c-slst) laminae upsection in the interbedded coarse-grained siltstone and fine-grained siltstone lithofacies. B, C: Flame, ball-and-pillow (bap) structures in thin sections from the upper section of the interbedded siltstone and claystone lithofacies at Outcrop A. Thicker and coarser grained siltstone laminae are also displayed upsection. Claystone (clst) laminae grade to fine-grained siltstone laminae upsection (C). D: Photomicrograph of the upper section of the interbedded siltstone and claystone lithofacies at Outcrop C displays slump (slp) structures.

from the continent due to rainfall (i.e. run-off).

Single grains of sand or coarse silt found locally within claystone micro-laminae were likely entrained in the flow (Reineck and Singh, 1980), although the isolated coarse grains may also have settled out from suspension as a result of aeolian deposition, or via ice-rafted debris (Powell and Domack, 2002). The micro-laminae may represent deposition resulting from high-density underflow currents generated by glaciofluvial activity (Smith and Ashley, 1985). Micro-lamina deposits, whether composed of siltstone or claystone, have also been observed in fine-grained turbidite depositional systems, with each lamina representing a single turbidite (Reineck and Singh, 1980). Storm reworking has also been suggested for micro-laminae found in Cretaceous mudstones (Plint, 2013). Another possible interpretation is that the multiple micro-laminae in the claystone layers may be the results of katabatic winds (Ashley, 2002). Katabatic winds, a common feature in the vicinity of glaciers, result when a cold air mass associated with a glacier drains to a lower, warmer, ice-free area. Katabatic winds tend to blow away from glacial ice and across the surface of a glacial lake, generating slow epilimnial currents that transport sediment away from the ice sheet (Parish and Bromwich, 1991; Ashley, 2002). The co-existence of siltstone and claystone micro-laminae in the interbedded siltstone and claystone lithofacies favours variations in flow energy, which supports the turbidite interpretation.

The thin bed of conglomerate found at Outcrop A (Figure 3-5-B) probably represents a bed of iceberg-dumped debris (Benn and Evans, 2010). When an iceberg overturns, surface material is dumped into the water, potentially forming a bed of glacial debris (Benn and Evans 2010).

The ca. 4 cm thick claystone bed that overlies a thick sequence of laminated siltstones and sandstones (Figure 3-7-A) indicates a reduction in sediment transport energy (Benn and Evans, 2010). This may indicate a period of clay rainout from suspension in a marine/lacustrine environment, or a period of fluvial avulsion during which the sandy-silty sediments were redirected to another part of the basin, and the finer clays resulted from overbank deposition (Reineck and Singh, 1980). A brecciated lamination (Figure 3-

7-C), possibly due to storm reworking, which was observed near the top of the lithofacies, which combined with an increase in the thickness of the siltstone layers may indicate a shallowing upward trend due to delta progradation (Reineck and Singh, 1980).

### 3.2.5 Sandstone Lithofacies

The sandstone lithofacies is represented at Outcrop C by an approximately 3 m thick bed of pink, massive sandstone (Figure 3-6). At Outcrop A, the sandstone bed is also pink (Figure 3-6-A, 3-7-B), is much thinner (ca. 10 cm), and has a rippled contact with both the underlying and overlying claystone beds. In thin section, the sandstone lithofacies displays cross-lamination and both normal and reverse grading. Sandstone grains are mainly angular to sub-angular, although the range extends to sub-rounded. The grains are mostly composed of quartz (64%) with the remaining grains composed of plagioclase (20%), chlorite (12%) potassium feldspar (2%) and mica (2%).

#### 3.2.5.1 Sandstone Lithofacies Interpretation

The sandstone lithofacies overlies the interbedded siltstone and claystone lithofacies at both Outcrop A and Outcrop C, and probably represents delta front sheet sand deposits (Reineck and Singh, 1980). Delta front sand sheet deposits that overlie laminated siltstone and claystone deposits are associated with delta progradation (Reineck and Singh, 1980). For example, delta front sheet sand deposits have been observed overlying a silt and mud lithofacies in the La Fourche-Mississippi delta (Fisk, 1955). At Outcrop A, the sandstone lithofacies composes a thin bed that is both underlain and overlain by the interbedded siltstone and claystone lithofacies, which may indicate that the lithofacies represents an isolated influx of bedload, perhaps resulting from a glacial outburst flood (jökulhlaup) or a precipitation-induced flash flood (Reineck and Singh, 1980; Benn and Evans, 2010). The pink colour in the sandstone beds appears to be the result of iron oxide, which occupies microscopic pits in some of the individual grains. This suggests that there was sufficient oxygen in Earth's atmosphere at the time of deposition to affect the oxidation of iron.

### 3.2.6 Siltstone Lithofacies

The siltstone lithofacies overlies the laminated siltstone and claystone lithofacies at Outcrop A and is 2.7 m thick (Figure 3-10). It is composed of siltstone beds ranging from 15 -25 cm thick that are interbedded with rhythmic intervals of siltstone and argillite. The rhythmic sequences of siltstone and argillite have a total thickness of 8-10 cm, and are composed of individual beds of siltstone averaging 1.5 cm thick and argillite laminations up to 1 cm thick.

#### 3.2.6.1 Siltstone Lithofacies Interpretation

The siltstone lithofacies represents a transition zone, marking a progression away from the rhythmic sedimentation of the underlying interbedded siltstone and claystone lithofacies to the overlying wavy argillite lithofacies. The intercalated siltstone and claystone beds indicate variations in the sedimentation rate that may result from short term, perhaps diurnal, stops and starts in glacial melting activity that could be associated with a cycle of freezing conditions at night and melting conditions during the day (Franco et al., 2011). Once the summer melt cycle was established, continuous, silty sedimentation could have led to the formation of the thicker siltstone beds (Benn and Evans, 2010). The siltstone lithofacies may also represent thin-bedded turbidite deposits (e.g. Basu and Bouma, 2000; Paull et al., 2014), which would indicate further delta progradation relative to the underlying deposits (e.g. Reineck and Singh, 1980). The absence of dropstones indicates that the glacial ice sheet had retreated from the area of deposition.

### 3.2.7 Interbedded Coarse-grained and Fine-grained Siltstone Lithofacies

The interbedded coarse-grained and fine-grained siltstone lithofacies comprises the entirety of Outcrop B (Figure 3-11). The lithofacies consists of thin, planar bedded coarse- and fine-grained siltstone couplets. On fresh surfaces, the rock is typically medium to dark grey, with the fine-grained siltstone layers displaying a darker grey colour than the thinner, coarse-grained siltstone layers. The rhythmites range from 3-31 mm thick.

## Outcrop A (15-18+ m)

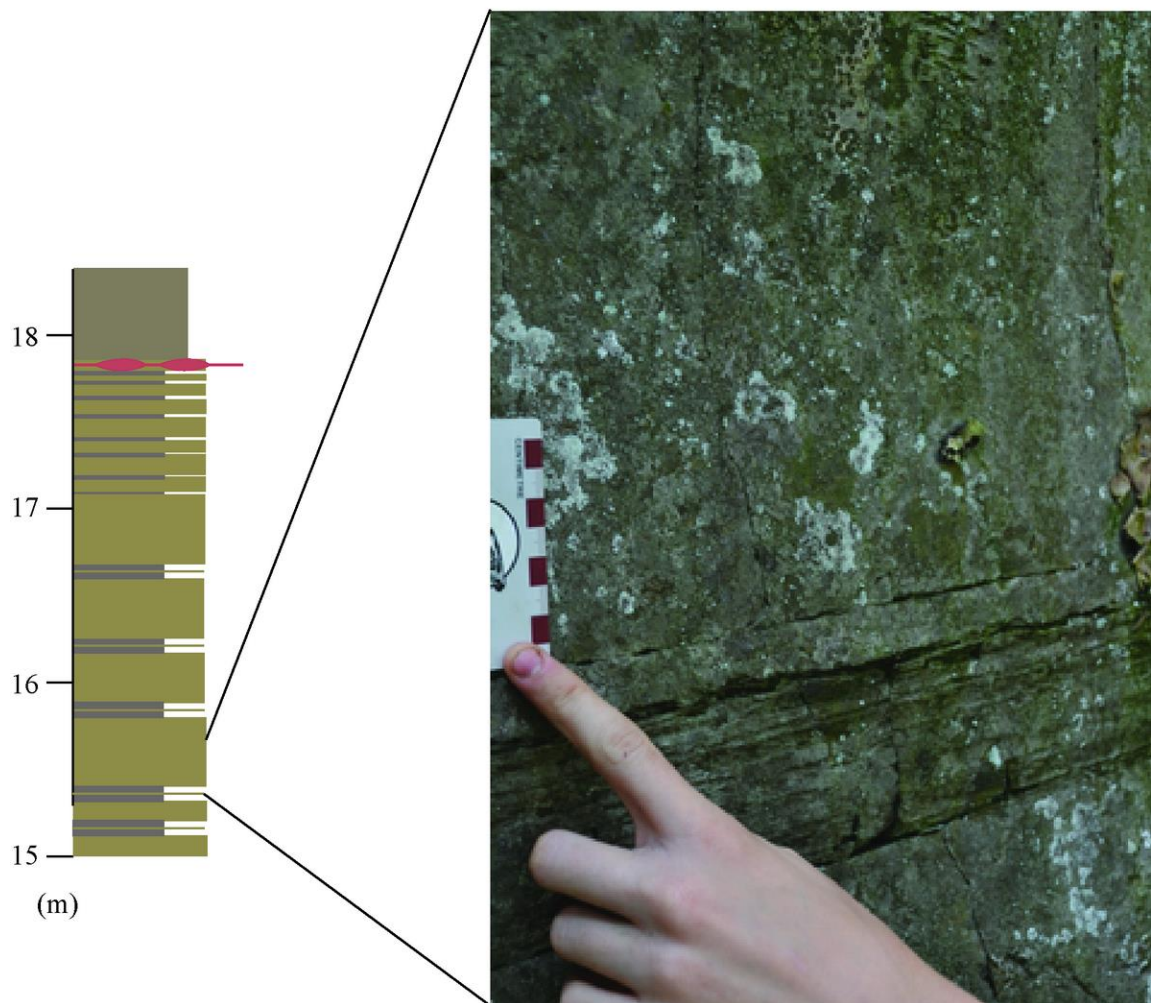


**Figure 3-10:** The siltstone lithofacies at Outcrop A is characterized by siltstone beds measuring 15 – 25 cm thick interbedded with thin beds of rhythmically layered siltstone and claystone that combine to form beds up to 10 cm thick.

## Outcrop B

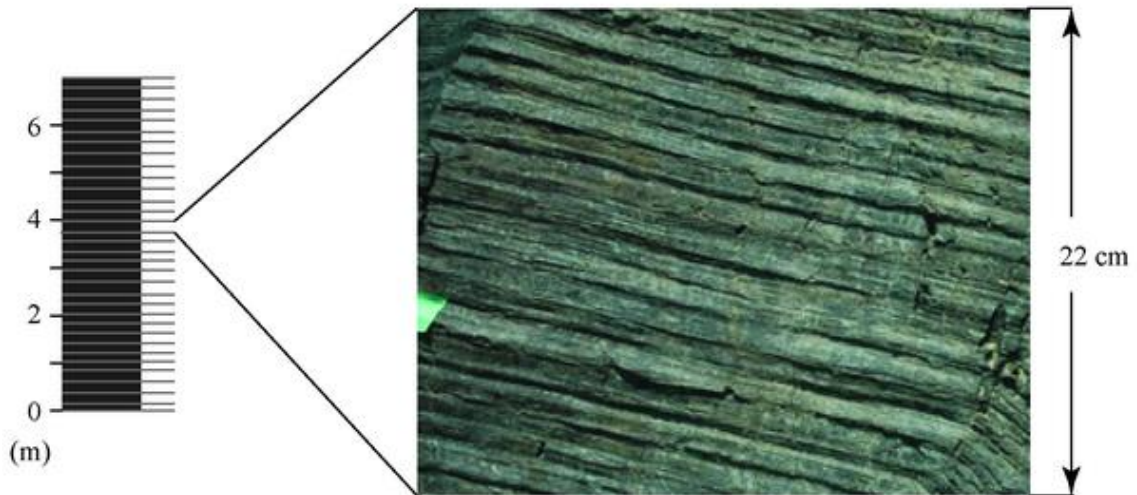
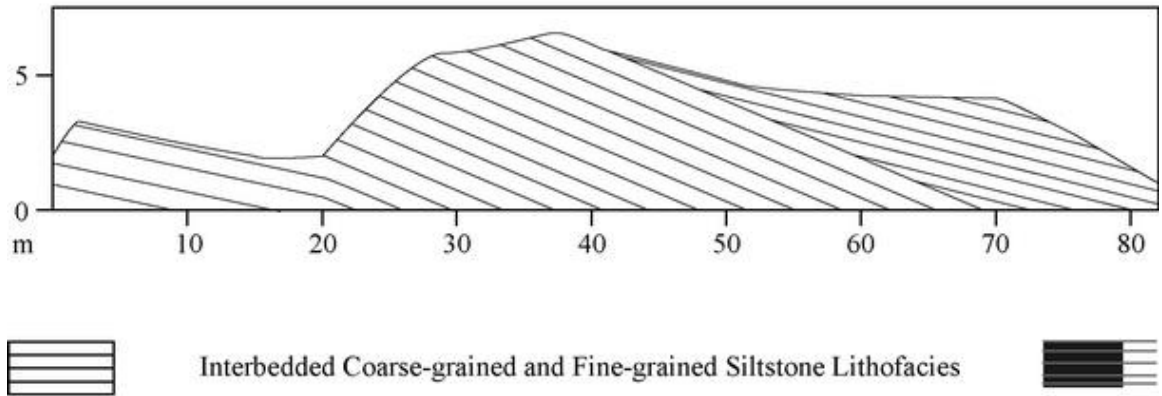


**Figure 3-11:** The rhythmic laminations that compose the interbedded coarse-grained siltstone and fine-grained siltstone lithofacies are evident at Outcrop B. Dropstones were not found in this lithofacies.

The fine-grained siltstone layers comprise anywhere from 40% to 90% of an individual couplet. Dropstones were not found within this lithofacies.

In thin section, the fine-grained siltstone layers are characterized by multiple planar, micro-laminae, which may be separated by a razor-thin silt parting (Figure 3-8-B), similar to the interbedded siltstone and claystone lithofacies. The number of micro-laminae is variable between fine-grained siltstone layers. Local grains of sand and coarsesilt were identified in this lithofacies. Grains are predominantly angular to sub-angular, ranging to sub-rounded. Sorting is generally good in the fine-grained siltstone layers and poor in the coarse-grained siltstone layers. Normal and reverse grading is common in the fine-grained siltstone layers, and less commonly displayed in the coarse-grained siltstone layers, in which interlamination with fine-grained siltstone is absent. Upsection, micro load and flame structures (Figure 3-9-A) were identified, as were lensoidal features in the coarse-grained siltstone layer. Quartz dominates the mineralogy, comprising 65% of the lithofacies, with plagioclase (10 - 15%), chlorite (5 - 10%) and mica (<5%) composing the remainder.

#### 3.2.7.1 Interbedded Coarse-grained and Fine-grained Siltstone Lithofacies Interpretation

The interbedded coarse-grained and fine-grained siltstone lithofacies is interpreted to represent fluvial deposits that were transported to a medial delta front, more distal from the delta than the sandstone facies, but more proximal than the interbedded siltstone and claystone lithofacies (Reineck and Singh, 1980). This facies is morphologically similar to the medial section of the interbedded siltstone and claystone lithofacies found at Outcrop A, but it lacks dropstones. Increasingly rapid deposition is indicated upsection by load and flame structures within the fine-grained siltstone layers, and by the formation of lensoidal features in the coarse-grained siltstone layers (Reineck and Singh, 1980).

#### 3.2.8 Wavy Argillite Lithofacies

The wavy argillite lithofacies overlies the siltstone lithofacies at Outcrop A. This lithofacies is approximately 35 m thick, and is composed of thin beds of argillite that as a group display a broad, wavy pattern. Two wavy bedforms were measured in the lower

part of the unit: 1) the lower bedform, located about 4 m above a 10 cm thick pink sandstone bed had a wavelength of 1.6 m and a height of 22 cm, and 2) a second wavy bedform, located a further 4 m above the first bedform, has a wavelength of 445 cm and a height of 13 cm.

### 3.2.8.1 Wavy Argillite Lithofacies Interpretation

The wavy argillite lithofacies represents a decrease in grain size relative to the underlying siltstone lithofacies. Fining upward sequences have been observed in ancient fluvial deposits (e.g. Cotter, 1978), and in this study, the decrease in grain size is interpreted to result from increasing transport distance from the sediment source (i.e. the glacier that fed sediment into the river that in turn fed the basin, is receding) (e.g. Clemmensen and Houmark-Nielsen, 1981; Dalrymple, 2010). There may also have been a marine or lacustrine transgression resulting from accumulated glacial melt in the basin (Benn and Evans, 2010). The wavy argillite facies may also represent overbank or inner bay floor deposits, with the waves being formed by marine/lake wave activity (Nichols, 2009; Ogami et al., 2015).

## 3.3 Depositional Model

The diamictite lithofacies, the contorted argillite lithofacies and the interlaminated siltstone and sandstone lithofacies were found only at Outcrop D in this study. The diamictite in this study is tillite, lithified glacial till composed of rock debris that was eroded, transported and ultimately deposited by a glacier (eg. Brodzikowski and van Loon, 1991). Till is often deposited in a ridge, such as in a moraine or esker. These ridges can be unstable, and subject to slumping. The diamictite lithofacies and contorted argillite lithofacies of this study represent the deposits of a local slumping event. The overlying interlaminated siltstone and sandstone lithofacies displays planar bedding and local asymmetrical ripples where it overlies contorted argillite and diamictite. The lithofacies at Outcrop D likely represent a slumped ridge that formed near the base of a delta/fan near the delta front. Asymmetrical ripples resembling lenticular bedding probably represent channel-mouth or mouth bar deposits.

The interlaminated siltstone and claystone lithofacies at Outcrop C lacks the interbedded lenticular beds that characterize the deposits at Outcrop A, which suggests an absence of fluvial activity in the former. This can be attributed to an interdistributary bay depositional environment (Reineck and Singh, 1980). Glaciofluvial outwash streams may form a series of deltas along the margin of a glaciofluvial water body, creating interdistributary bays between deltas (Ashley, 2002). Lakeshore-proximal sediments in interdistributary bays may be composed of sediments delivered to the zone from the adjacent continental landmass, which includes sediment originating from glacial melt (Ashley, 2002). The deposits may also be prodeltaic rhythmites, which form at the base of a delta distal to the bottomsets (Reineck and Singh, 1980). When prodeltaic rhythmites form, grain size decreases with distance from the delta front, ranging from sand-dominated near the delta front, to silt-dominated, to mud-dominated distally (Reineck and Singh, 1980). Rhythmites found at the base of Outcrop A and throughout Outcrop C are claystone-dominated and would therefore represent distal prodeltaic deposits. Prodeltaic deposits represent distal turbidite deposits. High sedimentation rates in an ice-contact to ice-proximal depositional environment support the formation of turbidites that can be initiated by slope failure in a subaqueous fan or deltaic environment (Benn and Evans, 2010).

One feature unique to Outcrop A is the sporadic presence of thin, rippled sandstone beds that morphologically display starved ripples or interconnected lenses. These beds are composed of a coarser grain size than the surrounding sediment, which may suggest reworking; however cross-bedding within the lenses indicates that they were formed by periodic events that delivered coarse-grained sediment from elsewhere. One explanation is that the lensoidal beds may have formed from sediment released from calved icebergs, an interpretation that is supported by the abundant dropstones in these beds (Thomas and Connell, 1985). Another possible interpretation is that the sediment was delivered from a neighbouring landmass during a rainstorm event. Evans et al., (2007) identified stratified lenses in laminated muds of glaciolacustrine sediments proximal to Loch Quoich, Scotland, which they interpreted to represent subaqueous mass flow deposits.

An increase in depositional rate is indicated by increasing bed thickness observed upsection in the interbedded siltstone and claystone lithofacies at Outcrop A, as well as by the increase in dewatering structures such as load and flame structures (Figure 3-10; Nichols, 2009). The accompanying upsection grain size increase is consistent with delta progradation (Reineck and Singh, 1980). Delta progradation displaying a coarsening upward sequence in a river-dominated environment requires adequate accommodation space in the receiving basin, mixed-load sediment transport, and minimal tidal activity if the receiving basin is marine (Ogami et al., 2015). Parallel and lenticular laminations that are locally breached by contorted slump deposits have been found at the base of shallow, interdistributary deltaic lake deposits (Coleman and Prior, 1982). Thus the interbedded siltstone and claystone lithofacies is interpreted to represent prograding delta deposits.

The sandstone lithofacies that composes the upper unit of Outcrop C may indicate interdistributary bay infilling by delta front sands as the delta progrades (Elliot, 1974). Cross-bedding was not apparent in the sandstone lithofacies at Outcrop C, which indicates a period of rapid deposition, perhaps via a large-scale turbidity current (Talling et al., 2012). The sandstone lithofacies may also represent deposition associated with further delta progradation (Reineck and Singh, 1980). The sandstone lithofacies that forms a thin bed at Outcrop A probably represents a single turbidite division or sedimentation resulting from a jökulhlaup (outburst flood).

The lack of dropstones in the siltstone lithofacies indicates that the glacial ice retreated to a point where ice-rafted debris (IRD) no longer found its way to the delta. The wavy argillite lithofacies indicates further retreat of glacial ice, resulting in the delivery of only fine-grained sediment to the delta (Benn and Evans, 2010). The complete lack of coarse-grained sediment may also indicate delta abandonment (Reineck and Singh, 1980).

In summary, the deposition of sediment in the study area was a result of two contemporaneous processes: delta progradation and glacial retreat. Glacial ice is inferred to have existed on a continental landmass proximal to a large body of water that could accommodate sediment deposition. The presence of dropstones in deposits lower in the stratigraphy indicates that glacial ice was proximal to the zone of deposition, providing a

source of IRD. Sedimentation was dominated by glacial melt: during periods of limited glacial melting, micro-layers of claystone were deposited whereas during periods of increased melting and associated increased depositional energy, siltstone layers were deposited. As glacial ice retreated from the continental margin, a glaciofluvial environment developed. Sedimentation continued to be dominated by glacial melting; however periods of greater fluvial transport energy initiated by jökulhlaups or periods of intense precipitation resulted in channel washout, leading to the deposition of sandy, cross-bedded lenticular beds within the rhythmite sequences. Calved glacial ice survived the transport distance from the area of calving to the area of deposition early in the cycle, but as the glacier retreated, icebergs melted completely before reaching the medial to distal river delta. A general coarsening-upward sequence indicates delta progradation over time, with the uppermost fine-grained unit representing either delta abandonment (fluvial avulsion) and/or further glacier retreat.

### 3.4 Sedimentology Summary

The sedimentological analysis of the four outcrops in this study identified eight lithofacies that are consistent with a depositional environment consisting of glacial recession, delta progradation, and local slumping. Although the outcrops are similar, morphological differences indicate that each outcrop represents a separate depositional event. Rhythmic deposits that morphologically resemble varves are composed of alternating layers of siltstone and claystone at Outcrops A and C, or alternating layers of coarse-grained and fine-grained siltstone at Outcrop B. Individual siltstone and claystone layers are composed of multiple micro-laminae, indicating that the layers are formed by multiple depositional events. This is significant because varved clay layers are generally described in the literature as being composed of homogenous or normally graded clay that settles from suspension during the winter freeze season.

### Depositional Model: Upper Gowganda Formation

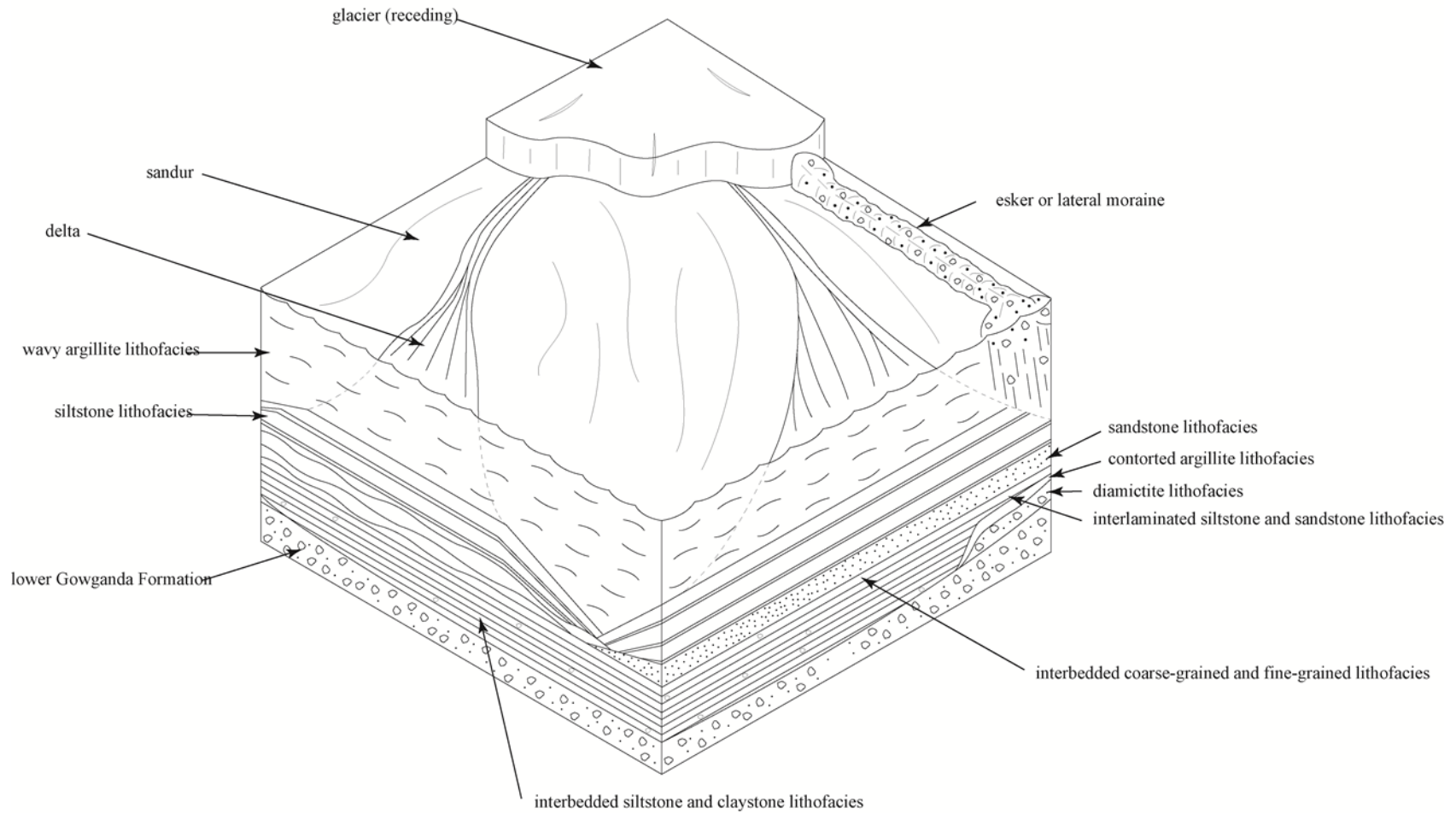


**Figure 3-12:** Depositional model of the upper Gowganda Formation based on lithofacies found in the study area.

## 4 Geochemistry

Sixteen samples were collected from the interbedded siltstone and claystone lithofacies at Outcrop A for geochemical analysis. Powder X-ray diffraction (pXRD) analysis, major and rare earth element (REE) analysis and stable isotope analysis of oxygen were conducted with the aim of determining the provenance of the sedimentary deposits, and determining whether there was chemical alteration and sedimentary recycling during the period encompassing erosion to deposition. Low levels of chemical alteration and sedimentary recycling would imply that the sediment was glacially eroded and regionally deposited when the glacier melted, without undergoing significant atmospheric weathering.

### 4.1 Sample Preparation

Eight rhythmites randomly collected over a stratigraphic interval of approximately 10m of the interbedded siltstone and claystone lithofacies at Outcrop A were separated into claystone and siltstone slices using an MK tile saw with a diamond blade. Each slice was pulverized using a tungsten carbide vibratory ring pulveriser to create a powder for geochemical analysis. Thus, a total of 16 powdered samples were prepared for powder XRD, major and REE, and stable isotope analyses.

### 4.2 Major, Trace and Rare Earth Element Analysis

The samples were analyzed at the Geoscience Laboratories of the Ontario Geological Survey in Sudbury, Canada. Fused-disc X-ray fluorescence (XRF) was used to determine the major elements. Loss on ignition values, as determined by gravimetric methods, ranged from 0.74 – 2.91 wt% (Table 4-1). Trace elements (Table 4-1), including REE (Table 4-2), were determined using inductively coupled plasma-mass spectrometry (ICP-MS). The accuracy and precision of this method is monitored through the use of the standard SY-2, which is syenite from the Bancroft area of Eastern Ontario (Gladney and Roelandts, 1990; Longrich et al., 1990). The relative standard deviation of the method is between 2% and 4% for 28 of 33 elements tested (Longrich et al., 1990). At the time of

**Table 4-1: Major and trace element compositions of the interlaminated siltstone and claystone lithofacies at Outcrop A of the Gowganda Formation**

Sample	OA-S1 (siltstone)	OA-S1 (claystone)	OA-S2-05 (siltstone)	OA-S2-05 (claystone)	OA-S2-05m (siltstone)	OA-S2-05m (claystone)	OA-S3-06 (siltstone)	OA-S3-06 (claystone)	OA-S5-01 (siltstone)	OA-S5-01 (claystone)	OA-S5-03 (siltstone)	OA-S5-03 (claystone)	OA-FRI-2a (siltstone)	OA-FRI-2a (claystone)	OA-FRI-2c (siltstone)	OA-FRI-2c (claystone)	
Element Detection (wt%)																	
Limit																	
SiO <sub>2</sub>	0.04	60.60	57.17	61.71	60.77	61.94	59.10	63.73	61.48	60.39	58.17	59.47	59.56	73.04	60.77	64.87	59.01
TiO <sub>2</sub>	0.01	0.53	0.55	0.52	0.47	0.44	0.63	0.45	0.52	0.56	0.70	0.59	0.54	0.36	0.47	0.39	0.61
Al <sub>2</sub> O <sub>3</sub>	0.02	16.51	18.58	16.27	17.56	15.62	17.61	15.51	16.42	17.43	17.46	17.76	17.36	13.15	17.56	15.27	17.34
Fe <sub>2</sub> O <sub>3</sub>	0.01	7.77	7.98	7.46	6.96	7.16	7.57	7.00	7.26	7.12	8.57	7.17	7.61	3.24	6.96	6.06	7.76
MnO	0.002	0.093	0.095	0.089	0.082	0.082	0.087	0.081	0.086	0.085	0.106	0.085	0.091	0.030	0.082	0.077	0.101
MgO	0.01	3.63	3.76	3.26	3.14	3.13	3.38	3.07	3.21	3.25	3.97	3.38	3.52	0.79	3.14	2.72	3.60
CaO	0.006	1.234	0.937	1.261	0.953	1.074	1.171	1.065	1.090	1.100	1.687	1.121	1.003	0.954	0.953	0.949	1.149
Na <sub>2</sub> O	0.02	3.90	4.90	3.96	4.71	3.76	4.31	3.84	4.13	4.83	4.20	4.73	4.43	5.31	4.71	4.17	4.68
K <sub>2</sub> O	0.01	2.87	3.00	2.86	3.00	2.91	3.10	2.83	2.85	3.18	2.80	3.31	2.97	2.28	3.00	3.38	3.11
P <sub>2</sub> O <sub>5</sub>	0.002	0.135	0.079	0.134	0.114	0.118	0.145	0.123	0.149	0.098	0.202	0.093	0.125	0.108	0.114	0.109	0.127
BaO	0.004	0.080	0.080	0.080	0.080	0.080	0.070	0.080	0.070	0.080	0.070	0.080	0.080	0.070	0.080	0.100	0.080
Cr <sub>2</sub> O <sub>3</sub>	0.002	0.020	0.030	0.020	0.020	0.020	0.020	0.020	0.020	0.020	0.020	0.020	0.020	0.010	0.020	0.010	0.020
LOI	0.05	2.50	2.91	2.36	2.36	2.31	2.57	2.27	2.42	2.24	2.68	2.35	2.55	0.74	2.36	1.91	2.51
Total		99.87	100.07	99.98	100.22	98.64	99.76	100.07	99.71	100.38	100.64	100.16	99.86	100.08	100.22	100.02	100.10
CIA		67	68	67	67	67	67	67	67	66	67	66	67	61	67	64	66
(ppm)																	
Ba	0.8	767.4	714.4	714.0	751.4	754.2	694.2	742.1	698.2	700.1	659.6	704.4	774.2	634.7	734.9	943.9	736.6
Be	0.04	1.57	1.81	1.71	1.62	1.48	1.84	1.47	1.61	1.80	1.63	1.89	1.69	1.00	1.96	1.43	1.83
Bi	0.47	<0.47	<0.47	<0.47	<0.47	<0.47	0.51	<0.47	<0.47	0.48	<0.47	<0.47	0.47	<0.47	0.57	<0.47	<0.47
Cd	0.013	0.027	0.019	0.020	0.014	0.030	0.026	0.027	0.027	0.026	<0.013	0.026	0.026	0.021	0.026	0.034	0.030
Co	0.13	27.93	22.21	24.37	19.45	23.24	22.80	23.00	22.91	22.73	27.24	22.13	23.13	12.89	28.17	20.42	21.51
Cr	3	139	179	145	153	118	187	121	152	143	163	142	161	65	179	77	148
Cs	0.013	2.279	2.560	2.412	2.456	2.425	2.896	2.396	2.608	2.534	2.427	2.942	2.483	1.131	2.884	1.982	2.500
Cu	1.4	56.8	9.8	70.9	14.6	97.8	17.1	104.5	27.3	10.7	10.6	7.5	21.0	290.7	2.2	294.9	3.2
Ga	0.04	22.12	24.02	21.09	21.07	19.95	22.55	19.38	20.97	23.46	25.75	23.20	21.84	10.91	28.83	19.24	25.15
Hf	0.14	3.23	2.07	3.24	2.00	3.53	2.94	3.00	3.04	3.34	2.96	3.25	2.64	4.14	3.67	4.07	3.56
In	0.0018	0.0459	0.0429	0.0445	0.0364	0.0370	0.0482	0.0376	0.0419	0.0388	0.0618	0.0382	0.0430	0.0145	0.0732	0.0300	0.0483
Li	0.4	44.7	47.1	42.0	40.1	41.4	45.2	40.1	43.1	42.9	49.7	43.5	43.0	10.0	50.5	31.0	41.8
Mo	0.08	1.86	2.17	1.89	1.94	1.57	2.03	1.62	1.85	2.06	2.55	1.79	1.92	1.30	3.04	1.56	2.09
Ni	1.6	78.4	78.7	71.4	67.8	68.5	70.6	66.2	69.0	66.3	77.5	68.0	71.7	20.7	91.0	51.3	69.3
Pb	0.18	6.50	4.70	6.50	4.90	6.50	5.60	6.30	5.60	11.10	12.50	12.00	5.10	46.30	12.20	16.80	11.30
Rb	0.11	119.18	136.96	122.08	131.91	123.02	145.55	112.82	124.11	128.96	113.43	139.11	125.85	70.74	117.51	119.06	114.53
Sb	0.04	0.51	0.54	0.56	0.52	0.47	0.64	0.47	0.54	0.46	0.54	0.50	0.50	0.25	0.59	0.33	0.49
Sc	1.1	18.4	18.1	17.5	15.8	13.6	19.5	14.4	17.4	17.1	20.0	16.8	17.3	8.9	21.9	11.4	18.3
Sn	0.16	1.62	1.69	1.61	1.41	1.37	1.72	1.44	1.60	1.87	2.30	2.02	1.54	1.07	2.52	1.39	2.04
Sr	0.6	230.4	172.4	221.4	183.8	224.3	197.0	216.9	206.8	194.0	245.1	190.8	184.8	185.1	240.6	194.9	190.7
Ta	0.007	0.610	0.628	0.625	0.514	0.546	0.728	0.529	0.629	0.891	0.871	0.941	0.642	0.454	1.153	0.583	0.892
Th	0.018	8.771	10.345	9.296	8.052	7.637	12.178	7.411	9.443	18.606	13.540	19.786	10.015	5.866	18.098	10.440	16.649
Ti	7	3066	3222	3127	2668	2635	3712	2731	3082	3371	4092	3496	3138	2141	4827	2325	3586
Tl	0.002	0.562	0.614	0.560	0.603	0.579	0.637	0.544	0.577	0.644	0.549	0.710	0.589	0.384	0.606	0.618	0.555
U	0.011	3.748	3.075	3.487	2.489	3.171	3.810	2.910	3.171	4.873	6.245	4.487	3.209	2.957	6.107	4.063	5.579
V	0.8	116.4	133.6	109.3	114.2	101.8	137.5	99.7	116.3	115.7	141.4	116.6	123.3	71.2	147.8	82.7	117.1
W	0.05	1.08	1.27	1.18	1.03	0.94	1.34	0.98	1.16	1.15	1.41	1.16	1.16	0.75	1.54	0.78	1.12
Y	0.05	14.98	14.36	15.45	11.99	12.40	17.26	13.07	15.11	14.63	19.67	14.33	15.13	10.39	22.58	12.08	16.97
Zn	1.8	88.0	88.0	80.0	76.0	77.0	81.0	75.0	78.0	90.0	108.0	90.0	85.0	26.0	117.0	79.0	101.0
Zr	6	122	75	123	72	137	109	113	113	118	109	114	95	160	134	153	129

Using molecular proportions, the CIA is calculated as: CIA =  $[Al_2O_3 / (Al_2O_3 + CaO + Na_2O + K_2O)] \times 100$

**Table 4-2: Rare earth element compositions of the interlaminated siltstone and claystone lithofacies at Outcrop A of the Gowganda Formation**

REE	La	Ce	Pr	Nd	Sm	Eu	Gd	Tb	Dy	Ho	Er	Tm	Yb	Lu
Detection Limit	0.1	0.12	0.014	0.06	0.026	0.0031	0.009	0.0023	0.009	0.0025	0.007	0.0019	0.009	0.002
Sample	ppm	ppm	ppm	ppm	ppm	ppm	ppm	ppm	ppm	ppm	ppm	ppm	ppm	ppm
OA-S1 (siltstone)	33.7	63.63	7.359	27.42	4.673	1.0837	3.613	0.4888	2.780	0.5270	1.466	0.2168	1.383	0.210
OA-S1 (claystone)	22.9	44.89	5.247	19.62	3.644	0.9219	3.030	0.4350	2.535	0.4924	1.436	0.2120	1.389	0.209
OA-S2-05 (siltstone)	28.7	56.16	6.506	23.82	4.230	1.0212	3.382	0.4707	2.799	0.5225	1.523	0.2180	1.422	0.216
OA-S2-05 (claystone)	21.7	42.02	4.917	18.06	3.216	0.7686	2.601	0.3556	2.065	0.4093	1.171	0.1708	1.145	0.175
OA-S2-05m (siltstone)	22.4	46.71	5.197	19.40	3.513	0.8541	2.713	0.3871	2.201	0.4225	1.247	0.1850	1.231	0.187
OA-S2-05m (claystone)	28.2	56.49	6.571	23.92	4.367	1.0732	3.486	0.5109	3.015	0.5740	1.698	0.2450	1.638	0.251
OA-S3-06 (siltstone)	26.3	49.73	5.853	21.32	3.780	0.9145	2.928	0.3999	2.369	0.4480	1.312	0.1923	1.229	0.191
OA-S3-06 (claystone)	27.9	53.39	6.330	23.10	4.146	1.0171	3.260	0.4643	2.739	0.5272	1.546	0.2228	1.454	0.222
OA-S5-01 (siltstone)	29.8	59.23	6.818	24.50	4.312	0.8913	3.273	0.4512	2.643	0.5001	1.472	0.2146	1.427	0.218
OA-S5-01 (claystone)	46.9	91.44	10.484	37.72	6.330	1.3458	4.721	0.6323	3.569	0.6835	1.894	0.2669	1.703	0.251
OA-S5-03 (siltstone)	30.2	58.71	6.751	24.08	4.206	0.9010	3.259	0.4582	2.574	0.5030	1.479	0.2218	1.464	0.225
OA-S5-03 (claystone)	26.0	50.18	6.030	21.85	3.995	0.9937	3.228	0.4731	2.724	0.5291	1.505	0.2223	1.430	0.217
OA-FRI-2a (siltstone)	21.7	41.75	4.958	18.28	3.156	0.7125	2.306	0.3210	1.794	0.3516	1.022	0.1525	1.020	0.157
OA-FRI-2a (claystone)	51.2	99.29	11.378	40.81	6.939	1.5742	5.346	0.7184	4.102	0.7771	2.197	0.3092	1.961	0.295
OA-FRI-2c (siltstone)	29.1	56.74	6.573	23.57	4.054	0.9121	2.997	0.3983	2.227	0.4070	1.181	0.1681	1.103	0.171
OA-FRI-2c (claystone)	35.4	70.41	8.022	28.41	5.096	1.0985	3.828	0.5464	3.072	0.5871	1.663	0.2362	1.545	0.233

major element analysis for this study, the relative standard deviation of the method as measured by the standard LK-NIP-1 was between 1 - 3% for 9 of the 10 elemental oxides measured. The precision, as measured by duplicates of the standard GSP-2, was between 0 – 1% for 9 of 11 elemental oxides, and the precision of duplicate measurements of the claystone sample OA-S5-01 was between 0 – 1% for 12 elemental oxides. The accuracy of the method for trace element determination was monitored through the use of the standards AGV-2, with 33 of 36 trace and rare earth elements found to be within the acceptable range; and BHVO-2, with 16 of 16 trace and rare earth elements found to be in the acceptable range. The precision, as measured by the standard deviation of duplicate measurements of the standard MRB-29, was between 0 and 4% for 39 of 44 trace and REE. The standard deviation of duplicate measurements of the claystone sample OA-S5-03 was 0 – 3% for 42 of 44 trace elements tested, and of duplicate measurements of OA-02-05 (claystone) was 0 – 3% for 41 of 44 trace elements.

The siltstone rhythmite layers contain 59.47-73.04 wt% SiO<sub>2</sub> (detection limit 0.04 wt%) with MgO ranging from 0.79-3.63 wt% (detection limit 0.01 wt%). The claystone rhythmite layers contain 57.17-61.48 wt% SiO<sub>2</sub> and 3.14-4.26 wt% MgO. The claystone samples generally contain slightly higher levels of Fe<sub>2</sub>O<sub>3</sub>, Na<sub>2</sub>O, K<sub>2</sub>O and Al<sub>2</sub>O<sub>3</sub> compared with the siltstones. In terms of the trace elements, the siltstone layers contain more Zr (113-160 ppm, detection limit 6 ppm) compared with the claystone samples (72-134 ppm), (t-test: p = 0.03), and have a higher Zr/Sc ratio (t-test: p = 0.03), (Figure 4-1-A). The claystone samples contain greater abundances of Ti (t-test: p = 0.04) and Sc (t-test: p = 0.02) relative to the siltstone layers (Table 4-1; Figure 4-1). These characteristics indicate that the claystone layers are composed of more mafic material than the siltstone layers. Plotting Th/Sc versus Zr/Sc (Figure 4-1-B) reveals a modest enrichment in Zr and a slight depletion in Th relative to Sc for all samples. Sc is typically compatible with igneous systems, whereas Zr and Th are typically not, leading to compositional variations that result from igneous differentiation (McLennan et al., 1993). Sc thus preserves a signature of provenance, whereas zircon enrichment occurs in a passive margin setting due to sedimentary sorting (recycling), (McLennan et al., 1993). Thus a low Zr/Sc ratio

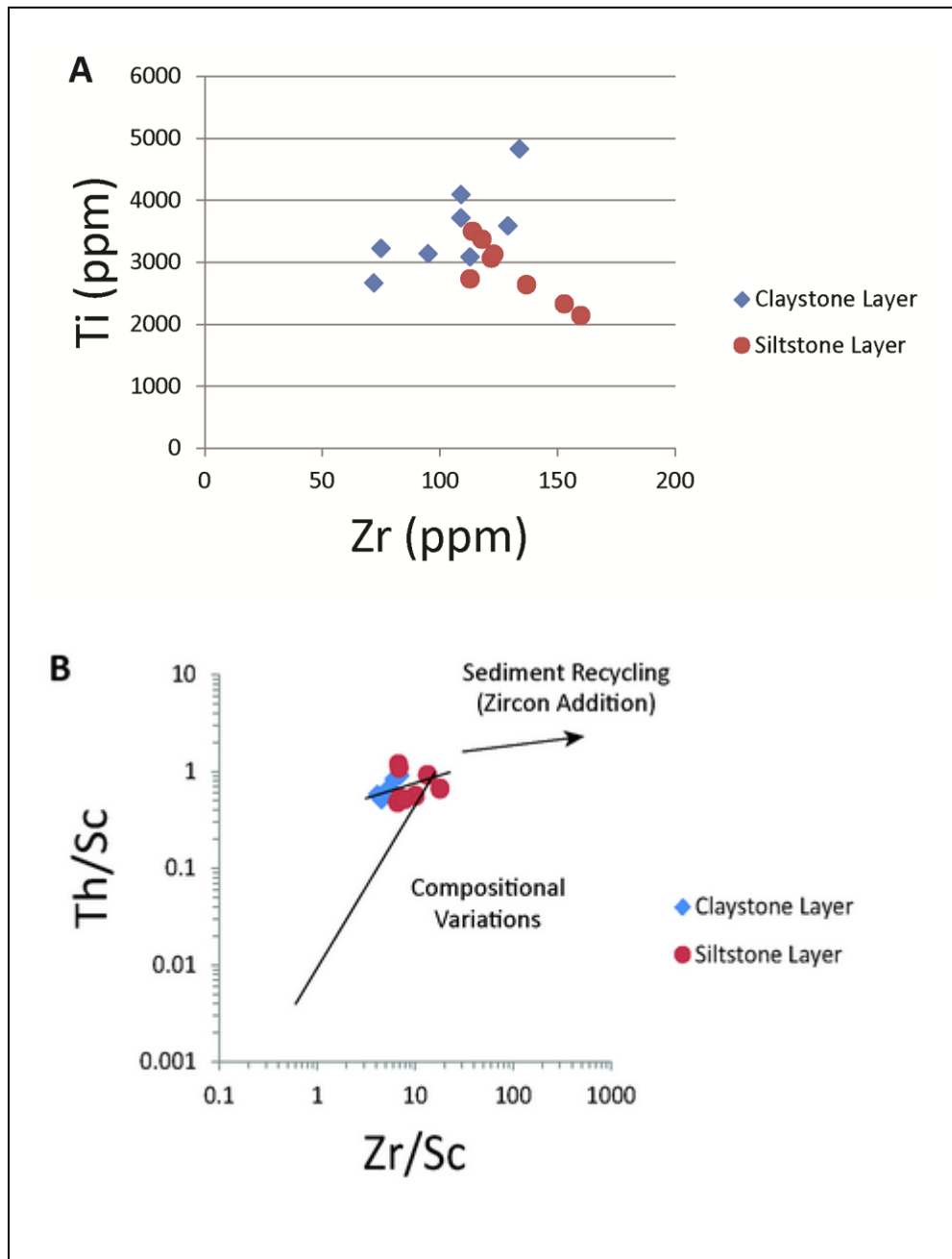


**Figure 4-1:** Trace element discrimination diagrams for the claystone and siltstone layers in rhythmites of Outcrop A. (A) Plot of Ti vs Zr showing the claystone layers to be enriched in Ti relative to the siltstone layers, and siltstone layers to be enriched in Zr relative to the claystone layers. (B) Plot of Th/Sc vs Zr/Sc shows little Zr enrichment (low Zr/Sc ratio), indicating that both layers underwent little recycling. Sediment recycling leads to zircon enrichment (upper trend line), whereas samples from active margins display a simple correlation between Th/Sc and Zr/Sc (compositional variations trend line). After McLennan et al. (1993).

for both the siltstone and claystone samples indicates that the sediment has undergone very little recycling.

Climatic conditions at the time of source rock erosion and sediment deposition can be inferred from the Chemical Index of Alteration (CIA), which is a measure of the amount of aluminous versus alkali minerals in a rock (Nesbitt and Young, 1982). Using molecular proportions, the CIA is calculated as:

$$\text{CIA} = [\text{Al}_2\text{O}_3 / (\text{Al}_2\text{O}_3 + \text{CaO}^* + \text{Na}_2\text{O} + \text{K}_2\text{O})] \times 100$$

where CaO\* is the amount of CaO incorporated in the silicate fraction of the rock.

Chemical weathering of feldspars in the upper crust leads to the formation of Al-rich clay minerals. Thus, a low CIA indicates mafic composition (fresh basalts have values between 30 and 45) whereas a high CIA indicates a high proportion of clays (kaolinite and chlorite have values approaching 100). Values within the range of 45 to 55 reflect the CIA values of unaltered granite or granodiorite (Nesbitt and Young, 1982). In this study, CIA values range from 61-68 (Table 4-1), which indicates a granite to granodiorite composition for the samples elevated by the presence of chlorite, and is consistent with values obtained previously for upper Gowganda Formation deposits (Nesbitt and Young, 1982; Young, 2001). This indicates that the material comprising the rhythmites has undergone very little chemical alteration (Nesbitt and Young, 1982; Young, 2001).

A Sc-Th-Zr/10 tectonic discrimination diagram is used to compare the relative abundances of Sc, Th and Zr/10 within measured samples to known values from passive margin, active continental margin, continental island arc, and ocean island arc depositional environments. On a Sc-Th-Zr/10 tectonic discrimination diagram (Figure 4-2), the samples plot within or proximal to the continental island arc field. This is consistent with derivation from the Archean Superior Province, which is interpreted as a collage of accreted active margin terrains (Ayer and Davis, 1997). As represented on a Sc-Th-Zr/10 tectonic discrimination diagram, oceanic island arc greywackes are relatively depleted in Th and Zr, indicating derivation from volcanics that are more mafic whereas active continental margin greywackes are enriched in Th and Zr, indicating derivation from volcanics that are more felsic (Bhatia and Crook, 1986). Greywackes that

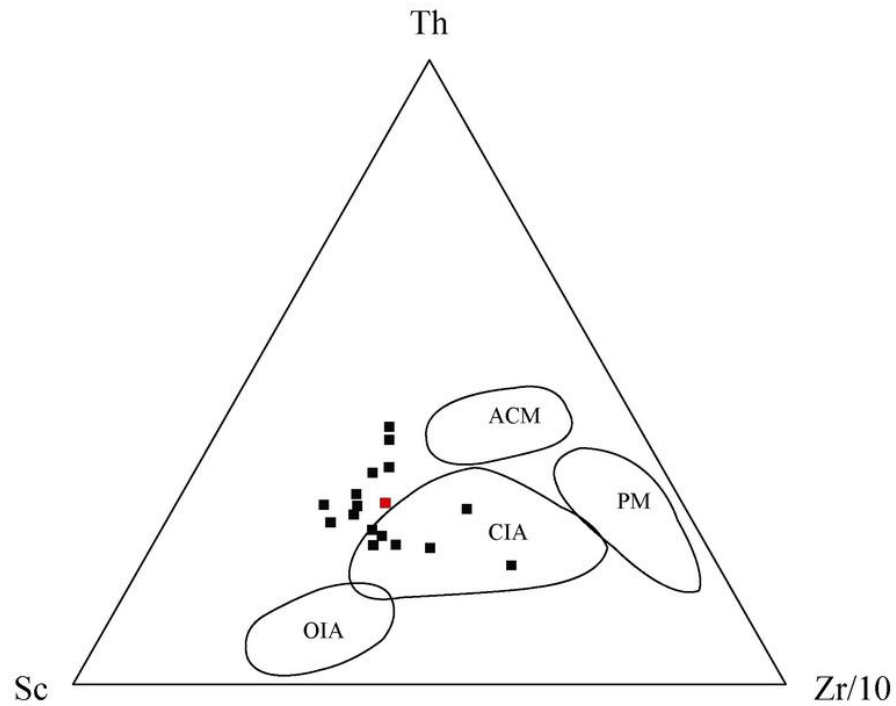


**Figure 4-2:** Tectonic discrimination diagram of samples from the interbedded siltstone and claystone lithofacies at Outcrop A, with the average of all samples shown in red. The average composition point plots just outside the continental island arc (CIA) field. Other fields shown are: passive margin (PM), active continental margin (ACM) and ocean island arc (OIA). After Bhatia and Crook (1986).

are significantly enriched in Zr are associated with sedimentary reworking found in a passive margin setting.

The REEs were normalized to the North American shale composite (NASC, Figure 4-3). All samples are enriched in the LREE compared with the HREE, with La/Yb<sub>n</sub> values ranging from 1.6-2.7 for the claystone samples and 1.8-2.6 for the siltstone samples. Enrichment in LREE with respect to HREE is typical of both potassium feldspar and plagioclase. Enrichment in HREE would be expected in the samples if feldspars were exposed to moderate chemical weathering leading to clay formation, thus these results indicate that the samples are derived from a crustal source rock (Taylor and McLennan, 1985). The samples are depleted in the HREE relative to NASC, which is expected because half of the Gowganda Formation samples are siltstones, and thus are richer in quartz and feldspars than the combined shales of NASC. This result is consistent with the results determined for Paleoproterozoic argillites by Young (2001) and with the results determined for different components of the Archean Superior Province by Fedo et al. (1997a). A slight enrichment in Eu indicates the presence of unaltered plagioclase (Panahi et al., 2000). Europium<sup>3+</sup> can be reduced to Eu<sup>2+</sup> in magmatic systems, where it can replace Ca<sup>2+</sup>, Sr<sup>2+</sup>, and Na<sup>+</sup> in plagioclase (Henderson, 1996). Eu measurements in this study have a range of 0.71-1.57 ppm (detection limit 0.0031); Eu measurements in the range of 0.88-1.17 ppm have been associated with continental crust (Taylor and McLennan, 1995). The REE plot also displays a modest Ce depletion. Negative Ce anomalies compared with NASC have been found in seawater and in marine carbonate (Liu et al., 1988; Shimizu et al., 1994); however marine conditions are characterized by an increase in the abundance of HREEs, a trait that is not observed in this study. Therefore marine conditions are not inferred from the negative Ce anomaly. The modest Nd depletion observed may be inherited from the source rock, and is not a result of post-depositional alteration (e.g. Chu et al., 2009).

### 4.3 Powder X-ray Diffraction

Sixteen powdered samples mounted in a back-packed, circular steel frame backed by a glass slide were analyzed using a Rigaku RU-200BVH rotating anode X-ray Diffractometer operating at 45 kV and 160 mA. The diffractometer employs CoK $\alpha$

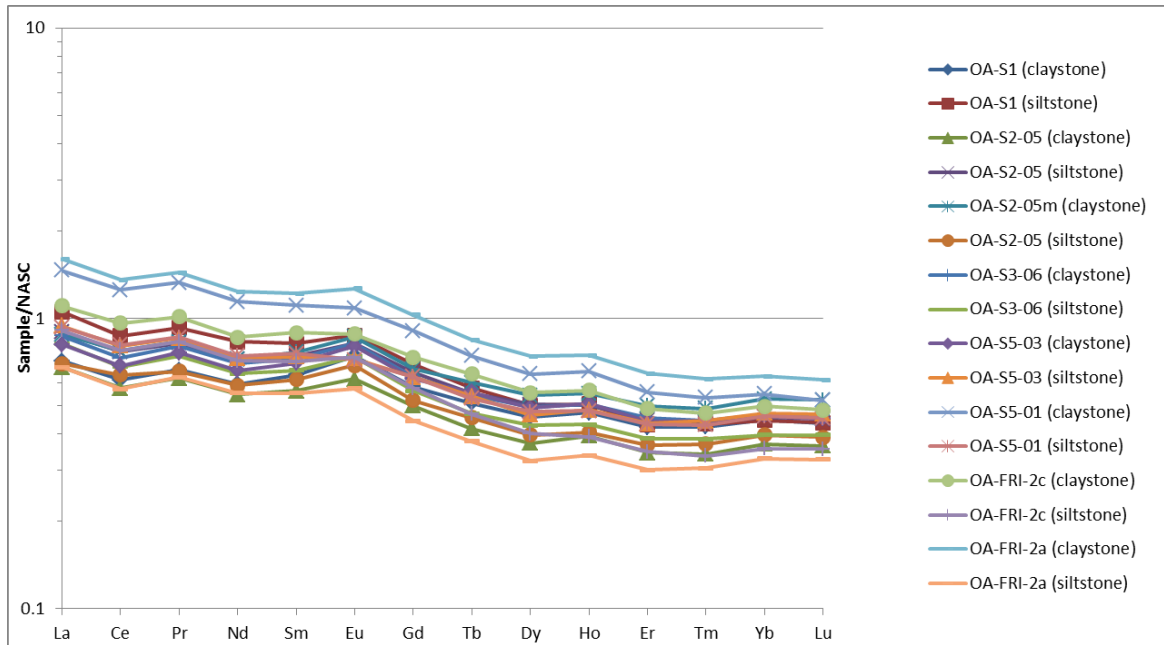


**Figure 4-3:** REE diagram of samples from the interbedded siltstone and claystone lithofacies at Outcrop A. NASC normalizing values are from Haskin et al. (1968) except for Dy, which is taken from Gromet et al. (1984).

radiation and uses a curved crystal diffracted beam graphite monochromator to achieve a monochromatic beam of wavelength  $\lambda=0.1790210$ . Using a step size of  $0.02^\circ$  and a scanning rate of  $10^\circ$  two-theta per minute, sample scans covered a range of  $2^\circ$  to  $82^\circ$  two-theta. X-rays were collimated using  $1^\circ$  divergent and scatter slits, and a 0.15mm receiving slit. The relative abundance of each mineral was estimated using the form-factor corrected background-subtracted peak height of the most intense, uniquely diagnostic diffractions of each phase. The form factors used to account for differences in crystallinity and intensity of measured diffractions among minerals, and the corresponding d-spacing, were x1 for quartz (0.343 nm) and plagioclase (0.319 nm), x2 for chlorite (1.4 nm) and x4 for mica (1.0 nm).

The results (Table 4-3) show that for claystone layers, the relative abundance of quartz ranged from 40 – 56 with an average of 49, the relative abundance of plagioclase ranged from 28 – 33 with an average of 33, the relative abundance of chlorite ranged from 6 – 13 with an average of 9 and the relative abundance of mica ranged from 5 – 13 with an average of 10. For the siltstone layers, the relative abundance of quartz ranged from 40 – 69 with an average of 56, the relative abundance of plagioclase ranged from 23 – 36 with an average of 29, the relative abundance of chlorite ranged from 2 – 13 with an average of 8 and the relative abundance of mica ranged from 2 – 12 with an average of 8. The results also show that the claystone layers have a greater content of plagioclase, chlorite and mica relative to the siltstone layers, and that the siltstone layers contain more quartz relative to the claystone layers.

## 4.4 Stable Isotopes

Whole-rock analysis of oxygen isotopes was conducted on the sixteen samples to evaluate the maturity of the sediments. Variations in the bulk oxygen-isotope composition of clastic sedimentary rocks reflect the contribution of: 1) fragmented rock and detrital minerals that have  $\delta^{18}\text{O}$  values characteristic of their igneous source ( $\sim+5\text{‰}$  to  $+10\text{‰}$ ), 2) weathering products such as clays, which are enriched in  $^{18}\text{O}$  ( $\sim+10\text{‰}$  to  $+30\text{‰}$ ) and 3) cements, which are also enriched in  $^{18}\text{O}$  (Savin and Epstein, 1970a,b; Longstaffe and Schwartz, 1977). Thus supracrustal weathering leads to the formation of

**Table 4-3: pXRD and stable isotope results for 16 powdered samples of the interbedded siltstone and claystone lithofacies from Outcrop A.**

<i>Claystone Layers</i>	$\delta^{18}\text{O}$ (‰)	Quartz (%)	Plagioclase (%)	Chlorite (%)	Mica (%)
OA-S1	7.1	40	40	8	12
OA-S2-05	7.7	52	31	7	10
OA-S2-05m	7.5	47	32	8	12
OA-S3-06	8.3	56	33	6	5
OA-S5-01	7.5	51	28	11	10
OA-S5-03	7.9	52	30	8	10
OA-FRI-02a	7.1	40	33	13	13
OA-Fri-02c	7.7	50	33	8	8
Average		49	33	9	10
<i>Siltstone Layers</i>					
OA-S1	7.8	59	25	9	8
OA-S2-05	7.7	55	31	8	7
OA-S2-05m	8.1	62	23	7	8
OA-S3-06	7.5	61	23	6	10
OA-S5-01	7.7	45	36	10	9
OA-S5-03	7.6	40	35	13	12
OA-Fri-02a	9.2	69	26	2	2
OA-Fri-02c	7.7	50	33	8	8
OA-Fri-2c	8.1	60	29	7	4
Average		56	29	8	8

Form factors used to correct for differences in crystallinity among minerals were x1 for quartz and plagioclase, x2 for chlorite and x4 for mica.  $\delta^{18}\text{O}$  results are relative to VSMOW.

shales and mudstones that are enriched in  $^{18}\text{O}$  with respect to crustal rock, due to the presence of clay minerals, and diagenetic silica cements that form in low temperature water (Longstaffe, 2003). Claystone and siltstone samples were evaluated separately to determine if conditions varied when each type was deposited.

The whole-rock oxygen isotope compositions were determined at the Laboratory for Stable Isotope Science (LSIS) located at the University of Western Ontario. Oxygen was extracted from silicates using the method of Clayton and Mayeda (1963), as modified by Borthwick and Harmon (1982) for use with  $\text{ClF}_3$ . Dried samples were heated and pumped in Ni-reaction vessels under vacuum at  $300^\circ\text{C}$  for 2 hours prior to reaction, and then reacted with  $\text{ClF}_3$  at  $580^\circ\text{C}$  overnight. Oxygen gas liberated by this process was quantitatively converted to  $\text{CO}_2$  by reaction with red-hot graphite. The  $\text{CO}_2$  gas was analyzed using an Optima dual-inlet mass spectrometer to determine the oxygen-isotope composition. Results are reported in the usual  $\delta$ -notation relative to Vienna Standard Mean Ocean Water (VSMOW). Details of the calibration to VSMOW are given in Polat and Longstaffe (2014). Accuracy was evaluated using the laboratory standard quartz (ORX), the laboratory standard basalt (BAS-206) and the laboratory standard carbon dioxide (Bleu) for which average values of +11.6‰, +7.5‰ and +10.3‰ were obtained, which compares well with their expected values of +11.5‰, +7.5‰ and +10.3‰, respectively. The reproducibility (SD) of  $\delta^{18}\text{O}$  values for replicates of the laboratory standards was  $\pm 0.08\text{‰}$ .

Whole-rock  $\delta^{18}\text{O}$  for the claystone layers ranged from +7.1 to +8.3‰ and for the siltstone layers  $\delta^{18}\text{O}$  ranged from +7.6 to +9.2‰ (Table 4-5). A t-test ( $p = 0.16$ ) shows that these results are not statistically different. The relationship between phyllosilicate content and whole-rock  $\delta^{18}\text{O}$  of all samples is illustrated in Figure 4-4.

## 4.5 Geochemistry Discussion

The aim of conducting pXRD, major and REE analysis, and oxygen isotope analysis was to determine the provenance of the sediment composing the rhythmites, and to assess whether there was chemical alteration and sedimentary recycling during the period encompassing erosion to deposition. If the depositional environment is glacially

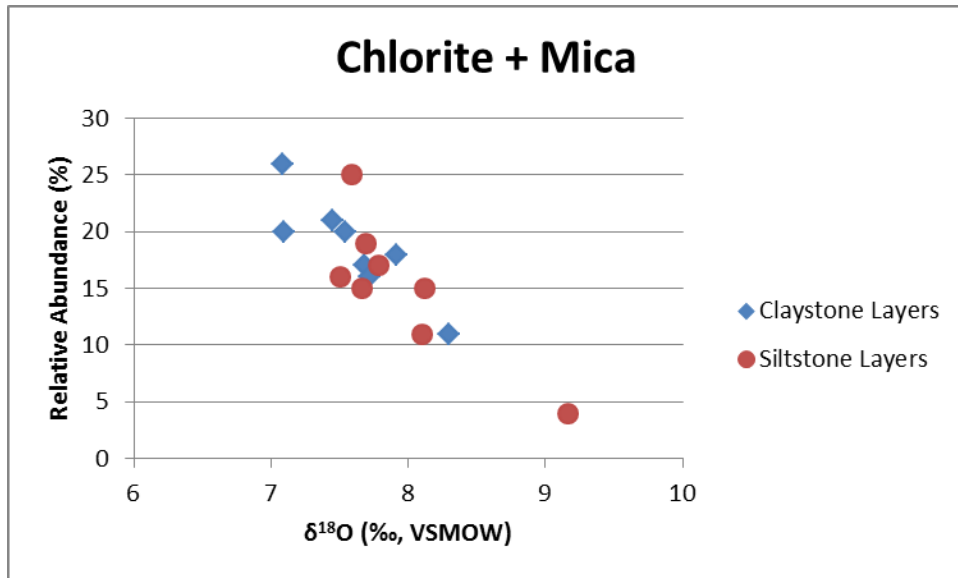


**Figure 4-4:** Relative abundance of chlorite + mica versus oxygen-isotope compositions of samples from the interbedded siltstone and claystone lithofacies at Outcrop A.

influenced, low levels of chemical alteration and sedimentary recycling would be expected.

The CIA values of 61-68 indicate a low degree of post-depositional alteration, which implies that very little clay formed as a result of supracrustal weathering processes. The trace element discrimination diagrams show very little enrichment in Zr, which also indicates little sediment recycling. Mafic source material (i.e. amphibole) in a sample is indicated by the presence of titanium, whereas Zr indicates the presence of felsic minerals (e.g. Morton, 1991). The rock composing the study area has been metamorphosed to greenschist grade, which has converted the previously existing amphiboles to chlorite. Titanium in the form of titanium dioxide could be produced as a by-product of the metamorphism, or titanium could be contained in chlorite (i.e. odinite). The plot of Ti vs Zr shows the claystone layers to be enriched in Ti relative to the siltstone layers, and the siltstone layers to be enriched in Zr relative to the claystone layers. This separation is a result of mechanical sorting of sediment derived from a single source. In a study of grain size and element distribution in river sediments, Dinelli et al. (2007) showed that Ti is positively correlated with the clay-sized fraction and Zr is positively correlated with the silt-sized fraction.

On the REE diagram, some of the claystone samples display a more mafic signature with respect to NASC (elevated levels of REE), and some of the siltstone samples display a more felsic signature (depleted levels of REE). This trend is consistent with a plot of the XRD value of Chlorite + Mica versus  $\delta^{18}\text{O}$  (Figure 4-4), which shows that chlorite and mica have modal mineralogical control on the whole-rock oxygen isotopic compositions – an increase in the relative abundance of chlorite + mica is associated with a decrease in the  $\delta^{18}\text{O}$  value. This indicates that the phyllosilicates (e.g. muscovite and chlorite were observed in thin section) are contributing a high temperature  $\delta^{18}\text{O}$  signature to the samples, not a low temperature signal as would be expected if the clays represented the products of weathering or low temperature alteration/diagenesis. Thus, the lack of clay minerals in the clay-sized fraction indicates that the clay-sized fraction is composed of glacially-pulverized rock flour.

Whole-rock  $\delta^{18}\text{O}$  values for the rhythmites, which range from 7.1 to + 9.2‰, are congruent with whole-rock  $\delta^{18}\text{O}$  results of +7.3 to +8.9‰ determined for Archean gneiss from the Superior Province (Longstaffe and Schwartz, 1977; Longstaffe and Gower, 1983). Elevated values in whole-rock  $\delta^{18}\text{O}$  values for the rhythmites would be expected if sedimentary recycling occurred due to the addition of low temperature phases resulting from post-depositional weathering (clay formation) and diagenetic processes (cementation). These results support the Sc-Th-Zr/10 tectonic discrimination diagram plot (Figure 4-2), which shows that the rhythmite samples compositionally resemble a continental island arc source, indicating little post-depositional weathering. Bhatia and Crook (1986) found that Archean samples from Australia, South Africa and Greenland plot mainly adjacent to and within the oceanic or continental island arc fields. The  $\delta^{18}\text{O}$  signals are those of primary granitoid rocks that have not been enriched in  $\delta^{18}\text{O}$  by silica overgrowths that would drive up their values. The formation of chlorite in the rhythmites composing the interbedded siltstone and claystone lithofacies at Outcrop A is probably predominantly due to greenschist metamorphism.

Together these results indicate that the minerals that compose the rhythmites have not undergone significant post-depositional alteration. It also indicates that the rhythmites do not contain a significant contribution from pre-existing supracrustally modified source rocks. These results are therefore consistent with what would be expected from sediment that was glacially eroded, transported within ice, and then deposited without being subjected to great transport distances or subaerial exposure.

## 5 Statistical Analysis of Rhythmites

### 5.1 Introduction

Sedimentary deposits from marine or lacustrine environments can be used to provide information about past climatic and depositional events. The sequential deposition of multiple, undisturbed varves within a basin provide a high-resolution record of a short, specific time interval (Ojala et al., 2012). Modern varve chronology relies on proving annual control on the deposition of rhythmic laminations because turbidite and contour current deposits in deep marine basins, and fluvial and tidal deposits in estuarine environments, can exhibit characteristics that are similar to those observed in varves (Eyles, 1993). Techniques used to constrain the annual periodicity of a series of rhythmites include isotope analysis ( $^{137}\text{Cs}$ ,  $^{210}\text{Pb}$ ,  $^{14}\text{C}$ ), pollen and diatom analysis, weather station records and the consideration of sedimentary budgets and structures (Ashley, 2002 and references therein). Once annual control has been demonstrated, varve deposits may be used to infer paleoclimate.

When considering Paleoproterozoic rhythmic deposits, annual control may be inferred, but not proven, due to the lack of biogenic or other markers that would allow annual control to be demonstrated. In an effort to fill this gap, spectral analysis has been used in this study to examine measured rhythmites from two outcrops: Outcrop A and Outcrop B. These results are first interpreted under the assumption of annual control, but consideration is also given to other depositional timeframes.

### 5.2 An Introduction to Spectral Analysis

Cyclic stratigraphic processes such as sedimentation can be described and interpreted as periodic oscillations. A periodic oscillation is mathematically described using a simple sinusoidal curve consisting of a fixed amplitude, frequency and phase. Geological oscillations describing cyclic stratigraphy are more complex in shape, and can be represented as a sum of multiple oscillations with particular frequencies. Multiple frequencies comprise a spectrum, and the analysis of a spectrum is called spectral analysis (Weedon, 2003).

Sedimentary deposits may be considered to be records of environmental change. When stratigraphic thicknesses are sequentially measured at constant intervals, based on observable parameters such as recognizable beds, a time series can be formed. This time series represents a spectrum. For the purpose of spectral analysis it is assumed that the stratigraphic record is composed of regular components (the signal) and irregular components (the noise). The signal represents a periodic oscillation in some variable whereas the noise represents an irregular oscillation (Weedon, 2003).

Fourier's Theorem states that any time series can be recreated as the sum of its underlying single frequency contributions. Fourier analysis uses sine and cosine waves to examine a time series. The discrete Fourier transform (DFT) is used to create a periodogram, which is a measure of the amplitude of each of a number of frequency components. Although the DFT is frequently used as the basis of many spectral analysis techniques, it is regarded as inappropriate for use in cyclostratigraphic studies due to the presence of red noise in geologic systems. Red noise, and the method chosen for use in this study, the multi-taper method, is discussed further in Section 5.4.2. Methods employing the DFT are termed "non-parametric", which implies that no assumptions are made about the frequency distribution. Parametric methods such as the maximum entropy method make the assumption that new values are partially dependent upon previous values (Weedon, 2003).

### 5.3 Prior Study: Hughes et al. (2003)

Hughes et al. (2003) conducted a small-scale spectral analysis study of 256 rhythmites from Outcrop A, denoted by them as the Wharncliffe argillite. Noting that it was not possible to determine the period of couplet deposition from field evidence, yet recognizing dropstones in beds of laminated couplets of siltstone and claystone, Hughes et al. (2003) proposed that the couplets formed in a glaciolacustrine environment in association with recurring, annual, freeze-thaw cycles. Within the framework of this assumption of annual control, the authors proposed that variations in the thicknesses of the couplets in the measured section resulted from variations in climate on a year-over-year basis. Hughes et al. (2003) measured the couplets from photographs of the outcrop, and used both the DFT and the maximum entropy method to assess the data. Both of

these methods provided profiles of average spectral power at a given frequency using the complete data set. In order to allow for the assessment of variations in spectral power within the data set, Hughes et al. (2003) also conducted a coherent state analysis using a window of 20 layer couplets. A coherent state analysis seeks correlation amongst spectral peaks, and effectively identifies which peaks recur, and can thus identify whether or not a spectral peak is persistent throughout the dataset. In the Hughes et al. (2003) study, the most prominent peak in the couplet pattern was found to be at 14.3 layer couplets, with lesser peaks found at 27.8, 10.7, and 9.9 layer couplets. Hughes et al. (2003) connected the peak they found at 14.3 layer couplets with a peak period of 14.2 years found in the spectral analysis results of a regional temperature time series taken from central England. The peak at 14.3 layer couplets and the peak at 27.8 layer couplets of the Hughes et al. (2003) study also correlated well with the range (10.4 years – 27.3 years) of spectral peaks found in a study of the historical rainfall records of the Los Angeles Basin in California, USA. The periodicities of 10.7 and 9.9 layer couplets were interpreted as belonging to a single coherent mode, which the authors correlated to variability in the historical sunspot cycle record. Hughes et al. (2003) postulated that solar cycle variations could influence temperature and precipitation levels on an interannual time scale, citing sedimentary examples from the Modern, Eocene and Proterozoic. From these results, the authors concluded that both temperature and rainfall could have potentially influenced the thickness of the couplet layers found in the Gowganda Formation.

Hughes et al. (2003) also described a number of spectral peaks as holding less statistical significance due to a lack of coherence throughout the entire sequence. Describing these signals as “quasi-periodic”, the authors noted that quasi-periodic signals have been observed in modern climatic studies. For example, the El Niño Southern Oscillation (ENSO) is described as having a quasi-periodic cycle that ranges from 3 to 7 years (e.g. Rittenour et al., 2000; Breckenridge, 2007). In the Hughes et al. (2003) study the following quasi-periodic peaks were observed:

a) 2.97 and 3.17 layer couplets – peaks in the range of 2 to 70 months resemble the Quasi Triennial Oscillation, which involve modelled variances in atmospheric pressure suspected to result from changes in solar flux (Hameed et al., 1995),

- b) 6.10 layer couplets – similar to a 6.24 year peak in the atmospheric pressure spectrum associated with the Atmospheric Pole Tide (Hameed et al., 1995),
- c) 4 – 5 layer couplets – several small, non-coherent peaks within this range are similar to peaks found in the modern record that result from the influence of ENSO (3 – 7 years) and the North Atlantic Oscillation (NAO, 5 – 7 years) (Appenzeller et al., 1998),
- d) 77.2 layer couplets – perhaps associated with an NAO spectrum in the 80 – 90 year range (Appenzeller et al., 1998).

In connection with (a) and (b) above, Hughes et al. (2003) note that variances in sedimentation rates, and thus in layer couplet thickness, do not result directly from changes in atmospheric pressure variances. Changes in atmospheric pressure result from variations in solar flux, which is implied to lead to variances in layer couplet thickness. Hughes et al. (2003) acknowledge that all the above-noted periodicity correlations assume annual control for the Gowganda rhythmites.

Within this context, Hughes et al. (2003) identify events that may lead to discrepancies within the sedimentary record, and thus in the spectral analysis results of the rhythmite measurements. First, turbidite deposits may result in the deposition of one or more rhythmites that are not associated with the inferred annual freeze-thaw cycle. Second, extended periods of warm climate could lead to the deposition of multiple interannual couplets, and extended periods of cold climate could lead to periods of no deposition at all. Irregular variations between warm and cold periods could also confound attempts to diagnose interannual periodicities. Hughes et al. (2003) demonstrate that minor irregularities in the depositional process will not significantly change the results of the spectral analysis; however larger temporal or depositional anomalies could significantly alter the spectral profile, diluting the accuracy of the results. In conclusion, Hughes et al. (2003) suggest that the rhythmic deposition of the Gowganda Formation couplets warrants the interpretation of annual deposition in a glaciolacustrine environment, and that the spectral profile obtained from the sequence measured provides a moderate to robust signal of Paleoproterozoic climate. It should be noted however that not all authors agree with this interpretation. Citing the paleomagnetic results of Williams and Schmidt

(1997), which place the deposition of Huronian rocks at between 4° and 11° latitude (where seasonal freeze-thaw cycles generally do not exist in modern time), Young (2013) suggests that an alternate, non-seasonal mechanism may have produced the varve-like rhythmities.

## 5.4 The Present Study

This study expands upon the work of Hughes et al. (2003) by examining one record of 229 couplets and a second record of 585 couplets at Outcrop A, as well as one record of 216 couplets and a second record of 119 couplets at Outcrop B (refer to Figure 2-3 for location of outcrops). The goal was to determine if the results of Hughes et al. (2003) can be replicated in two similar sections of Outcrop A, and two similar sections of Outcrop B.

### 5.4.1 Field Sampling and Data Plotting

Rhythmities that form the interbedded siltstone and claystone lithofacies at Outcrop A, and the interbedded coarse-grained and fine-grained siltstone lithofacies at Outcrop B, are morphologically very similar, and were thus measured in the field for the purpose of spectral analysis. Outcrop A and Outcrop B emerge from the local soil on an angle, increasing in exposure height from right to left, and thus they were measured in sections of intervals in a stair-case fashion, with each section being horizontally continuous with the previous section. Each record was composed of 30 cm intervals, with each couplet being measured in the field using a tape measure from the base of a siltstone bed, which generally had higher relief, to the base of the overlying siltstone bed.

In Outcrop A, the lower record contains six 30 cm intervals for a total thickness of 180 cm. The couplets range from 1 - 18 mm thick, with an average thickness of about 7 mm (SD (standard deviation) 3; Figure 5-1). The rhythmite measurements in the lower record of Outcrop A do not display a trend of either increasing or decreasing thickness. The upper record of Outcrop A contains sixteen 30 cm intervals and one 20 cm interval for a total thickness of 5.0 m. The average couplet thickness for the upper record of Outcrop A was about 9 mm (SD 5), with couplets measuring 1 - 32 mm thick (Figure 5-2). The data for the upper record of Outcrop A shows a general increase in rhythmite thickness up-section, indicative of an increasing sedimentation rate that may be a result of increased

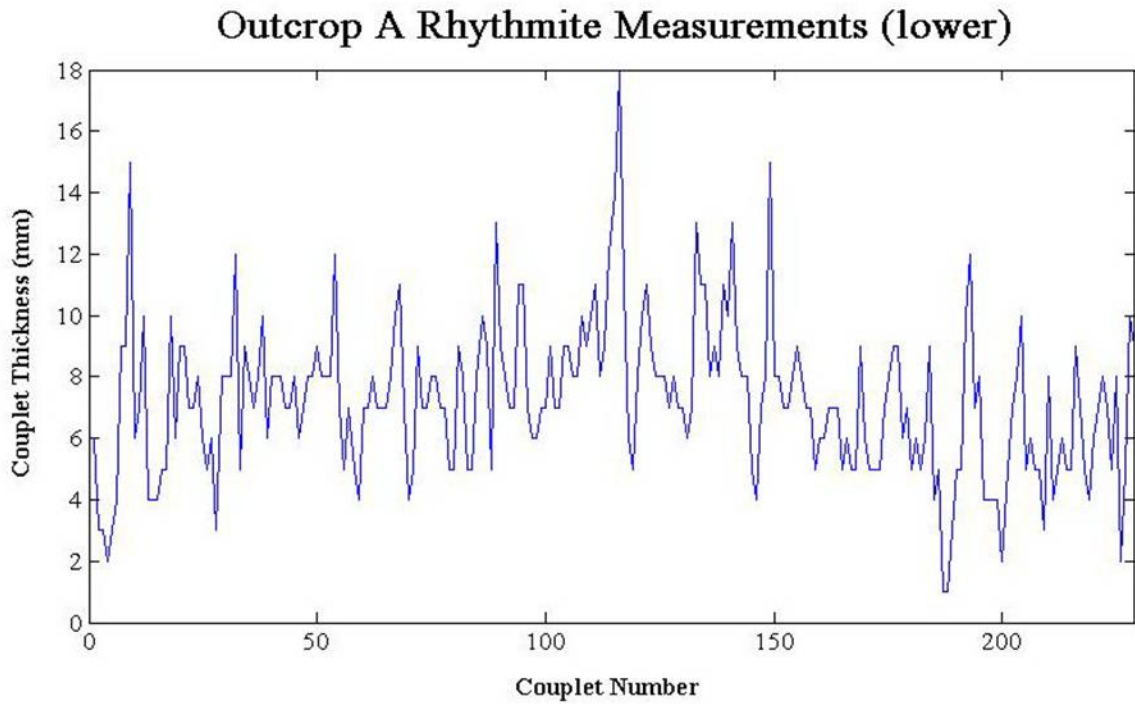


**Figure 5-1:** Plot showing the thickness of the 229 couplets that compose the lower set of measurements from Outcrop A.

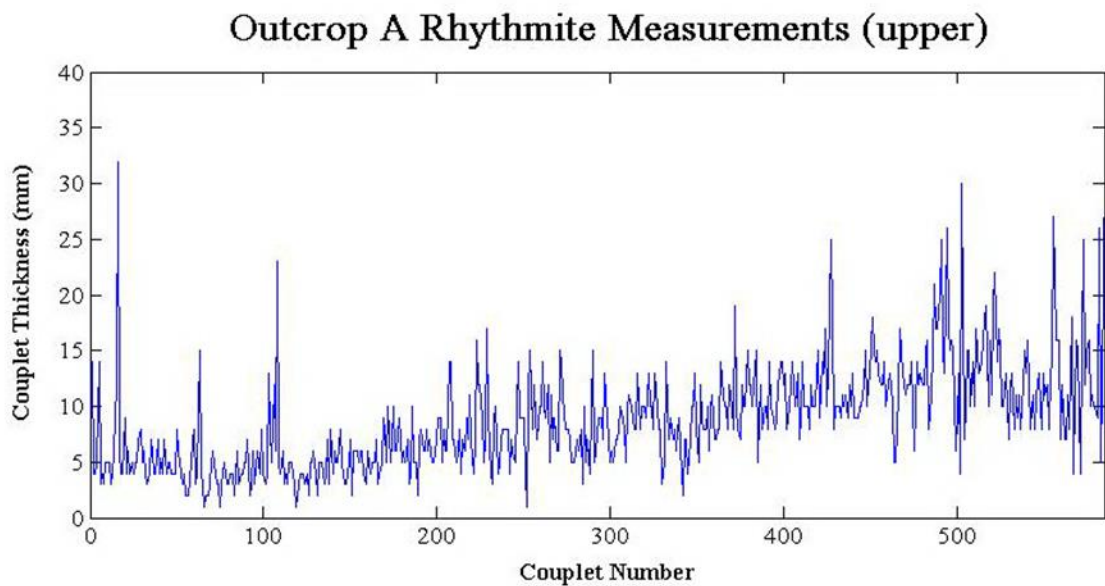


**Figure 5-2:** Plot showing the thickness of the 585 couplets that compose the upper set of measurements from Outcrop A.

glacial melting in a warming environment (Ridge et al., 2012). The lower and upper records of Outcrop A are separated by a 109 cm thick bed that is likely a slump deposit. Therefore, the lower and upper records comprise sequential, yet separated, data sets. Outcrop B was also measured from two records, with the lower record containing ten 30 cm intervals for a total thickness of 300 cm. The couplets range from 3 - 31 mm thick, with an average thickness of ~13 mm (SD 5; Figure 5-3). The upper record of Outcrop B was measured as five 30 cm intervals for a total thickness of 150 cm, with couplets ranging from 5 - 28 mm thick and having an average thickness of ~12 mm (SD 4; Figure 5-4). The lower and upper records of Outcrop B are separated by 80 cm of rhythmites that were too fractured to measure, and thus both records of Outcrop B comprise sequential, yet separated, data sets. The thickness measurements from both the lower and upper records of Outcrop B do not indicate an overall trend of increasing or decreasing thickness, which may indicate a period of steady sedimentation or reflect data sets that are too small to indicate an overall trend. Although the rhythmites that form the interbedded siltstone and claystone lithofacies at Outcrop A and the interbedded coarse-grained and fine-grained siltstone lithofacies at Outcrop B are morphologically similar, it is not known whether they represent the same, different, or overlapping depositional events.

#### 5.4.2 The Multi-Taper Method of Spectral Analysis

The multitaper method of spectral analysis (“MTM”) uses the average of multiple independent trials to estimate power spectra (Thomson, 1982). The MTM is a non-parametric method that employs the DFT. In a climate time series, the MTM can be used to separate climatic signals from the background noise in which they exist (Mann and Lees, 1996). Mann and Lees (1996) describe the background noise in climate systems as red noise, which is defined to be composed of white noise and an enhanced, low-frequency, slow-response climate signal such as that induced by the thermal inertia of the oceans. Red noise may comprise a significant proportion of the signal-plus-noise time series, leading to a low signal-to-noise ratio. The MTM Toolkit of Mann and Lees (1996) uses a parametric first-order autoregressive process (AR(1) process) to model the noise level, and fit this model to the data in order to estimate the noise. The AR(1) process

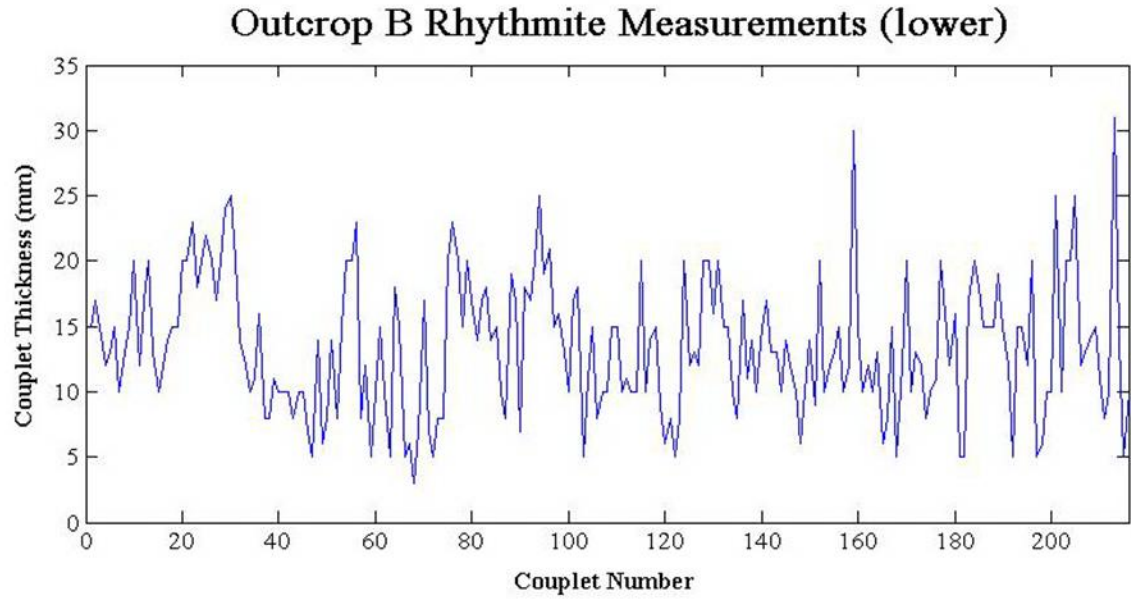


**Figure 5-3:** Plot showing the thickness of the 216 couplets that compose the lower set of measurements from Outcrop B.

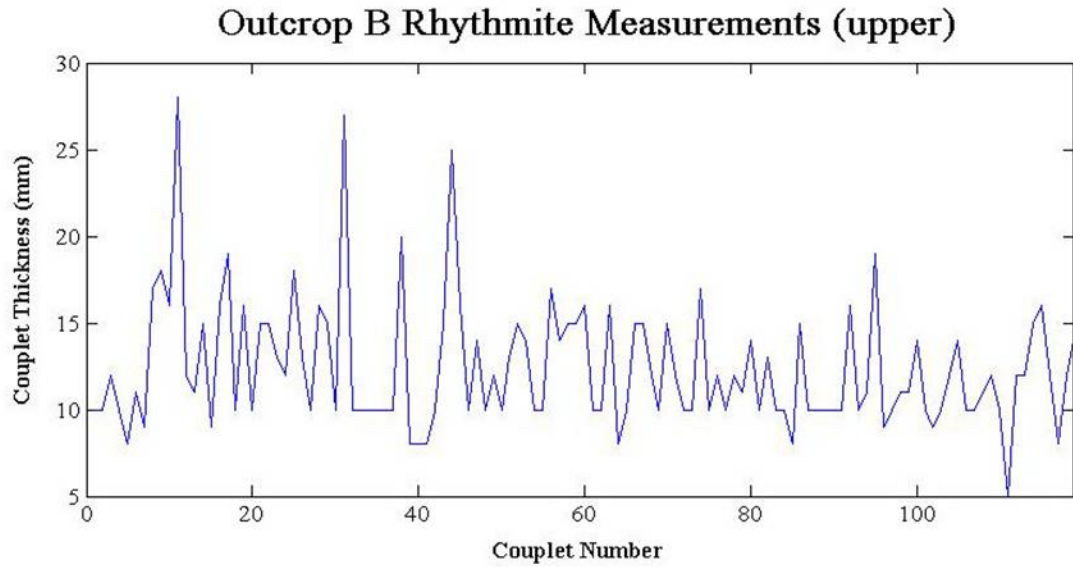


**Figure 5-4:** Plot showing the thickness of the 119 couplets that compose the upper set of measurements from Outcrop B.

is used to represent a noise series by expressing each sample in a time series using a linear combination of the previous sample and a white noise contribution. By applying an AR(1) process to white noise, the lower frequencies are naturally enhanced, leading to a red noise spectrum. Therefore, the MTM combined with the red noise model allows for improved noise identification, which leads to enhanced statistical significance of identified signals. In this study, the datasets are sufficiently small to allow for the use of 3 tapers (where the number of tapers used is  $K = 2p - 1$ ) and a time-frequency bandwidth  $p$  of 2.

### 5.4.3 Spectral Analysis Results

The spectral analysis results produced by the Hughes et al. (2003) data (G Hughes 2014, pers. comm., 5 July) using the MTM Toolkit are shown in Figure 5-5, and the spectral analysis results for the measurements of the four rhythmite records are provided in Figures 5-6 to 5-9. Harmonic peaks, shown in black, represent periodic signals that correspond to singular peaks in the power spectrum estimated by the MTM. The reshaped spectrum, which is calculated using a modified version of the reshaping process of Thomson (1982), is shown in red. The AR(1) red noise spectrum is estimated from the median-smoothed spectrum to provide a robust model for the noise background. The median line, shown in green, depicts the red-noise fit to the median-smoothed spectrum, and is calculated by replacing each frequency point in the reshaped spectrum with its median value. Three confidence levels are used to evaluate the distribution of the frequency as depicted by the reshaped spectrum, relative to background noise: 1) the 90% certainty line is shown in blue 2) the 95% certainty line is shown in yellow and 3) the 99% certainty line is shown in brown.

In the lower record of Outcrop A (Figure 5-6) quasi-periodic cycles of 4.4 and 9.2 couplets were noted with a 90% degree of certainty. Quasi-periodic cycles of 2.2 and 6.6 couplets were noted with a 95% degree of certainty, and a quasi-periodic cycle of 2.9 couplets was detected with a 99% degree of certainty. In the upper record of Outcrop A (Figure 5-7), a number of quasi-periodic cycles in the range of 2.3 to 4.4 couplets were found, in addition to quasi-periodic cycles of 4.9 and 8.8 couplets, all having a 90%

### MTM Spectrum Hughes et al. (2003) Data

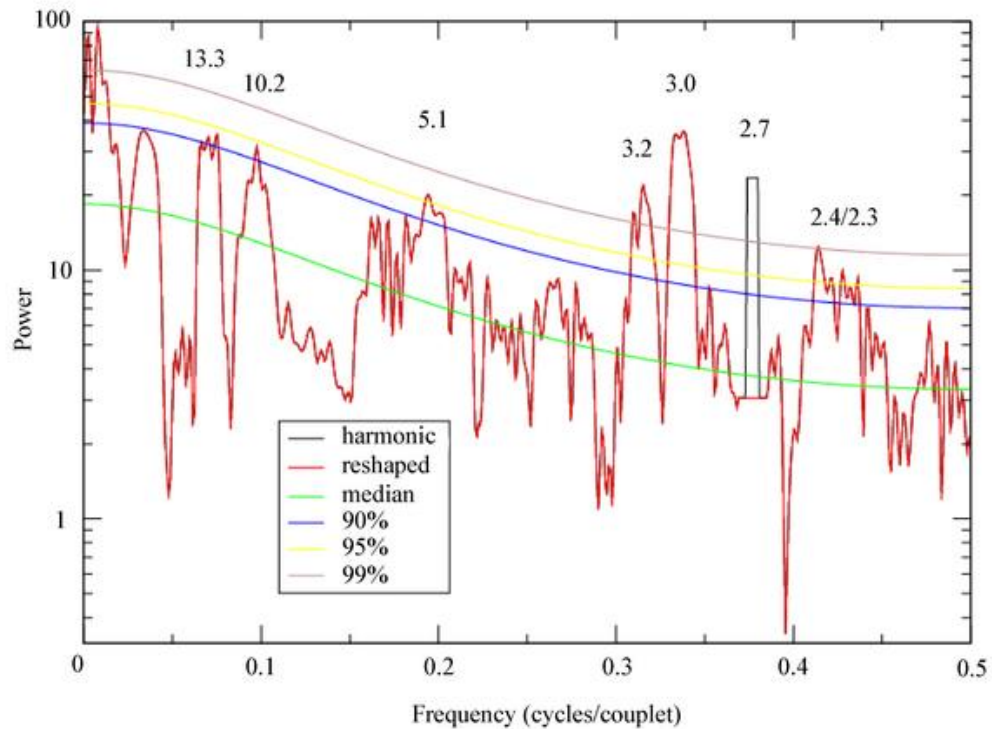


**Figure 5-5:** Spectral analysis results using the method of Mann and Lees (1996) for the rhythmite measurements of Hughes et al. (2003)(G Hughes 2014, pers. comm., 5 July). Quasi-periodic cycles with periods ranging from 2.3 to 13.3 couplets are shown. A harmonic cycle of period 2.7 couplets is indicated by the open black rectangle. The default frequency resolution of 2 and 3 tapers was used under the assumption of background red noise.

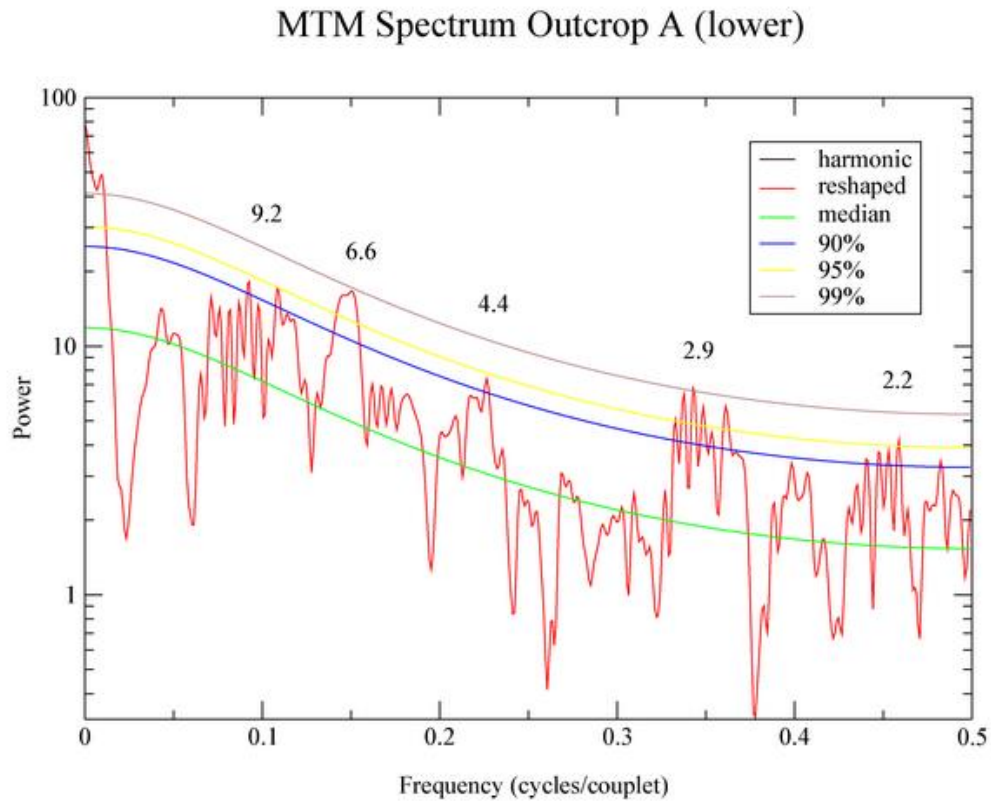


**Figure 5-6:** Spectral analysis results using the method of Mann and Lees (1996) for the lower rhythmite measurements from Outcrop A. Quasi-periodic cycles with periods ranging from 2.2 to 9.2 couplets are shown. The default frequency resolution of 2 and 3 tapers was used under the assumption of background red noise.

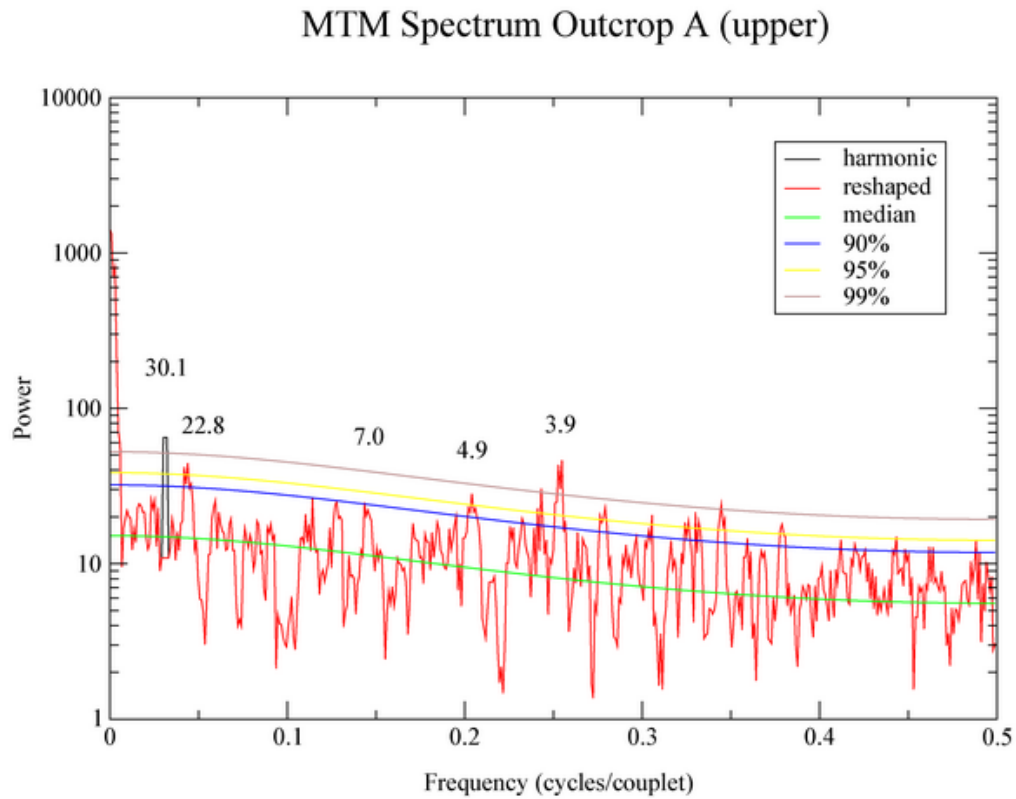


**Figure 5-7:** Spectral analysis results using the method of Mann and Lees (1996) for the upper rhythmite measurements from Outcrop A. Quasi-periodic cycles with periods ranging from 2.3 to 56.9 couplets are shown. A harmonic cycle of about 2.5 couplets is indicated in black by an open black rectangle. The default frequency resolution of 2 and 3 tapers was used under the assumption of background red noise.

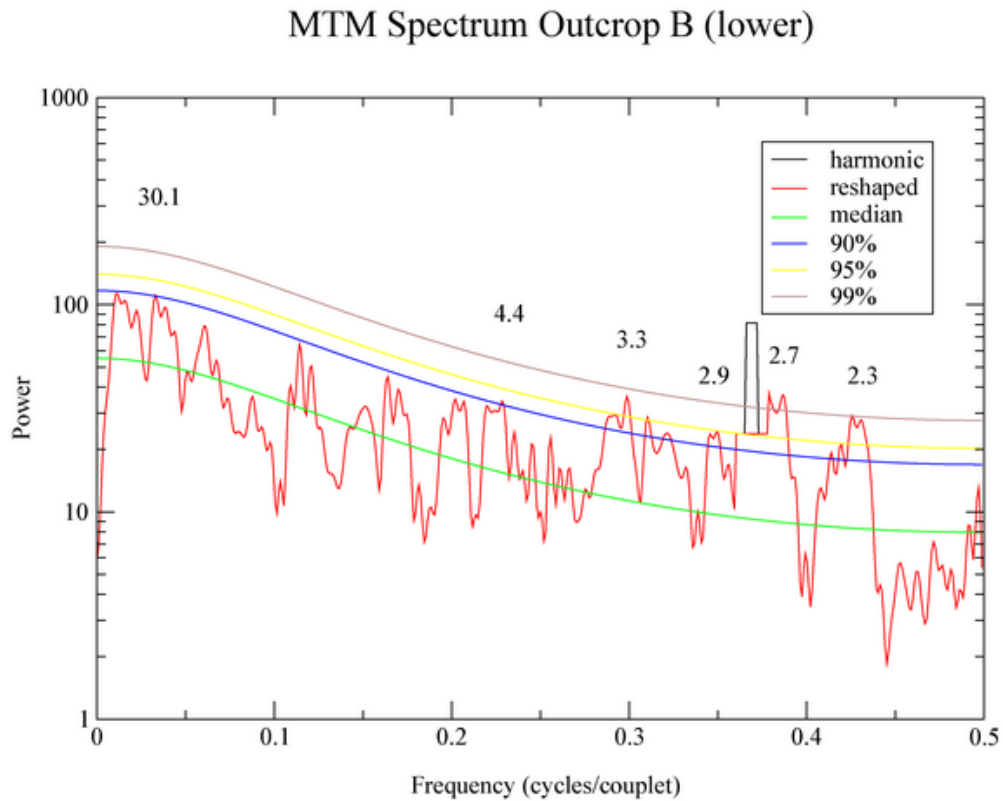


**Figure 5-8:** Spectral analysis results using the method of Mann and Lees (1996) for the lower rhythmite measurements from Outcrop B. Quasi-periodic cycles with periods ranging from 2.3 to 30.1 couplets are shown. A harmonic cycle with a period of about 2.8 couplets is indicated by the open black rectangle. The frequency resolution of 2 and 3 tapers was used under the assumption of background red noise.

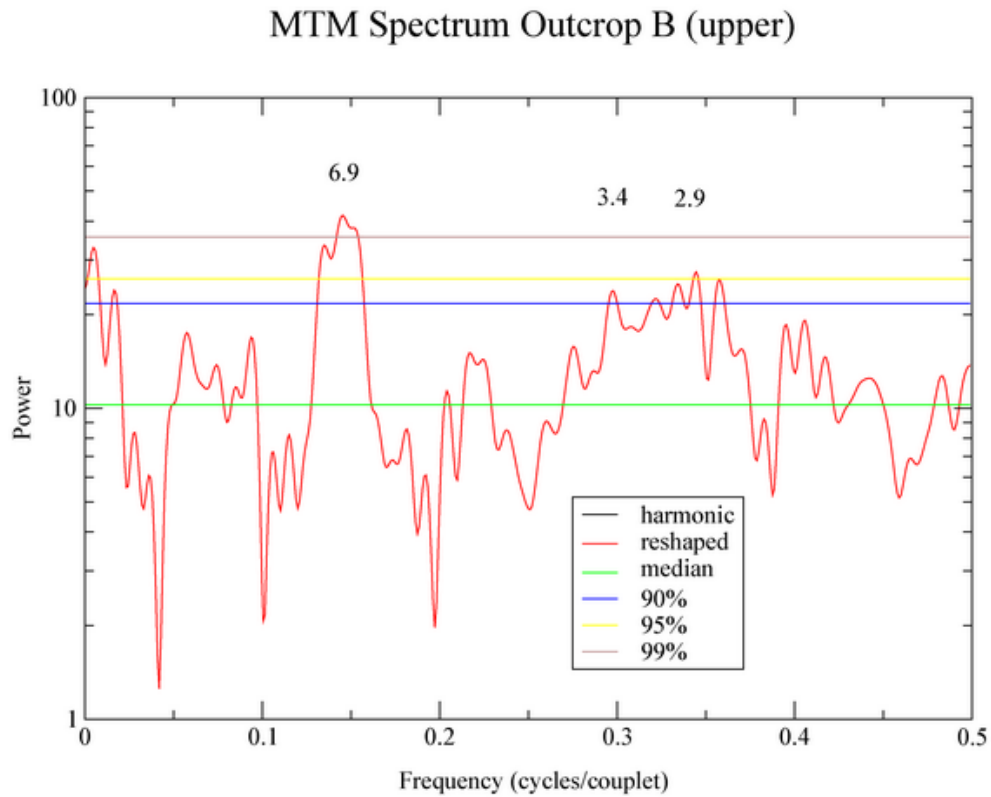


**Figure 5-9:** Spectral analysis results using the method of Mann and Lees (1996) for the upper rhythmite measurements from Outcrop B. Quasi-periodic cycles with a period ranging from 2.9 to 6.9 couplets are shown. The default frequency resolution of 2 and 3 tapers was used under the assumption of background red noise.

degree of certainty. A quasi-periodic cycle of 22.8 couplets, having a 95% degree of certainty, was also identified. Quasi-periodic cycles of 56.9 and 31.0 couplets (99% certainty) were also evident in the results. A harmonic cycle of 2.4 couplets was also identified.

The results from the lower record of Outcrop B (Figure 5-8) show a number of quasi-periodic cycles in the range of 2.3 to 4.4 couplets, and a quasi-periodic cycle of 30.1 couplets all having a 90% degree of certainty. A harmonic cycle of 2.8 couplets was also observed. The results from the upper record of Outcrop B (Figure 5-9) indicate a quasi-periodic cycle of 6.9 couplets having a 99% degree of certainty, and a few quasi-periodic cycles in the range of 2.9 to 3.4 couplets (90% - 95% degree of certainty).

#### 5.4.4 Spectral Analysis Interpretation

The spectral analysis results are summarized in Table 5-1. For comparison purposes, the spectral analysis results as originally published by Hughes et al. (2003) are also shown in Table 5-1. With one exception, the MTM Toolkit identifies similar peaks in the Hughes data to those published in Hughes et al. (2003).

If the deposits of Outcrop A are considered to represent annual rhythmites, as proposed by Hughes et al. (2003), and a similar interpretation is extended to Outcrop B, then the results of this study can be compared to both the Hughes et al. (2003) results and similar results obtained from Holocene and Pleistocene varve studies. Two spectral analysis studies have been conducted in the Great Lakes region of North America recently: Godsey et al. (1999) on Lake Huron varves, and Breckenridge (2007) on Lake Superior varves. In addition, Rittenour et al. (2000) conducted a spectral analysis study of the varves in glacial Lake Hitchcock, a proglacial lake that existed in the Connecticut River valley of the New England region of the United States during the late Pleistocene/early Holocene.

A cluster of periodicities within the range of 2.2 – 2.9 years was determined for all four rhythmite records in this study. Cycles within this range are reminiscent of the modern day quasi-biennial oscillation (QBO), periodic changes in stratospheric equatorial wind

**Table 5-1: Summary of spectral analysis results from this study, and the Hughes et al. (2003) study**

Outcrop A (lower) n=229 <i>period (couplets)</i>	Outcrop A (upper) n=585 <i>period (couplets)</i>	Outcrop B (lower) n=216 <i>period (couplets)</i>	Outcrop B (upper) n=119 <i>period (couplets)</i>	Hughes (MTM) <sup>1</sup> n=256 <i>period (couplets)</i>	Hughes (published) <sup>2</sup> n=256 <i>period (couplets)</i>
	56.9				
	31	30.1			
	22.8			13.3	14.3
9.2	8.8			10.2	10.7, 9.9
6.6			6.9		6.1
4.4	3.0 - 4.9	3.3 - 4.4	3.0 - 3.4	3.0 - 3.2, 5.1	3.0 - 5.0
2.2 - 2.9	2.3 - 2.9	2.3 - 2.9	2.8 - 2.9	2.3 - 2.9	2.3 - 2.9

Results are shown for detected signal periods (in couplets).

Results from the Hughes et al. (2003) study as published<sup>1</sup>, and as produced by the MTM Toolkit<sup>2</sup>, are shown with this study's results.

directions that cyclically vary with a period of 22 to 34 months (Baldwin et al., 2001). The QBO impacts the stratospheric polar vortex, which in turn influences weather patterns on the surface of the Earth. Godsey et al. (1999) also attributed periodicities within the range of 2 - 3 years to the Southern Oscillation Index.

A number of low periodicity events within the range of 3.0 – 6.9 years were also determined from the four rhythmite records. Godsey et al. (1999) and Rittenour et al. (2000) attribute periodicities of three to seven years to climatic fluctuations associated with ENSO, the El Niño – Southern Oscillation. Hughes et al. (2003) and Breckenridge (2007) attribute periodicities of three to six years to ENSO, and periodicities of six to seven years to NAO, the North Atlantic Oscillation. A summary comparison of the results of this study and the results of similar studies is provided in Table 5-2.

Table 5-1 shows that some periodicities appear in more than one record. A periodicity of 9.2 years was identified in the lower record of Outcrop A, which is similar to the periodicity of 8.8 years found in the upper record of Outcrop A. This periodicity, however, was not evident in the results from Outcrop B. The periodicity of 31 years determined from the upper record of Outcrop A is similar to the periodicity of 30.1 years determined from the lower record of Outcrop B. This periodicity, however, was not characteristic of the lower record of Outcrop A or the upper record of Outcrop B. Periodicities of 56.9 and 22.8 years occur only once, in the upper record of Outcrop A and in the lower record of Outcrop A, respectively. Thus, the four records measured, as well as the Hughes et al. (2003) data, reveal periodicities in the order of 3 years (couplets). This suggests that climate systems such as QBO and ENSO may have been operational in the Paleoproterozoic, and supports the hypothesis that the rhythmic couplets were deposited on an annual basis.

**Table 5-2: Comparison of this study with similar studies conducted near the Great Lakes region.**

<b>Study</b>	<b>Deposits</b>	<b>ENSO</b>	<b>NAO</b>
Godsey et al. (1999)	Lake Huron sediments	3 - 7 years	n/a
Rittenour et al. (2000)	Lake Hitchcock sediments	3 - 7 years	n/a
Breckenridge (2007)	Lake Superior sediments	3 - 6 years	6 - 7 years
Hughes et al. (2003)	Gowganda Fm sediments	3 - 6 years	6 - 7 years
This study (2015)	Gowganda Fm sediments	3 - 6 years	6 - 7 years

If the period of deposition is interpreted to be one year then spectral signals in the 3 - 6 year range may result from oceanic oscillations similar to the El Niño Southern Oscillation (ENSO) and periods of 6 – 7 years may indicate the influence of an oceanic oscillation similar to the North Atlantic Oscillation (NAO).

## 6 Discussion

The sedimentological, geochemical and spectral analysis results from the studied deposits enable interpretation of the paleoenvironmental conditions operating during deposition of the upper Gowganda Formation. The geochemical results indicate that the minerals that compose the rhythmites have not undergone significant post-depositional alteration and do not contain a significant contribution from pre-existing supracrustally modified source rocks. Thus, the geochemical results are consistent with what would be expected from sediment that was glacially eroded, transported within ice, and then deposited without being subjected to great transport distances or subaerial exposure. The presence of clasts interpreted to be dropstones throughout many of the lithofacies also imply a depositional environment that is proximal to glacial ice and a body of water (Benn and Evans, 2010). Therefore, a description of key glacial landforms near the land-water interface is important, and is provided below. The focus is mainly on the two varve-like rhythmite-containing lithofacies: the interbedded coarse-grained siltstone and fine-grained siltstone lithofacies, and the interbedded siltstone and claystone lithofacies.

### 6.1 Deltas and Fans in Glacially-Influenced Environments

Where glacial ice is present along the margin of a basin, one or more ice-contact deltas or subaqueous fans may form (Ashley, 2002). Deltas form as a result of the fluvial transport of sediment into a standing body of water (Benn and Evans, 2010). As river water meets a water body the flow decelerates, resulting in the immediate deposition of coarse-grained sediment, and a merging of fine-grained suspended sediment, with the water body (Reineck and Singh, 1980). Fine-grained sediment that settles out of suspension contributes to the building of the delta, as do turbidity currents/turbidites, which are initiated by the gravitational failure of sediment that accumulates on the upper delta slope (Benn and Evans, 2010). Deltas are broadly defined to consist of three components: 1) Topsets, which are the deposits that exist on the upper delta surface; topsets may be deposited on the delta plain, or overlie foresets; 2) Foresets, also called clinofolds, are the layers that form the delta front, the shallow or steeply dipping face of the delta that builds out into the water body, and 3) Bottomsets, which are the deposits that form at the

base of the delta, beyond the foresets. The prodelta environment extends from the bottomsets to the non-deltaic basinal deposits (Reineck and Singh, 1980; Ashley, 2002; Benn and Evans, 2010). The total energy dissipated by the fluvial system upon reaching the water body determines the type of delta formed (Ashley, 2002). The following discussion considers the formation of glacially influenced deltas and fans in a lacustrine environment; however deltas and fans may also form in marine environments (Benn and Evans, 2010).

### 6.1.1 Ice-contact Deltas

Ice-contact deltas are subaerial to subaqueous sediment masses that expand into a lake as a result of the delivery of local glaciofluvial detritus. A stable meltwater stream will form a single delta whereas a meltwater stream that redirects itself (avulses) over time, or that splits into secondary branches, will form multiple deltas (Ashley, 2002). The bedding and textural characteristics of the delta foresets depends on the energy of the fluvial system. A higher energy system forms a Gilbert-type delta, which is characterized by steeply dipping beds composed of sand and clasts (Gilbert, 1890). Sediment transport from the upper reaches of the delta to the base is accomplished by mass movement ranging from avalanching, to creep and slump, to turbidity flows (Nemec, 1990; Benn and Evans, 2010). A lower energy system produces fine-grained, shallowly-dipping foresets that are characterized by rapid sedimentation and dewatering structures (Ashley, 2002), lithological attributes observed in the present study. Sediment transport is dominated by underflow currents (turbidites), with intermittent deposition of ice-rafted debris and diamictite (Smith and Ashley, 1985; Ashley, 2002). Post-depositional deformation of beds is common given high rates of sedimentation, and gravitational collapse results when adjacent or underlying ice melts (Ashley, 2002). Sandy delta foresets transition to clay-draped climbing ripple deposits, which transition distally to planar bottomsets composed of clay laminations that form as density underflows abate (Kelly and Martini, 1986).

### 6.1.2 Ice-contact Subaqueous Fans

Subaqueous fans form where glaciofluvial sediment is transported to an adjacent water body via basal glacial tunnels (e.g. Donnelly and Harris, 1989). The elevation of a subaqueous fan is independent of lake level, which distinguishes a fan from an ice-contact delta. The latter forms its topset-foreset contact at lake level (Ashley, 2002). Multiple fans formed along a glacial front may coalesce to form an end moraine (Sharpe and Cowan, 1990). Proximal deposits consist of sands containing large clasts whereas the mid-fan region is composed of mass flow deposits. Both environments display dewatering structures that indicate rapid deposition (Ashley, 2002 and references therein). Distal fan deposits are inferred to be constructed in the same manner as distal deltaic deposits, with clay-draped climbing ripples giving way distally to parallel laminations (Ashley, 2002).

### 6.1.3 Glaciofluvial Deltas

Glaciofluvial lakes are primarily fed by the outwash stream(s) of a glacier that is not in direct contact with the lake (Benn and Evans, 2010). Stream channel diversion into a lake basin leads to an increase in the rate of sedimentation (Coleman and Prior, 1982). Gilbert (1975) demonstrated that river sediment discharge rates directly influence the thickness and composition of basin deposits. Coleman and Prior (1982) confirmed this observation, recognizing an upsection increase in layer thickness, wherein sandstone and siltstone interbedded with thinly laminated claystone layers coarsen upwards into sandstone-dominated deposits. Coarse-grained outwash sediment is predominantly deposited on the sandur (outwash plains) that separates the glacier from the glacial lake, resulting in lake deposits that are finer-grained and well sorted (Ashley, 2002).

The deltas that form in glaciofluvial lakes may be steeply dipping, composed of gravels and coarse-grained material if the ice face is proximal to the lake, or deltas may have low-angle foresets ( $5^{\circ}$  to  $15^{\circ}$ ) and be mostly composed of finer-grained materials (sands and silts) if the ice-face is distal (Benn and Evans, 2010). In the upper delta of both types, rhythmic beds of upward-fining sand and gravel are common, generally resulting from distributary channel relocation or intermittent periods of high discharge (Ashley, 2002).

Low-angle deltas are primarily composed of climbing-ripple sequences draped by clay that has been dispersed distally above the thermocline by sediment influx momentum and wind stress before settling from suspension (Ashley, 2002). Although the clay drapes in this environment have been interpreted to result from clay rainout during the winter freeze season (Gustavson et al., 1975), flume studies and field evidence suggest that lapses in depositional energy can lead to the deposition of clay layers over climbing ripples multiple times within the summer melt season, and thus a layer of clay does not necessarily indicate a varve terminus (Smith and Ashley, 1985). Proximal to the base of the delta climbing ripple sequences, which are formed by the virtually steady supply of glaciofluvial sediment, may be interbedded with turbidite sequences resulting from gravitational failure on the delta slope (Smith and Ashley, 1985; Ashley, 2002).

Glaciofluvial outwash streams may form a series of deltas along the margin of a glaciofluvial lake (Ashley, 2002). Lakeshore-proximal sediments in the zones between neighbouring deltas are mostly composed of re-worked coarse-grained sediments delivered to the zones from the adjacent continental landmass, and clays that settle from suspension (Ashley, 2002). Near-shore beach deposits grade into unstratified silts and muds in deeper water (Sturm and Matter, 1978).

Lake basin deposits are controlled by their proximity to the delta(s) that formed them (Ashley, 2002). Distally, lake basin deposits are primarily composed of parallel-laminated rhythmites (Benn and Evans, 2010). Coleman and Prior (1982) note that the rhythmic laminations found in the lower part of lacustrine delta-fill deposits resemble varve deposits. Overlying rhythmites become thicker and coarser-grained as a delta progrades into a basin (Smith and Ashley, 1985). As the delta progrades, basinal beds become rippled and multi-laminated, and can eventually display deltaic characteristics as lake basin infilling proceeds (Ashley, 2002). Rhythmites may become thinner and finer-grained as a delta is abandoned (Smith and Ashley, 1985). Interbedded mass movement deposits such as turbidites and slumps can also be found locally (Smith and Ashley, 1985). As turbidity currents decelerate at the base of a delta they may also form rhythmic deposits that resemble varves (e.g. Bouma sequence  $T_d$  deposits, Bouma, 1962).

## 6.2 Gowganda Formation Rhythmites: Varves, Turbidites or Both?

Rhythmites of the upper Gowganda Formation in the study area display the characteristics of both varves and turbidites. Lindsey (1969) and Hughes et al. (2003) have proposed that the rhythmites are varves, whereas Eyles (2008) suggests that most Gowganda Formation deposits resulted from debris flows. In order to properly characterize the rhythmites of the Gowganda Formation, various descriptions of varve classification are provided in the following sections.

### 6.2.1 Grouping Varves by Fine-grained Layer Thickness

Ashley (1975) classified the types of varves found in glacial Lake Hitchcock, New England, USA based on their composition. Ashley (1975) identified three types of varves: Group I varves have a fine-grained (clay) layer that is thicker than the coarse-grained (silt) layer, Group II varves have a fine-grained layer that is approximately the same thickness as the coarse-grained layer, and Group III varves have a coarse-grained layer that is thicker than the fine-grained layer.

### 6.2.2 Group I Varves

Group I varves as described by Ashley (1975) closely resemble the rhythmic couplets that compose the lower section of the interbedded siltstone and claystone lithofacies found at Outcrop A, where the claystone layers are thicker than the siltstone layers. Ashley (1975) interpreted Group I varves as being deposited within a lake basin distal to major river deltas. Coarser grained layers were proposed to be deposited by turbidity flows that reached the area of varve deposition only during periods of high runoff, while fine-grained layers were deposited by clay rainout during periods of quiescence. On an annual basis, the quiescent period was thought to dominate, accounting for the thicker clay layer. The couplets that compose the lower section of the interbedded siltstone and claystone lithofacies have previously been interpreted as varves (e.g. Lindsey, 1969; Hughes et al., 2003); however micro-laminae, which were identified in the Gowganda rhythmites, may be present in both varve and turbidite deposits.

### 6.2.3 Micro-laminae within Varve Layers

The presence of multiple micro-laminae is a distinguishing feature of many of the rhythmite layers in the interbedded siltstone and claystone lithofacies, and in the morphologically similar interbedded coarse siltstone and fine siltstone lithofacies. The claystone layers contain multiple planar micro-laminae, each displaying minor variations in colour and texture and often separated by a very thin siltstone layer (Figure 3-8-A, -D). Micro-laminae in siltstone layers display a wavy pattern, and often alternate between siltstone and claystone. Gilbert (1975) observed micro-laminae within both the finer-grained winter layers and the coarser-grained summer layers in varves of glaciofluvial Lillooet Lake, British Columbia, which were attributed to intermittent underflow events. Micro-laminae in silt layers were recently observed in glaciolacustrine varves in Scotland, and photomicrographs also appear to display micro-laminae in some mud layers (Bendle et al., 2015). Micro-laminae have also been identified by Leckie and McCann (1982) in deltaic deposits of a proglacial lake constructed when an ice dam formed near the mouth of the Conne River in southern Newfoundland during the late-Wisconsinan. Hambley and Lamoureux (2006) also observed multiple micro-laminae in varves formed by seasonal snowmelt in a closed lacustrine, non-glacial environment. Thus, micro-laminae are clearly associated with depositional environments influenced by seasonal glacial and nival melt, suggesting that starts and pauses in melting result in minor pulses of sediment transport.

### 6.2.4 Micro-laminae in Turbidite Deposits

Fine-grained, mud-rich turbidite systems characterize medium- to large-sized basins. (Bouma, 2000). The depositional environment associated with fine-grained mud-rich turbidite systems is typically long, wide and flat. Sediment is normally fine-grained sand or finer with low sand/clay ratios, and sediment volume is typically large. Progradation is likely rapid as basin infilling proceeds, and slows or ceases as the sediment source avulses. In a fluvial environment, the strength of the flow of water often varies with changes in seasons, which can lead to variations in both the grain size that is entrained and in the quantity of sediment that is transported (Bouma, 2000).

### 6.2.5 The Micro-laminae in this Study

The micro-laminae in the claystone layers of this study resemble distal  $T_d$  turbidite deposits (planar laminated mud). Glacial melt would have produced muddy water that experienced gravitational acceleration and turbulence as it travelled down the delta front. Planar layers would have formed in the prodelta or deep basin setting as energy dissipated. Each discrete lamina represents a period of runoff that was interrupted by a short- or long-term freeze cycle. At the time of deposition, the claystone layers would have been composed of rock flour (mostly pulverized quartz and feldspar) and very little clay, and thus the depositional flows were likely non-cohesive. Non-cohesive turbidites are characterized by low density, high turbulence and rapid deposition (Talling et al., 2012). Particle aggregation and flocculation is low, with any suspension settling being reworked by subsequent turbidity flows.

Siltstone micro-laminae in the Gowganda deposits are mainly parallel and wavy. Combined with the coarser grain size, these structures indicate higher transport energy, which is inferred to have been provided by greater volumes of water from glacial melt. These laminae are interpreted to represent distal  $T_c$  deposits (ripple or climbing ripple cross-lamination). Therefore, the rhythmites of this study are interpreted as repeating  $T_c$  and  $T_d$  turbidites. Whether a  $T_c$  layer or  $T_d$  layer is formed depends upon fluvial depositional energy, which is inferred to be controlled by the rate of glacial melting. The fact that  $T_c$  layers and  $T_d$  layers form in groups, and that these groups alternate with each other, suggests that periods of warm weather that led to extensive glacial melting alternated with periods of cold weather. Thus, each micro-lamina is interpreted to represent a single depositional event. Each siltstone layer and claystone layer consists of a composite of micro-laminae that accumulate during periods of greater melting and lesser melting respectively. In the modern world this activity is associated with an annual winter/summer, freeze/thaw cycle in temperate regions. If the same freeze/thaw cycle can be applied to the Paleoproterozoic environment this implies that each couplet is in fact a varve. Sequential rhythmic layering of hundreds of couplets strongly argues for annual control. It therefore follows that varves, at least in this study, are composed of grouped couplets of micro-turbidites.

### 6.2.6 Group II Varves

Varves that contain a clay layer that is approximately the same thickness as the silt layer are classified as Group II varves (Ashley, 1975). Group II varves vary considerably in overall thickness from one lake locality to another, and are therefore divided into three subgroups. Subgroup IIa varves are thinly laminated (average 0.25 cm thick), found only in the upper parts of a lake section, and interpreted to represent distal delta deposits that form during the terminal phase of sedimentation. Subgroup IIb varves are moderately laminated (average 0.5 cm to 0.75 cm thick), and have silt layers that contain erosional contacts, graded beds and small scale cross-lamination. Varves of this type form beyond the bottomsets of a delta, but not as distally as Subgroup IIa varves. Subgroup IIc varves are bedded (averaging  $\geq 1.25$  cm thick) and are confined to topographic lows (basin or trough) at least 1.5 km away from a delta.

The Subgroup IIb varves as described by Ashley (1975) closely resemble the rhythmic couplets that compose the upper section of the interbedded siltstone and claystone lithofacies that are found at Outcrop A (Figure 6-1), where claystone and siltstone layers have similar thicknesses, and where rhythmic beds are frequently interbedded with rippled lenses of sandstone. Subgroup IIb varves, which were identified at a water depth of 26 m and in excess of 3 km from shore, were interpreted by Ashley (1975) to have been deposited by turbidity currents. Reineck and Singh (1980) place similar deposits (their Figure 454a) in a delta front environment. In this study, the rhythmites that resemble Subgroup IIb varves overlie rhythmites that resemble Group I varves, and are interpreted to represent prodelta-to-delta front deposits, deposited by turbidites. Deposits resembling Group III varves described by Ashley (1975) were not found in the study area.

## 6.3 Spectral Analysis of the Rhythmite Measurement Data

If the couplets are interpreted to represent annual depositional events, the short term periodicities of 2 – 4 couplets found in all rhythmite records may indicate the influence of climatic systems, similar to the modern day QBO and ENSO, which may have been operational during the Paleoproterozoic. This interpretation would support the hypothesis

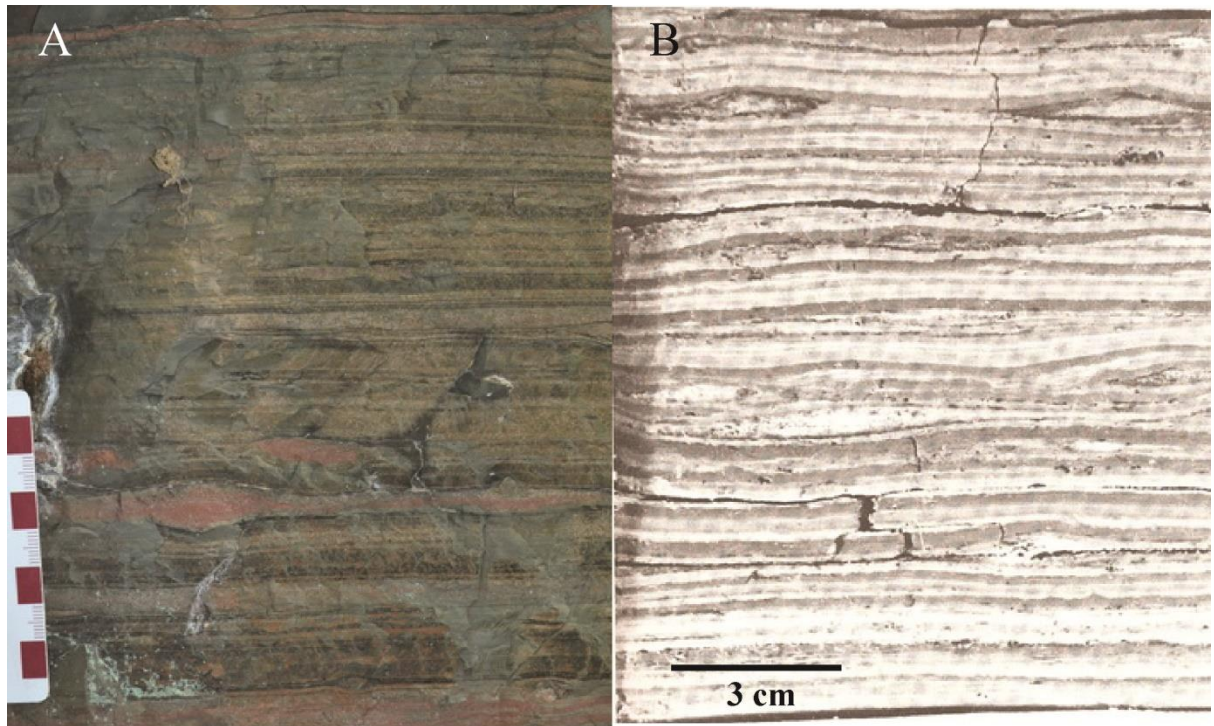


**Figure 6-1:** Centimetre-scale rhythmic deposits found in the upper section of the interbedded siltstone and claystone lithofacies at Outcrop A (A) bear a strong resemblance to Subgroup IIb varves (B) formed by turbidity currents 3 km from shore in 26 m of water in glacial Lake Hitchcock (Ashley, 1975). Scale in A is in cm.

that the rhythmic couplets represent annual deposits. Longer term periodicities were also identified in all four records; however these periodicities lacked consistency, appearing in some records but not others (Figure 5.1). For example, a periodicity of about 9 couplets (9.2 for the lower record of Outcrop A; 8.8 for the upper record of Outcrop A) was not identified in Outcrop B. Similarly, a periodicity of about 31 couplets (31 for the upper record of Outcrop A; 30.1 for the lower record of Outcrop B) was not identified in the other two records. In addition, periodicities of 22.8 and 56.9 couplets were found only in the upper record of Outcrop A. Possible explanations for these inconsistencies include variations in the depositional environment, gaps in the varve chronology, the varve formation process, and errors attributable the model.

### 6.3.1 Variations in the Depositional Environment

Longer term periodicities identified in some records were at best only confirmed in one additional record, which indicates either that the model has produced a false positive result, or that the longer term results are not consistent from one record to the next. This may be a function of the nature of the sedimentary structures and grain sizes at different outcrops, the uncertainty in stratigraphic level, and gaps in the stratigraphic record.

The depositional environments of the measured rhythmite records at Outcrop A and Outcrop B are not the same. The couplets of the former are composed of claystone and siltstone, whereas the couplets of the latter are composed of fine- and coarse-grained siltstone. This variance may be attributed to different locations within one deltaic environment, different locations in separate deltaic or basinal environments, temporal variations in deposition, or a combination of these factors.

In addition, Outcrop A is characterized by sandy, cross-bedded lenticular/wavy beds. Greater accuracy in the spectral analysis results for Outcrop A could potentially be achieved by removing the measurements of the lenticular/wavy beds. These beds have erosional bases, however, implying that the layers underlying them are thinner than when they were originally deposited. It is reasonable to expect the spectral analysis results of the lower and upper records at each of the two studied sites to show a high degree of correlation if in fact rhythmite deposition was influenced by a consistent external

mechanism. Unfortunately, this could not be demonstrated due to gaps in the rhythmite chronology, which may be attributable to one or more of the following factors.

### 6.3.1.1 Gaps in the Varve Chronology

If glacial melting ceases completely for an extended time period, the “missing data” is not accounted for in the spectral analysis model. Rittenour et al. (2000) found it necessary to exclude ice-proximal and thin ice-distal varves in glacial Lake Hitchcock from their spectral analysis, stating that these varves failed to provide accurate data about annual glacial melt and the regional climate. Where accuracy ceased and inaccuracy commenced was not elucidated. Also, the failure of modern varve chronologies to correlate well with  $^{14}\text{C}$  dating can suggest gaps (missing varves) in the chronology (e.g. Breckenridge, 2007; Hyodo and Longstaffe, 2011; Prasad and Baier, 2014).

### 6.3.1.2 Varve Formation is a Complex Process

The interpreted depositional environment for the upper Gowganda Formation in the study area is dynamically complex, with sedimentation influenced by both delta progradation and glacial recession. Locally, delta progradation results in increasingly thicker beds (Reineck and Singh, 1980) whereas glacial recession results in lower sedimentation rates (Fleisher et al., 2003). Thus, variances in rhythmite thickness can result independent of external forcing. Ridge et al., (2012) also noted that prodeltaic varves may be difficult to correlate on a regional basis due to the influence of local processes.

The processes involved in the formation of varves remain controversial. For example, sediments in Lake Huron and Lake Superior are characterized by red and grey layers (e.g. Godsey et al., 1999; Breckenridge, 2007; Hyodo and Longstaffe, 2011). Farrand (1969a, 1969b) proposed that the sediment composing the red layers in the Lake Superior deposits originated from a different source than the sediment composing the grey layers. In this model, the grey sediment was derived from northern glacial tills during the colder part of a year and red sediment is derived from southern, iron-rich tills during the warmer part of a year. This model allows for sedimentation resulting from both glacial outwash and precipitation, which maintains an annual formation cycle but may complicate spectral analysis if the goal is to identify external influences on glacial ice. Alternatively,

Breckenridge (2007) argued that both the grey and red clay layers of the Lake Superior varves were derived from the receding ice sheet at the time of deposition (possibly combined with outflows from Lake Agassiz), allowing for the use of spectral analysis on a Lake Superior varve dataset to seek periodicities. The Breckenridge (2007) model, however, does not account for sedimentation that may have resulted from fluctuations in precipitation. Carbon and oxygen isotope analysis of detrital calcite derived from both the red and grey clay layers indicated that they are derived from different sources (Hyodo and Longstaffe, 2011), which may indicate that some Lake Superior varves are glacially derived while others are not.

Multiple depositional processes may also be contained within the annual boundaries delineating a single varve. In a study of Nicolay Lake, located on Cornwall Island in the Canadian High Arctic, Hambley and Lamoureux (2006) identify three subannual depositional layers found within the annual parameters that define a varve: 1) a basal layer that is deposited by sedimentation resulting from nival melt in the spring; 2) a layer resulting from hydrological events induced by precipitation, and 3) a layer resulting from sporadic mass wasting events such as turbidites or slumps. In proximal, near-shore locations, varve deposits are thick, and subannual rhythmite layers are more easily identified. Distal deposits from the deeper basin are composed of “simple couplets” that apparently have the subannual layers intermixed.

By comparing local weather station records with nival melt rhythmite thicknesses, Hambley and Lamoureux (2006) found a strong correlation between nival melt sedimentation and cumulative seasonal melt degree days. The combined measured thickness variations in meteoric-induced hydrological events and mass wasting events were demonstrated to be randomly variable and not associated with cumulative melt degree days in a season. Hambley and Lamoureux (2006) also concluded that although distal couplets deposited in the lake basin present a varve facies, they are composed of an unknown combination of nival melt, hydrologic precipitation and mass wasting. It is therefore likely that any climatic signal identified in distal varves (i.e. through the use of spectral analysis) represents a nival melt signal weakened by hydrological and mass wasting events. This result implies that for the spectral analysis of glacially induced

rhythmic deposits, it is the thickness of the silt layer that preserves climatic information whereas the clay layer formed by particle rainout indicates that fluvial sedimentation has been suspended. Hambley and Lamoureux (2006), however, demonstrated that silt rhythmite layers are composed of both nival melt deposits and sediment transported with meteoric water, components that may be induced by unrelated climatic events. This suggests that the silt rhythmite layers, as a whole, may not be particularly useful for isolating climatic events, which may partially account for the inconclusive spectral analysis results of their study.

Low sedimentation rates can also lead to further complications. In years of reduced winter precipitation deltaic bifurcation resulted in the summer melt season, leading to sediment dilution. This resulted in the formation of multiple sets of thin, simple couplets in the proximal environment that resembled distal varves (Hambley and Lamoureux, 2006). Distal varves, however, were found to be too thin to display a distinct nival melt sedimentary layer, demonstrating that a connection between melt degree days and nival melt sedimentation may not be evident if deltaic bifurcation occurs (Hambley and Lamoureux, 2006). This result suggests that a full understanding of the depositional environment, and changes in depositional conditions, needs to be accounted for when considering varves for use with spectral analysis.

### 6.3.1.3 Errors Attributable to the Model

Spectral analysis investigations often invoke the use of two models to demonstrate that results are consistent (e.g. Andrews et al., 2010; Ojala et al., 2015). In the present study, the model that was chosen (Mann and Lees, 1996) was designed for, and has been demonstrated to work with, natural phenomena such as rhythmic laminations and tree-ring growth. Notwithstanding the designed intention of the model, the output may contain a false-positive result (Mann and Lees, 1996). This study, however, is predominantly concerned with relative comparisons between similar deposits, and therefore a single model was deemed sufficient for the purposes of this study.

Another issue that faces spectral analysis modelling is that of persistence, which relates to zones (subsets) of anomalous data that may influence the results of the entire dataset. In

geological terms, this may be represented by a period of extended warmth leading to rhythmites that are generally thicker than the contextual rhythmites that make up the rest of the record.

This study also utilized small datasets, which limited the output potential to decadal-scale results. Although this allowed for the possibility of finding short-term solar cycles due to sunspot activity (11 yr and 22 yr periodicities), none were consistently identified. This result is consistent with those of Zhao and Feng (2015), who found no connection between short-term solar cycles (11 yr and 22 yr periodicities) and local temperatures in modern Antarctica.

## 7 Conclusions

Within the study area, eight lithofacies compose a glaciomarine/glaciolacustrine depositional environment. The diamictite and contorted argillite lithofacies represent slumped sediments that were overlain by the interlaminated siltstone and sandstone lithofacies in a delta front/submarine fan environment. Prodelta deposits represented by the interbedded siltstone and claystone lithofacies became coarser grained (represented by the coarse-grained and fine-grained siltstone lithofacies) as the delta prograded, with sand sheet deposits represented by the sandstone lithofacies deposited at the delta front. Retreating ice, perhaps in concert with marine/lacustrine transgression, led to deposition of increasingly finer-grained deposits, represented first by the siltstone lithofacies and finally by the wavy argillite lithofacies. Micro-laminae within siltstone and claystone layers represent micro-turbidites, which collectively form rhythmite sequences that are interpreted to be varves (annually deposited couplets).

Petrographic examination of six of the lithofacies revealed the majority of individual grains to be consistently angular to sub-angular, indicating little mechanical reworking during the cycle of erosion through to re-deposition. Geochemical results confirm that the sediments underwent very little chemical weathering during the erosional cycle.

Spectral analysis revealed periodicities of circa three couplets, congruent with climatic cycles such as the QBO and the ENSO observed in modern times, strongly indicating that the rhythmic couplets represent annual deposits (i.e. varves). Longer term periodicities were not consistently observed, perhaps due to changes in sedimentary depositional processes. The concurrence of locally increasing sedimentation due to delta progradation and locally decreasing sedimentation resulting from glacial recession and marine/lacustrine transgression may have led to the lack of preservation of a meaningful longer term climatic signal within the rhythmites.

The presence of dropstones and micro-laminae within the mechanically and geochemically unaltered rhythmite sequences of the interbedded siltstone and claystone lithofacies supports the conclusion that the rhythmites represent varve deposits,

confirming that the upper Gowganda Formation represents some of the oldest glaciogenic deposits found on Earth.

## References

- Agterberg, F.P. and Banerjee, I., 1969. Stochastic model for the deposition of varves in glacial Lake Barlow-Ojibway, Ontario, Canada. *Can. J. Earth Sci.* 6, 625-652.
- Andrews, S.D., Trewin, N.H., Hartley, A.J., Weedon, G.P., 2010. Solar variance recorded in lacustrine deposits from the Devonian and Proterozoic of Scotland. *J. Geol. Soc.* 167, 847-856.
- Antevs, E., 1925. Retreat of the last ice sheet in eastern Canada. *Geol. Surv. Can. Mem.* 146, 142pp.
- Appenzeller, C., Stocker, T. F., Anklin, M., 1998. North Atlantic Oscillation dynamics recorded in Greenland ice cores. *Science* 282, 446-449.
- Archer, A.W., Johnson, T.W., 1997. Modelling of cyclic tidal rhythmites (Carboniferous of Indiana and Kansas, Precambrian of Utah, USA) as a basis for reconstruction of intertidal positioning and palaeotidal regimes. *Sedimentol.* 44, 991-1010.
- Archer, A.W., Kuecher, G.J., Kvale, E.P., 1995. The role of tidal-velocity asymmetries in the deposition of silty tidal rhythmites (Carboniferous, Eastern Interior Coal Basin, U.S.A.). *J. Sediment. Res.* 65, 408-416.
- Archer, A.W., Kvale, E.P., Johnson, H.R., Williams, G., 1990. Discussion on Late Precambrian tidal rhythmites in South Australia and the history of the Earth's rotation-reply. *J. Geol. Soc.* 147, 401-407.
- Ashley, G.M., 1975. Rhythmic sedimentation in glacial Lake Hitchcock, Massachusetts-Connecticut. In: Jopling, A.V. and McDonald, B.C., (Eds.), *Glaciofluvial and Glaciolacustrine Sedimentation*, Soc. Econ. Paleon. Mineral. Spec. Pub. 23, 304-320.
- Ashley, G.M., 2002. Glaciolacustrine Environments. In: Menzies, J. (Ed.), *Modern and Past Glacial Environments*, Butterworth-Heinemann, Oxford, pp. 335-359.

- Ayer, J.A., Davis, D.W., 1997. Neoproterozoic evolution of differing convergent margin assemblages in the Wabigoon Subprovince: geochemical and geochronological evidence from the Lake of the Woods greenstone belt, Superior Province, northwestern Ontario. *Precambrian Res.* 81,155–178.
- Baldwin, M.P., Gray, L.J., Dunkerton, T.J., Hamilton, K., Haynes, P.H., Randel, W.J., Holton, J.R., Alexander, M.J., Hirota, I., Horinouchi, T., Jones, D.B.A., Kinnersley, J.S., Marquardt, C., Sato, K., Takahashi, M., 2001. The quasi-biennial oscillation. *Rev. Geophys.* 39, 179-229.
- Basu, D., Bouma, A.H., 2000. Thin-bedded turbidites of the Tanqua Karoo: physical and depositional characteristics. *SEPM Spec. Pub.* 68, 263-278.
- Bekker, A., Rasmussen, B., Fletcher, I.R., 2010. Fixing the correlation among Paleoproterozoic glaciations and their relationship with the rise of atmospheric oxygen. AGU, Fall Meeting 2010, abstract #U32A-06.
- Bendle, J.M., Palmer, A.P., Carr, S.J., 2015. A comparison of micro-CT and thin section analysis of Lateglacial glaciolacustrine varves from Glen Roy, Scotland. *Quatern. Sci. Rev.* 114, 61-77.
- Benn, D., Evans, D.J., 2010. *Glaciers and Glaciation*. Hodder Education, London, UK, 802pp.
- Bennett, G.B., Dressler, B.O., Robertson, J.A., 1991. The Huronian Supergroup and associated intrusive rocks. In: Thurston, P.C., Williams, H.R., Sutcliffe, R.H., Stott, G.M. (Eds.), *Geology of Ontario*. Ont. Geol. Surv., Spec. 4, 549-591.
- Bernstein, L., Young, G., 1990. Depositional environments of the Early Proterozoic Espanola Formation, Ontario, Canada. *Can. J. Earth Sci.* 27, 539-551.
- Bhatia, M.R., Crook, K.A., 1986. Trace element characteristics of graywackes and tectonic setting discrimination of sedimentary basins. *Contrib. Mineral. Petrol.* 92, 181-193.

- Borthwick, J., Harmon, R.S., 1982. A note regarding  $\text{ClF}_3$  as an alternative to  $\text{BrF}_5$  for oxygen isotope analysis. *Geochim. Cosmochim. Acta* 46, 1665-1668.
- Bouma, A.H., 1962. *Sedimentology of some flysch deposits: a graphic approach to facies interpretation*, Elsevier, Amsterdam, 168pp.
- Bouma, A.H., 2000. Fine-Grained, Mud-Rich Turbidite Systems: Model and Comparison with Coarse-Grained, Sand-Rich Systems. In: Bouma, A.H., Stone, C.G. (eds.), *Fine-Grained Turbidite Systems*, Am. Assoc. Pet. Geol. Mem. 72, 9-20.
- Bramlette, M.N., 1946. The Monterey Formation of California and the origin of its siliceous rocks. U.S. Geol. Surv. Prof. Pap. 212, 57pp.
- Breckenridge, A., 2007. The Lake Superior varve stratigraphy and implications for eastern Lake Agassiz outflow from 10,700 to 8900 cal ybp (9.5–8.0 14C ka). *Palaeogeogr. Palaeoclimatol. Palaeoecol.* 246, 45-61.
- Brodzikowski, K., van Loon, A.J., 1990. *Glacigenic sediments*. Elsevier, Amsterdam, 674pp.
- Card, K., 1978. *Geology of the Sudbury-Manitoulin Area, Districts of Sudbury and Manitoulin*. Ont. Geol. Surv. 166, 29-118.
- Card, K., Jackson, S., 1995. *Tectonics and Metallogeny of the Early Proterozoic Huronian Foldbelt and the Sudbury Structure of the Canadian Shield: Field Trip Guidebook*. Geol. Surv. Can., Open File Report 3139.
- Casshyap, S.M., 1969. Petrology of the Bruce and Gowganda formations and its bearing on the evolution of Huronian sedimentation in the Espanola-Willisville area, Ontario (Canada). *Palaeogeogr. Palaeoclimatol. Palaeoecol.* 6, 5-36.
- Chan, M.A., Kvale, E.P., Archer, A.W., Sonett, C.P., 1994. Oldest direct evidence of lunar-solar tidal forcing encoded in sedimentary rhythmites, Proterozoic Big Cottonwood Formation, central Utah. *Geology* 22, 791-794.

- Chandler, F., 1986. Sedimentology and paleoclimatology of the Huronian (Early Aphebian) Lorrain and Gordon Lake Formations and their bearing on models for sedimentary copper mineralization. *Geol. Surv. Can.*, Pap 86-1A, 121-132.
- Chu, M-F., Wang, K-L., Griffin, W.L., Chung, S-L., O'Reilly, S.Y., Pearson, N.J., Iizuka, Y., 2009. Apatite composition: tracing petrogenetic processes in Transhimalayan granitoids. *J. Petrol.* 50, 1829-1855.
- Clayton, R.N., Mayeda, T.K., 1963. The use of bromine pentafluoride in the extraction of oxygen from oxides and silicates for isotopic analysis. *Geochim. Cosmochim. Acta* 27, 43-52.
- Clemmensen, L.B., Houmark-Nielsen, M., 1981. Sedimentary features of a Weichselian glaciolacustrine delta. *Boreas* 10, 229-245.
- Coleman, A. P., 1907. The lower Huronian ice age. *Am. Jour. Sci.* 23, 187-192.
- Coleman, J.M., 1966. Ecological changes in a massive fresh-water clay sequence. *Am. Geol. Soc.* 16, 159-174.
- Coleman, J.M., Prior, D.B., 1982. Deltaic environments of deposition. Scholle, P.A., Spearing, D. (Eds.), *Sandstone Depositional Environments*, *Am. Assoc. Pet. Geol. Mem.* 31, 115-137.
- Collins, W.H., 1925. North shore of Lake Huron. *Geol. Surv. Can. Mem.*, 143.
- Corfu, F., Andrews, A., 1986. A U-Pb age for mineralized Nipissing diabase, Gowganda, Ontario. *Can. J. Earth Sci.* 23, 107-109.
- Cotter, E., 1978. The evolution of fluvial style, with special reference to the central Appalachian Paleozoic. In: Miall, A.D. (Ed.), *Fluvial Sedimentology*. *Can. Soc. Petrol. Geol. Mem.* 5, 361-383.
- Dake, J.M., Harleman, D.R., 1969. Thermal stratification in lakes: analytical and laboratory studies. *Water Resour. Res.* 5, 484-495.

- Dalrymple, R.W., 2010. Introduction to siliciclastic facies models. In: James, N.P., Dalrymple, R.W. (Eds.), *Facies Models 4*, Geological Association of Canada, Newfoundland, Canada, pp.59-72.
- de Alvarenga, C.J., Trompette, R., 1992. Glacially influenced sedimentation in the later Proterozoic of the Paraguay Belt (Mato Grosso, Brazil). *Palaeogeogr. Palaeoclimatol. Palaeoecol.* 92, 85-105.
- De Geer, G., 1912. A Geochronology of the last 12,000 years. In: 11th International Geological Congress (1910), Stockholm, Sweden, vol. 1, pp. 241-253.
- Delaney, C., 2005. Seasonal controls on deposition of Late Devensian glaciolacustrine sediments, central Ireland. In: Hambrey, M.J., Christofferson, P., Glasser, N.F., Hubbard, B. (Eds.), *Glacial Sedimentary Processes and Products*, Int. Assoc. Sedimentologists Spec. Pub. 39, 149-163.
- Dietz, R.S., 1964. Sudbury structure as an astrobleme. *J. Geol.* 72, 412-434.
- Dinelli, E., Tateo, F., Summa, V., 2007. Geochemical and mineralogical proxies for grain size in mudstones and siltstones from the Pleistocene and Holocene of the Po River alluvial plain, Italy. In: Arribas, J., Critelli, S., Johnson, M.J., (Eds.), *Sedimentary Provenance and Petrogenesis: Perspectives from Petrography and Geochemistry*, Geol. Soc. Am. Spec. Pap. 420, 25-36.
- Donnelly, R. and Harris, C., 1989. Sedimentology and origin of deposits from a small ice-dammed lake, Lierbreen, Norway. *Sedimentol.* 36, 581-600.
- Donnelly, T.H., Jackson, M.J., 1988. Sedimentology and geochemistry of a mid-Proterozoic lacustrine unit from northern Australia. *Sediment. Geol.* 58, 145-169.
- Dowdeswell, J.A., Hogan, K.A., Arnold, N.S., Mugford, R.I., Wells, M., Hirst, J.P.P., Decalf, C., 2015. Sediment-rich meltwater plumes and ice-proximal fans at the margins of modern and ancient tidewater glaciers: Observations and modelling. *Sedimentol.* 6, 1665-1692.

- Dressler, B.O., 1984. The effects of the Sudbury Event and the intrusion of the Sudbury Igneous Complex on the footwall rocks of the Sudbury Structure. In: Pye, E.G., Naldrett, A.J., Giblin, P.E. (Eds.), *The Geology and Ore Deposits of the Sudbury Structure*, Ont. Geol. Surv. Spec. Vol. 1, pp 97-136.
- Elliott, T., 1974. Interdistributary bay sequences and their genesis. *Sedimentol.* 21, 611-622.
- Eriksson, K.A., Simpson, E.L., 2000. Quantifying the oldest tidal record: the 3.2 Ga Moodies Group, Barberton greenstone belt, South Africa. *Geology* 28, 831-834.
- Evans, D.J.A., Hiemstra, J.F., O’Cofaigh, C., 2007. Glaciotectonic structures and landforms. In: Elias, S.A. (Ed.), *Encyclopedia of Quaternary Science*, Elsevier, Rotterdam, 831-838.
- Eyles, N., 1993. Earth’s glacial record and its tectonic setting. *Earth-Sci. Rev.* 35, 1-248.
- Eyles, N., 2008. Glacio-epochs and the supercontinent cycle after ~ 3.0 Ga: Tectonic boundary conditions for glaciation. *Palaeogeogr. Palaeoclimatol. Palaeoecol.* 258, 89-129.
- Eyles, N., Eyles, C.H., 1989. Glacially-influenced deep-marine sedimentation of the Late Precambrian Gaskiers Formation, Newfoundland, Canada. *Sedimentol.* 36, 601-620.
- Farrand, W.R., 1969a. The Quaternary history of Lake Superior. In: *Proc. 12th Conf. Great Lakes Research*. Int’l Assoc. for Great Lakes Research, Ann Arbor, MI, pp. 181-197.
- Farrand, W.R., 1969b. Late-glacial and postglacial sedimentation in the deep basins of Lake Superior, USA. *Mitteilungen International Verein Limnologie* 17, 34-42.
- Fedo, C.M., Young, G.M., Nesbitt, H.W., 1997a. Paleoclimatic control on the composition of the Paleoproterozoic Serpent Formation, Huronian Supergroup, Canada: a greenhouse to icehouse transition. *Precambrian Res.* 86, 201-223.

- Fedo, C.M., Young, G.M., Nesbitt, H.W., Hanchar, J.M., 1997b. Potassic and sodic metasomatism in the southern province of the Canadian Shield: evidence from the Paleoproterozoic serpent formation, Huronian Supergroup, Canada. *Precambrian Res.* 84, 17-36.
- Fleisher, P.J., Bailey, P.K., Cadwell, D.H., 2003. A decade of sedimentation in ice-contact, proglacial lakes, Bering Glacier, AK. *Sediment. Geology* 160, 309-324.
- Fisk, H.N., 1955. Sand facies of recent Mississippi delta deposits. *Proceedings of the Fourth World Petroleum Congress, Sec. I/C, 3, 377-398.*
- Flint, R.F., 1971. *Glacial and Quaternary Geology.* John Wiley and Sons, New York, 906pp.
- Fralick, P.W., Miall, A.D., 1989. Sedimentology of the Lower Huronian Supergroup (Early Proterozoic), Elliot Lake area, Ontario, Canada. *Sediment. Geol.* 63, 127-153.
- Franco, D.R., Hinnov, L.A., Ernesto, M., 2011. Spectral analysis and modeling of microcyclostratigraphy in late Paleozoic glaciogenic rhythmites, Paraná Basin, Brazil. *Geochem. Geophys. Geosyst.* 12, Q09003.
- Frarey, M.J., 1977. *Geology of the Huronian Belt between Sault Ste. Marie and Blind River, Ontario.* *Geol. Surv. Can. Mem.*, 383.
- Freeman, E. B., 1978. *Geological Highway Map, Southern Ontario; Ont. Geol. Surv., Map 2418*
- Gilbert, G.K., 1890. *Lake Bonneville.* U. S. Geol. Surv. Monogr. vol. 1, 438pp.
- Gilbert, R., 1975. Sedimentation in Lillooet Lake, British Columbia. *Can. J. Earth Sci.* 12, 1697-1711.
- Gladney, E.S., Roelandts, I., 1990. 1988 Compilation of Elemental Concentration Data for CCRMP Reference Rock Samples SY-2, SY-3 and MRG-1. *Geostand. Newsl.* 14, 373-458.

Godsey, H.S., Moore, T.C., Rea, D.K., Shane, L.C.K., 1999. Post-Younger Dryas seasonality in the North American midcontinent region as recorded in Lake Huron varved sediments. *Can. J. Earth Sci.* 36, 533-547.

Greb, S., Archer, A., 1998. Annual sedimentation cycles in rhythmites of carboniferous tidal channels. *Soc. Sed. Geol. Spec. Pub.* 61, 75-84.

Gromet, L.P., Haskin, L.A., Korotev, R.L., Dymek, R.F., 1984. The "North American shale composite": its compilation, major and trace element characteristics. *Geochim. Cosmochim. Acta*, 48, 2469-2482.

Gustavson, T.C., Ashley, G.M., Boothroyd, J.C., 1975. Depositional sequences in glaciolacustrine deltas. In: Jopling, A.V. and McDonald, B.C. (Eds.), *Glaciofluvial and glaciolacustrine sedimentation*, Soc. Econ. Paleon. Mineral. Sp. Pub. 23, 249-263.

Hambley, G.W., Lamoureux, S.F., 2006. Recent summer climate recorded in complex varved sediments, Nicolay Lake, Cornwall Island, Nunavut, Canada. *J. Paleolimnol.* 35, 629-640.

Hameed, S., Currie, R.G., Lagrone, H., 1995. Signals in atmospheric pressure variations from 2 to ca. 70 months: Part I, simulations by two coupled ocean—atmosphere GCMs. *Int. J. Climatol.* 15, 853-871.

Hampton, M.A., 1972. The role of subaqueous debris flow in generating turbidity currents. *J. Sediment. Res.* 42, 775-793.

Haskin, L.A., Haskin, M.A., Frey, F.A., Wildeman, T.R., 1968. Relative and absolute terrestrial abundances of the rare earths. In: Ahrens, L.H. (Ed.), *Origin and Distribution of the Elements*, Pergamon Press, Oxford, pp. 889-912

Henderson, P., 1996. The rare earth elements: Introduction and review. In: Jones, A.P., Wall, F., Williams, C.T. (Eds.), *Rare Earth Minerals: Chemistry, Origin and Ore Deposits*, Chapman & Hall, UK, 372pp.

Hofmann, H., Pearson, D., Wilson, B., 1980. Stromatolites and fenestral fabric in early Proterozoic Huronian Supergroup, Ontario. *Can. J. Earth Sci.* 17, 1351-1357.

Holm, D.K., Van Schmus, W.R., MacNeill, L.C., Boerboom, T.J., Schweitzer, D., Schneider, D., 2005. U-Pb zircon geochronology of Paleoproterozoic plutons from the northern midcontinent, USA: Evidence for subduction flip and continued convergence after geon 18 Penokean orogenesis. *Geol. Soc. Am. Bull.* 117, 259-275.

Huang, S.Y., Chen, Y.G., Burr, G.S., Jaiswal, M.K., Lin, Y.N., Yin, G., Liu, J., Zhao, S., Cao, Z., 2014. Late Pleistocene sedimentary history of multiple glacially dammed lake episodes along the Yarlung-Tsangpo river, southeast Tibet. *Quat. Res.* 82, 430-440.

Hughes, G.B., Giegengack, R., Kritikos, H.N., 2003. Modern spectral climate patterns in rhythmically deposited argillites of the Gowganda Formation (Early Proterozoic), southern Ontario, Canada. *Ear. Plan. Sci. Lett.* 207, 13-22.

Hyodo, A., Longstaffe, F.J., 2011. The chronostratigraphy of Holocene sediments from four Lake Superior sub-basins 1 1 Laboratory for Stable Isotope Science (LSIS) Contribution 264. *Can. J. Earth Sci.* 48, 1581-1599.

Jackson, M.J., 1985. Mid-Proterozoic dolomitic varves and microcycles from the McArthur Basin, northern Australia. *Sediment. Geol.* 44, 301-326.

Junnila, R., Young, G., 1995. The Paleoproterozoic upper Gowganda Formation, Whitefish Falls area, Ontario, Canada: subaqueous deposits of a braid delta. *Can. J. Earth Sci.* 32, 197-209.

Kelly, R.I. and Martini, I.P., 1986. Pleistocene glacio-lacustrine deltaic deposits of the Scarborough Formation, Ontario, Canada, *Sediment. Geol.* 47, 27-52.

Ketchum, K.Y., Heaman, L.M., Bennett, G., Hughes, D.J., 2013. Age, petrogenesis and tectonic setting of the Thessalon volcanic rocks, Huronian Supergroup, Canada. *Precambrian Res.* 233, 144-172.

- Klein, G.D., 1971. A sedimentary model for determining paleotidal range. *Geol. Soc. Am. Bull.* 82, 2585-2592.
- Klein, C., 2005. Some Precambrian banded iron-formations (BIFs) from around the world: Their age, geologic setting, mineralogy, metamorphism, geochemistry, and origins. *Am. Mineral.* 90, 1473-1499.
- Koglin, N., Frimmel, H.E., Minter, W.L., Brätz, H., 2010. Trace-element characteristics of different pyrite types in Mesoarchaeon to Palaeoproterozoic placer deposits. *Miner. Deposita* 45, 259-280.
- Krapež, B., Barley, M.E., Pickard, A.L., 2003. Hydrothermal and resedimented origins of the precursor sediments to banded iron formation: sedimentological evidence from the Early Palaeoproterozoic Brockman Supersequence of Western Australia. *Sedimentol.* 50, 979-1011.
- Krogh, T., Davis, D., Corfu, F., 1984. Precise U-Pb zircon and baddeleyite ages for the Sudbury area, in: Pye, E.G., Naldrett, A.J., Giblin, P.E. (Eds.), *The Geology and Ore Deposits of the Sudbury Structure*, Ont. Geol. Surv., Spec., Vol. 1, pp. 431–446.
- Kuenen, P.H., 1957. Sole markings of graded graywacke beds. *J. Geol.* 65, 231-258.
- Lacelle, D., Brooker, A., Fraser, R.H., Kokelj, S.V., 2015. Distribution and growth of thaw slumps in the Richardson Mountains–Peel Plateau region, northwestern Canada. *Geomorphol.* 235, 40-51.
- Landmann, G., Reimer, A., Lemcke, G., Kempe, S., 1996. Dating Late Glacial abrupt climate changes in the 14,570 yr long continuous varve record of Lake Van, Turkey. *Palaeogeogr. Palaeoclimatol. Palaeoecol.* 122, 107-118.
- Leckie, D.A., McCann, S.B., 1982. Glacio-lacustrine sedimentation on low slope prograding delta, in: Davidson-Arnott, R., Nickling, W., Fahey, B.D. (Eds.), *Research in glacial, glacio-fluvial and glacio-lacustrine systems: proceedings of the 6th Guelph Symposium on Geomorphology*, 1980. *Guelph Symp. Geomorph.* 6, 261-278.

Lindsey, D.A., 1969. Glacial sedimentology of the Precambrian Gowganda Formation, Ontario, Canada. *Geol. Soc. Am. Bull.* 80, 1685-1702.

Liu, Y.G., Miah, M.R.U., Schmitt, R.A., 1988. Cerium: a chemical tracer for paleo-oceanic redox conditions. *Geochim. Cosmochim. Acta* 52, 1361–1371.

Long, D.G., 1976. The stratigraphy and sedimentology of the Huronian (lower Aphebian) Mississagi and Serpent Formations. Ph.D. thesis, University of Western Ontario, London, Ont. Canada, 291 pp.

Long, D.G., 1978. Depositional environments of a thick Proterozoic sandstone: the (Huronian) Mississagi Formation of Ontario, Canada. *Can. J. Earth Sci.* 15, 190-206.

Long, D.G., 1986. Stratigraphic and depositional setting of placer gold concentrations in basal Huronian strata of the Cobalt Plain. *Ont. Geol. Surv., Open File Rep.* 5593, 125 pp.

Long, D.G., 2004. The tectonostatigraphic evolution of the Huronian basement and the subsequent basin fill: geological constraints on impact models of the Sudbury event. *Precambrian Res.* 129, 203-223.

Long, D.G., 2009. The Huronian Supergroup, in: Rousell, D.H. and Brown, G.H. (Eds.), *A Field Guide to the Geology of Sudbury, Ontario*, *Ont. Geol. Surv., Open File Rep.* 6243, pp. 14-30.

Long, D., Ulrich, T., Kamber, B., Bentley, S., 2011. Laterally extensive modified placer gold deposits in the Paleoproterozoic Mississagi Formation, Clement and Pardo Townships, Ontario. *Can. J. Earth Sci.* 48, 779-792.

Longerich, H.P., Jenner, G.A., Fryer, B.J., Jackson, S.E., 1990. Inductively coupled plasma-mass spectrometric analysis of geological samples: a critical evaluation based on case studies. *Chem. Geol.* 83, 105-118.

Longstaffe, F.J., 2003. Isotopic Methods in Sedimentology, in: Middleton, G.V. (Ed.), *Encyclopedia of Sediments and Sedimentary Rocks*. Kluwer Academic Publishers, The Netherlands, pp. 385-397.

Longstaffe, F.J., Gower, C.F., 1983. Oxygen-isotope geochemistry of Archean granitoid gneisses and related rocks in the English River Subprovince, Northwestern Ontario

Longstaffe, F.J., Schwartz, H.P., 1977.  $^{18}\text{O}/^{16}\text{O}$  of Archean elastic metasedimentary rocks: a petrogenetic indicator for Archean gneisses? *Geochim. Cosmochim.* 41, 1303-1312.

Lowe, D.R., 1982. Sediment gravity flows: II. Depositional models with special reference to the deposits of high-density turbidity currents. *J. Sediment. Res.* 52, 279-297.

Lowey, G., 1985. Stratigraphy and sedimentology of the Lorrain Formation, Huronian Supergroup (Aphebian), between Sault Ste. Marie and Elliot Lake, Ontario, and implications for stratiform gold mineralization. *Geol. Surv. Can., Open File Rep.* 1154, 56 pp.

Mann, M.E., Lees, J.M., 1996. Robust estimation of background noise and signal detection in a climatic time series. *Clim. Change* 33, 409-445.

Martins-Neto, M.A., Pedrosa-Soares, A.C., Lima, S.A.D.A., 2001. Tectono-sedimentary evolution of sedimentary basins from Late Paleoproterozoic to Late Neoproterozoic in the Sao Francisco craton and Araçuaí fold belt, eastern Brazil. *Sediment. Geol.* 141, 343-370.

Mazumder, R., 2004. Implications of lunar orbital periodicity from the Chaibasa tidal rhythmite (India) of late Paleoproterozoic age. *Geology* 32, 841-844.

McLennan, S.M., Hemming, S., McDaniel, D.K., Hanson, G.N., 1993. Geochemical approaches to sedimentation, provenance, and tectonics. *Geol. Soc. Am. Spec. Pap.* 284, 21-40.

Miall, A.D., 1985. Sedimentation on an early Proterozoic continental margin under glacial influence: the Gowganda Formation (Huronian), Elliot Lake area, Ontario, Canada. *Sedimentol.* 32, 763-788.

- Morgenstern, N., 1967. Submarine slumping and the initiation of turbidity currents. Richards, A.F. (ed.), *Marine Geotechnique*, Int. Res. Conf. Marine Geotechnique, 189–220.
- Morton, A.C., 1991. Geochemical studies of detrital heavy minerals and their application to provenance research. In: Morton, A.C., Todd, S.P., Haughton, P.D.W. (Eds.), *Developments in Sedimentary Provenance Studies*. Geol. Soc. Spec. Pub. 57, 31-45.
- Mulder, T., Alexander, J., 2001. The physical character of subaqueous sedimentary density flows and their deposits. *Sedimentol.* 48, 269-299.
- Mustard, P., Donaldson, J., 1987. Early Proterozoic ice-proximal glaciomarine deposition: the lower Gowganda Formation at Cobalt, Ontario, Canada. *Geol. Soc. Am. Bull.* 98, 373-387.
- Mutti, E., 1977. Distinctive thin-bedded turbidite facies and related depositional environments in the Eocene Hecho Group (South-Central Pyrenees, Spain). *Sedimentol.* 24, 107-131
- Nemec, W., 1990. Aspects of sediment movement on steep delta slopes. In: Colella, A. and Prior, D.B. (Eds.), *Coarse-Grained Deltas*. Int. Assoc. Sedimentologists Sp. Pub. 10, 29-73.
- Nesbitt, H.W., Young, G.M., 1982. Early Proterozoic climates and plate motions inferred from major element chemistry of lutites. *Nature* 299, 715-717.
- Nichols, G., 2009. *Sedimentology and Stratigraphy*, Wiley-Blackwell, UK, 419pp.
- Nio, S., Yang, C., 1991. Diagnostic attributes of clastic tidal deposits: a review. In: Smith, D.G., Reinson, G.E., Zaitlin, B.A., Rahmani, R.A. (Eds.), *Clastic Tidal Sedimentology*, Can. Soc. Pet. Geol. Mem. 16, 3-28.
- Ogami, T., Sugai, T., Fujiwara, O., 2015. Dynamic particle segregation and accumulation processes in time and space revealed in a modern river-dominated delta: A spatiotemporal record of the Kiso River delta, central Japan. *Geomorphology* 235, 27-39.

- Ojala, A.E.K., Francus, P., Zolitschka, B., Besonen, M., & Lamoureux, S.F., 2012. Characteristics of sedimentary varve chronologies—a review. *Quat. Sci. Rev.*, 43, 45-60.
- Palonen, P., 1973. Paleogeography of the Mississagi Formation and lower Huronian cyclicity, in: Young, G.M. (Ed.), *Huronian Stratigraphy and Sedimentation*, Geol. Assoc. Canada Spec. Pap. 12, pp. 157-167.
- Panahi, A., Young, G.M., Rainbird, R.H., 2000. Behavior of major and trace elements (including REE) during Paleoproterozoic pedogenesis and diagenetic alteration of an Archean granite near Ville Marie, Quebec, Canada. *Geochim. Cosmochim.* 64, 2199-2220.
- Parish, T.R., Bromwich, D.H., 1991. Continental-scale simulation of the Antarctic katabatic wind regime. *J. Clim.* 4, 135-146.
- Paull, C.K., McGann, M., Sumner, E.J., Barnes, P.M., Lundsten, E.M., Anderson, K., Gwiazda, R., Edwards, B., Caress, D.W., 2014. Sub-decadal turbidite frequency during the early Holocene: Eel Fan, offshore northern California. *Geol.* 42, 855-858.
- Plint, A.G., 2013. Mud dispersal across a Cretaceous prodelta: Storm-generated, wave-enhanced sediment gravity flows inferred from mudstone microtexture and microfacies. *Sedimentol.* 61, 609-647.
- Polat, A., Longstaffe, F.J., 2014. A juvenile oceanic island arc origin for the Archean (2.97Ga) Fiskenæsset anorthosite complex, southwestern Greenland: Evidence from oxygen isotopes. *Earth Planet. Sci. Lett.* 396, 252-266.
- Powell, R., Domack, E., 2002. Glaciolacustrine Environments. In: Menzies, J. (Ed.), *Modern and Past Glacial Environments*, Butterworth-Heinemann, Oxford, pp. 361-389.
- Prasad, S., Baier, J., 2014. Tracking the impact of mid- to late Holocene climate change and anthropogenic activities on Lake Holzmaar using an updated Holocene chronology. *Global Planet. Change* 122, 251-264

Prothero, D.R., Schwab, F., 1996. *Sedimentary Geology: An Introduction to Sedimentary Rocks and Stratigraphy*, W.H. Freeman and Company, New York, 575pp.

Rainbird, R., Donaldson, J., 1988. Nonglaciogenic deltaic deposits in the early Proterozoic Gowganda Formation, Cobalt Basin, Ontario. *Can. J. Earth Sci.* 25, 710-724.

Rainbird, R.H., 1985. Sedimentology and geochemistry of the Firstbrook Member of the Gowganda Formation in the eastern Cobalt Basin, M.Sc. thesis, Carleton University, Ottawa, Ont., Canada, 157 pp.

Rasmussen, B., Bekker, A., Fletcher, I.R., 2013. Correlation of Paleoproterozoic glaciations based on U–Pb zircon ages for tuff beds in the Transvaal and Huronian Supergroups. *Earth Planet. Sci. Lett.* 382, 173-180.

Reineck, H.E., Singh, I.B., 1972. Genesis of laminated sand and graded rhythmites in storm-sand layers of shelf mud. *Sedimentol.* 18, 123-128.

Reineck, H.E., Singh, I.B., 1980. *Depositional Sedimentary Environments: With Reference to Terrigenous Clastics*. Springer-Verlag, Berlin, 549pp.

Reineck, H.E., Wunderlich, F., 1968. Classification and origin of flaser and lenticular bedding. *Sedimentol.* 11, 99-104.

Ridge, J.C., Balco, G., Bayless, R.L., Beck, C.C., Carter, L.B., Dean, J.L., Voytek, E.B., Wei, J.H., 2012. The new North American Varve Chronology: A precise record of southeastern Laurentide Ice Sheet deglaciation and climate, 18.2-12.5 kyr BP, and correlations with Greenland ice core records. *Am. J. Sci.* 312, 685-722.

Rittenour, T.M., Brigham-Grette, J., Mann, M.E., 2000. El Niño-like climate teleconnections in New England during the late Pleistocene. *Science* 288, 1039–1042.

Robertson, J.A., 1976. *Geology of the Massey Area, Districts of Algoma, Manitoulin and Sudbury*. Ont. Div. Mines, Geosci. Rep. 136, 130 pp.

Robertson, J.A., 1986. Huronian geology and the Blind River (Elliot Lake) uranium deposits, in: Evans, E.L. (Ed.), *Uranium Deposits of Canada*, Can. Inst. Min. and Metall. Spec. Vol. 33, pp 7-33.

Roscoe, S.M., 1969. Huronian rocks and uraniferous conglomerates in the Canadian Shield. *Geol. Surv. Can. Paper 68-40*, 205 pp.

Roscoe, S.M., 1981. Temporal and other factors affecting deposition of uraniferous conglomerates, in: Armstrong, F.C. (Ed.), *Workshop on genesis of uranium- and gold-bearing Precambrian quartz-pebble conglomerates*, USGS Prof. Pap. 1161-W, pp. W1-W17.

Rousell, D.H., Gibson, H.L., Jonasson, I.R., 1997. The tectonic, magmatic and mineralization history of the Sudbury Structure. *Explor. Min. Geol.* 6, 1-22.

Rousell, D.H., Long, D.G., 1998. Are outliers of the Huronian Supergroup preserved in structures associated with the collapse of the Sudbury impact crater? *J. Geol.* 106, 407-420.

Savin, S.M., Epstein, S., 1970a. The oxygen and hydrogen isotope geochemistry of clay minerals. *Geochim. Cosmochim. Acta* 34, 25-42.

Savin, S.M., Epstein, S., 1970b. The oxygen and hydrogen isotope geochemistry of ocean sediments and shales. *Geochim. Cosmochim. Acta* 34, 43-63.

Shanmugam, G., 1997. The Bouma sequence and the turbidite mind set. *Earth-Sci. Rev.* 42, 201-229.

Sharpe, D.R. and Cowan, W.R., 1990. Moraine formation in northwestern Ontario: product of subglacial fluvial and glaciolacustrine sedimentation. *Can. J. Earth Sci.* 27, 1478-1486.

Shimizu, H., Tachikawa, K., Masuda, A., Nozaki, Y., 1994. Cerium and neodymium isotope ratios and REE patterns in seawater from the North Pacific Ocean. *Geochim. Cosmochim. Acta* 58, 323-333.

Siegenthaler, C., Sturm, M., 1991. Slump induced surges and sediment transport in Lake Uri, Switzerland. *Verh.-Int. Ver. Limnol.* 24, 955–958.

Sims, P., Schmus, W.V., Schulz, K., Peterman, Z., 1989. Tectono-stratigraphic evolution of the Early Proterozoic Wisconsin magmatic terranes of the Penokean Orogen. *Can. J. Earth Sci.* 26, 2145-2158.

Smith, N.D. and Ashley, G.M., 1985. Proglacial Lacustrine Environment. In: Ashley, G.M., Shaw, J., & Smith, N.D. (Eds.), *Glacial sedimentary environments*. SEPM Short Course 16, pp. 135-216.

Stow, D.A.V., Reading, H.G., Collinson, J.D., 1996. Deep seas, In: Reading, H.G. (Ed.), *Sedimentary environments: processes, facies and stratigraphy* 3, 395-453.

Sturm, M. and Matter, A., 1978. Turbidites and varves in Lake Brienz (Switzerland): deposition of clastic detritus by density currents. In: Matter, A. and Tucker, M.E. (Eds.), *Modern and Ancient Lake Sediments*. *Int. Assoc. Sedimentologists Spec. Pub.* 2, 147-168.

Talling, P.J., Masson, D.G., Sumner, E.J., Malgesini, G., 2012. Subaqueous sediment density flows: Depositional processes and deposit types. *Sedimentol.* 59, 1937-2003.

Tang, H., Chen, Y., 2013. Global glaciations and atmospheric change at ca. 2.3 Ga. *Geosci. Front.* 4, 583-596.

Taylor, S.R., McLennan, S.M., 1985. *The Continental Crust: It's Composition and Evolution*, Blackwell, Oxford, UK, 312pp.

Taylor, S.R., McLennan, S.M., 1995. The geochemical evolution of the continental crust. *Reviews of Geophysics* 33, 241-265.

Tessier, B., 1993. Upper intertidal rhythmites in the Mont-Saint-Michel Bay (NW France): perspectives for paleoreconstruction. *Mar. Geol.* 110, 355-367.

- Tessier, B., 1998. Tidal cycles: annual versus semi-lunar records. In: Alexander, C., Davis Jr, R.A., Henry, V.J. (Eds.), *Tidalites: Processes and Products*, Soc. Sed. Geol. Spec. Pub. 61, 69-74.
- Thomas, G.S. and Connell, R.J., 1985. Iceberg drop, dump, and grounding structures from Pleistocene glacio-lacustrine sediments, Scotland. *J. Sediment. Res.* 55, 243-249.
- Thomson, R., 1957. The Proterozoic of the Cobalt area, in: Gill, J.E., *The Proterozoic of Canada*, Roy. Soc. Can. Spec. Pub. 2, pp. 40-45.
- Thomson, D.J., 1982. Spectrum estimation and harmonic analysis. *Proc IEEE* 70: 1055-1096.
- Trendall, A.F., 1983. The Hamersley Basin. In: Trendal, A.F., Morris, R.C., (Eds.), *Iron Formation, Facts and Problems*, Dev. Precambrian Geol. 6, 69-129.
- Trendall, A.F., 2002. The significance of iron-formation in the Precambrian stratigraphic record. In: Altermann, W., Corcoran, P.L. (Eds.), *Precambrian Sedimentary Environments: A Modern Approach to Ancient Depositional Systems*, Spec. Publ. Int. Assoc. Sedimentol. 33, 33-66.
- Udden, J.A., 1914. Mechanical composition of clastic sediments. *Bull. Geol. Soc. Am.* 25, 655-744.
- Van Schmus, W. R., 1976. Early and middle Proterozoic history of the Great Lakes area, North America. *Philos. Trans. R. Soc. Lond. Ser. A*, 280.1298, 605-628.
- Veizer, J., Clayton, R., Hinton, R., 1992. Geochemistry of Precambrian carbonates: IV. Early Paleoproterozoic ( $2.25 \pm 0.25$  Ga) seawater. *Geochim. Cosmochim. Acta* 56, 875-885.
- Weedon, G.W., 2003. *Time-Series Analysis and Cyclostratigraphy: Examining stratigraphic records of environmental cycles*, Cambridge University Press, UK, 259pp.

- Wentworth, C.K., 1922. A scale of grade and class terms for clastic sediments. *J. Geology* 30, 377-392.
- Williams, G., 1981. Sunspot periods in the late Precambrian glacial climate and solar–planetary relations. *Nature* 291, 624-628.
- Williams, G., 1985. Solar affinity of sedimentary cycles in the late Precambrian Elatina Formation. *Australian J. Physics* 38, 1027-1044.
- Williams, G.E., 1989. Late Precambrian tidal rhythmites in South Australia and the history of the Earth's rotation. *J. Geol. Soc.* 146, 97-111.
- Williams, G.E., 1991. Upper Proterozoic tidal rhythmites, South Australia: sedimentary features, deposition, and implications for the earth's paleorotation. In: Smith, D.G., Reinson, G.E., Zaitlin, B.A., Rahmani, R.A. (Eds.), *Clastic Tidal Sedimentology*, Can. Soc. Pet. Geol. Mem. 16, 161-177.
- Williams, G.E., 2000. Geological constraints on the Precambrian history of Earth's rotation and the Moon's orbit. *Rev. Geophys.* 38, 37-59.
- Williams, G.E., Schmidt, P.W., 1997. Paleomagnetism of the Paleoproterozoic Gowganda and Lorrain Formations, Ontario: low paleolatitude for Huronian glaciation. *Earth Planet. Sci. Lett.* 153, 157-169.
- Willingham, T.O., Nagy, B., Nagy, L.A., Krinsley, D.H., Mossman, D.J., 1985. Uranium-bearing stratiform organic matter in paleoplacers of the lower Huronian Supergroup, Elliot Lake-Blind River region, Canada. *Can. J. Earth Sci.* 22, 1930-1944.
- Wood, J., 1973. Stratigraphy and depositional environments of upper Huronian rocks of the Rawhide Lake-Flack Lake area, Ontario, in: Young, G.M. (Ed.), *Huronian Stratigraphy and Sedimentation*, Geol. Assoc. Canada Spec. Pap. 12, pp. 73-95.
- Wright, D.J., Rust, B.R., 1985. Preliminary report on the stratigraphy and sedimentology of the Bar River Formation, in: Milne, V.G. (Ed.), *Geoscience Research Program, Summary of Research 1984-1985*, Ont. Geol. Surv. Misc. Pap.127, pp.119-123.

- Young, G.M., 1970. An extensive early Proterozoic glaciation in North America? *Palaeogeogr. Palaeoclimatol. Palaeoecol.* 7, 85-101.
- Young, G. M., 1982. The late Proterozoic Tindir Group, east-central Alaska: Evolution of a continental margin. *Geol. Soc. Am. Bull.* 93, 759-783.
- Young, G.M., 2001. Comparative geochemistry of Pleistocene and Paleoproterozoic (Huronian) glaciogenic laminated deposits: relevance to crustal and atmospheric composition in the Last 2.3 Ga. *J. Geol.* 109, 463-477.
- Young, G.M., 2013. Climatic catastrophes in Earth history: two great Proterozoic glacial episodes. *Geol. J.* 48, 1-21.
- Young, G.M., 2014. Contradictory correlations of Paleoproterozoic glacial deposits: local, regional or global controls? *Precambrian Res.* 247, 33-44.
- Young, G.M., Nesbitt, H.W., 1985. The Gowganda Formation in the southern part of the Huronian outcrop belt, Ontario, Canada: Stratigraphy, depositional environments and regional tectonic significance. *Precambrian Res.* 29, 265-301.
- Young, G.M., Long, D.G.F., Fedo, C.M., Nesbitt, H.W., 2001. Paleoproterozoic Huronian basin: product of a Wilson cycle punctuated by glaciations and a meteorite impact. *Sediment. Geol.* 141, 233-254.
- Zhao, X.H., Feng, X.S., 2015. Correlation between solar activity and the local temperature of Antarctica during the past 11,000 years. *J. Atmos. Sol. Terr. Phys.* 122, 26-33.
- Zolitschka, B., 2007. Varved lake sediments. In: Elias, S.A. (Ed.), *Encyclopedia of Quaternary Science*, Elsevier, Amsterdam, pp. 3105-3114.
- Zolnai, A.I., Price, R.A., Helmstaedt, H., 1984. Regional cross section of the Southern Province adjacent to Lake Huron, Ontario: implications for the tectonic significance of the Murray Fault Zone. *Can. J. Earth Sci.*, 21, 447-456.

## Appendices

### Appendix A: Core Logs, Gowganda Formation

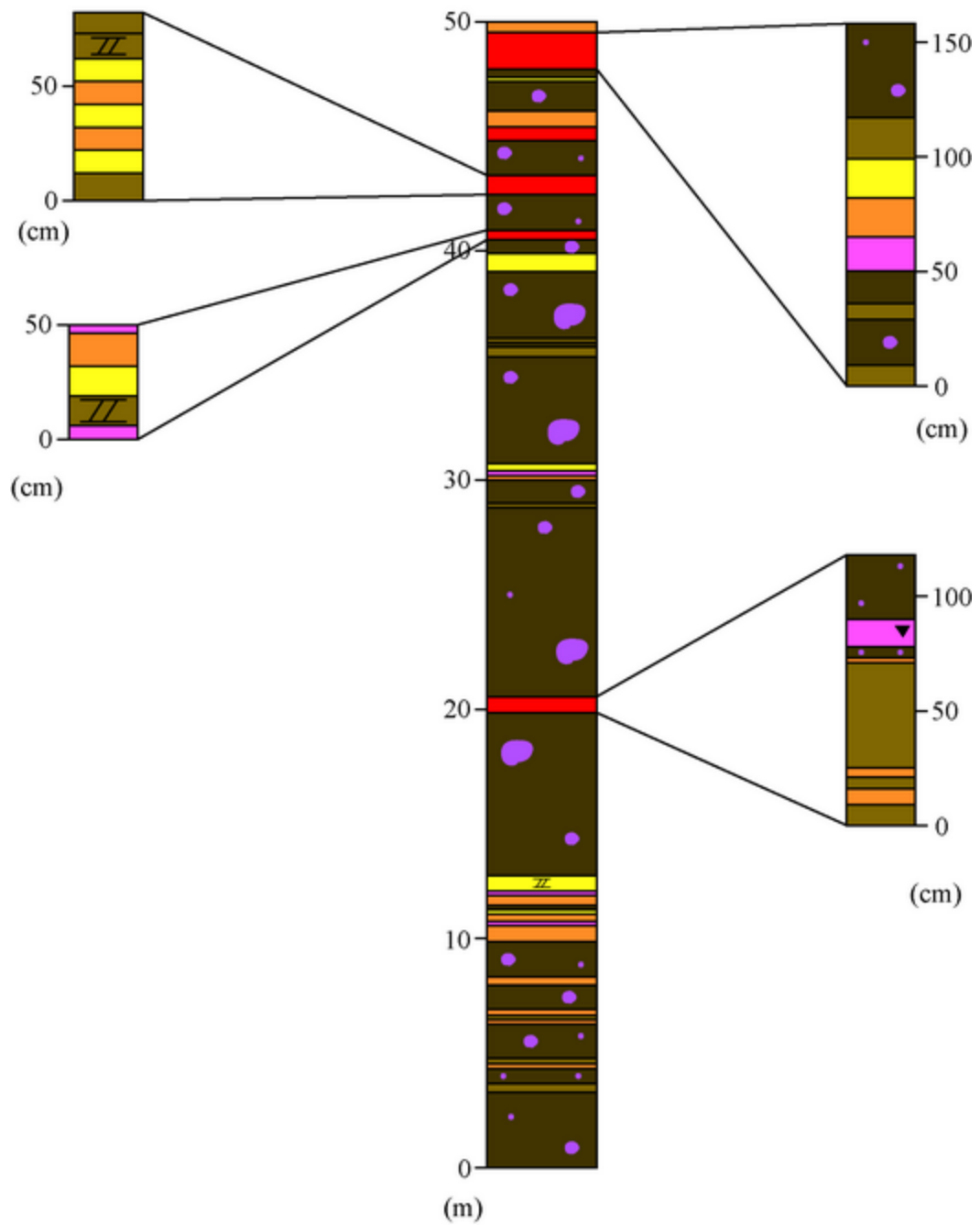
(Refer to Figure 2.3 for drill core locations)

## Legend

	Black/Grey Sandstone		Crossbedding
	Diamictite (mixed clasts)		Contorted bedding
	Yellow Sandstone		Planar Lamination
	Mixed Unit		Graded bedding
	Argillite		
	Granulestone		
	Diamictite (pebbly)		
	Ortho-conglomerate		
	Pink Sandstone		



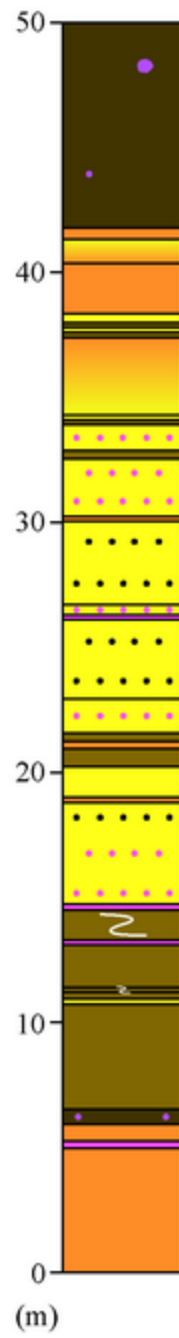
## Core - Gowganda, Lower, Hole 150-1 (b)



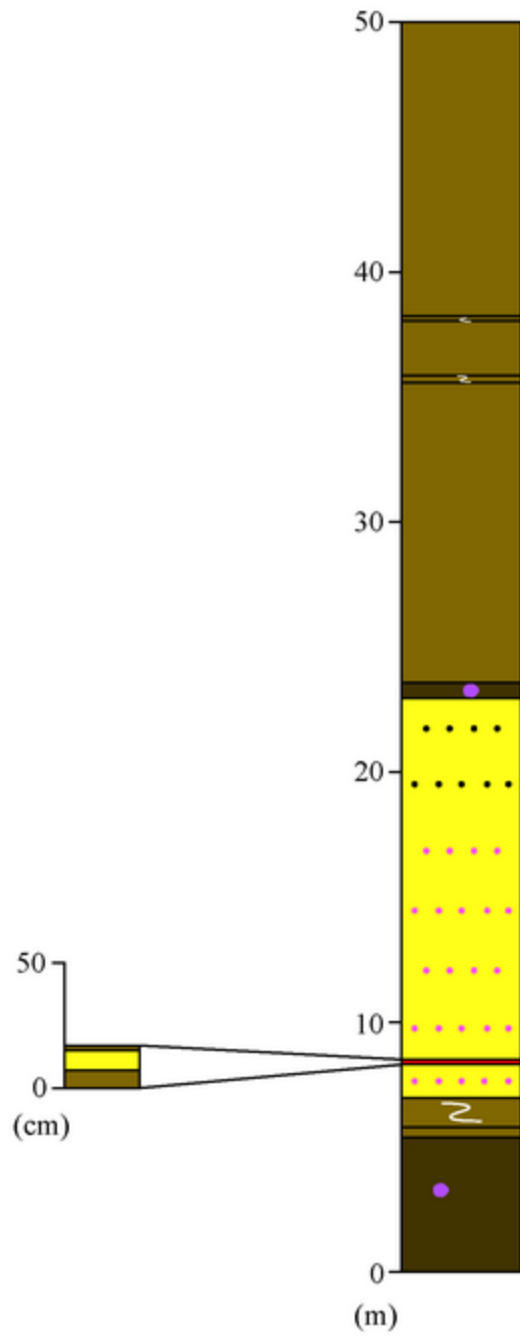
# Core - Gowganda, Lower, Hole 150-1 (c)



## Core - Gowganda, Lower, Hole 150-1 (d)



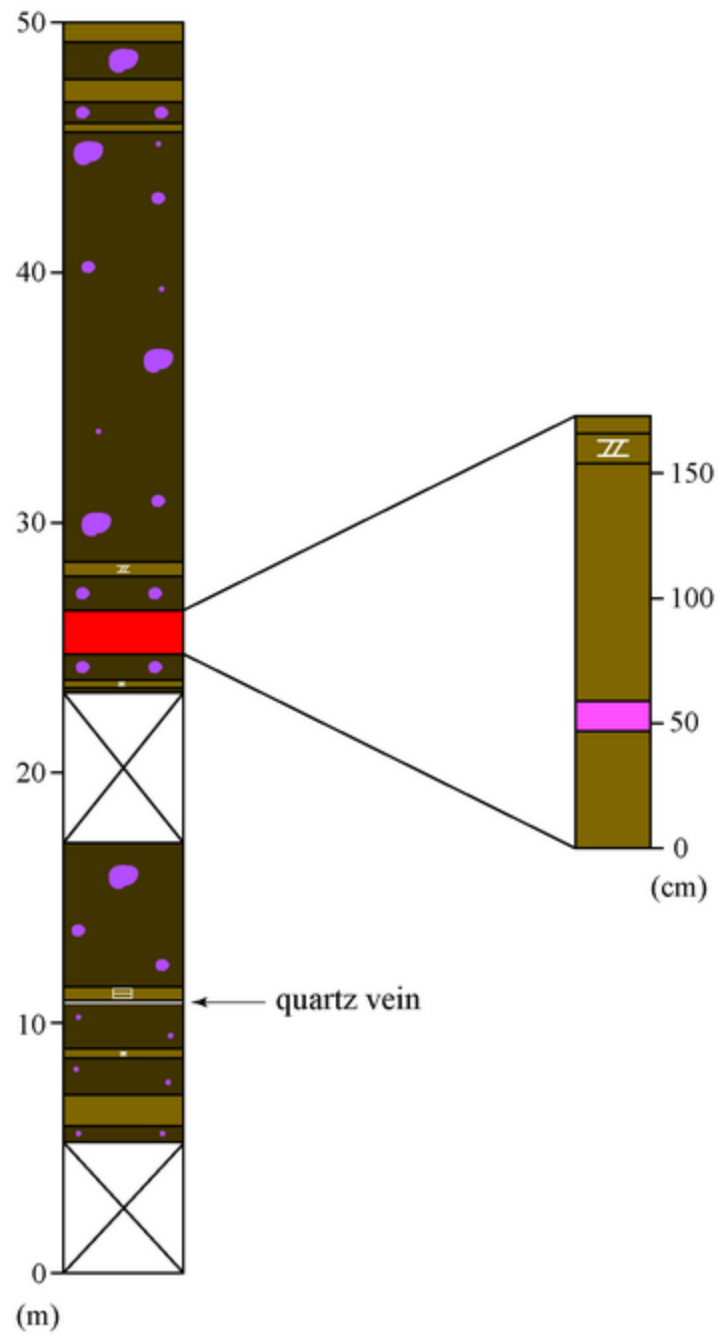
## Core - Gowganda, Lower, Hole 150-1 (e)



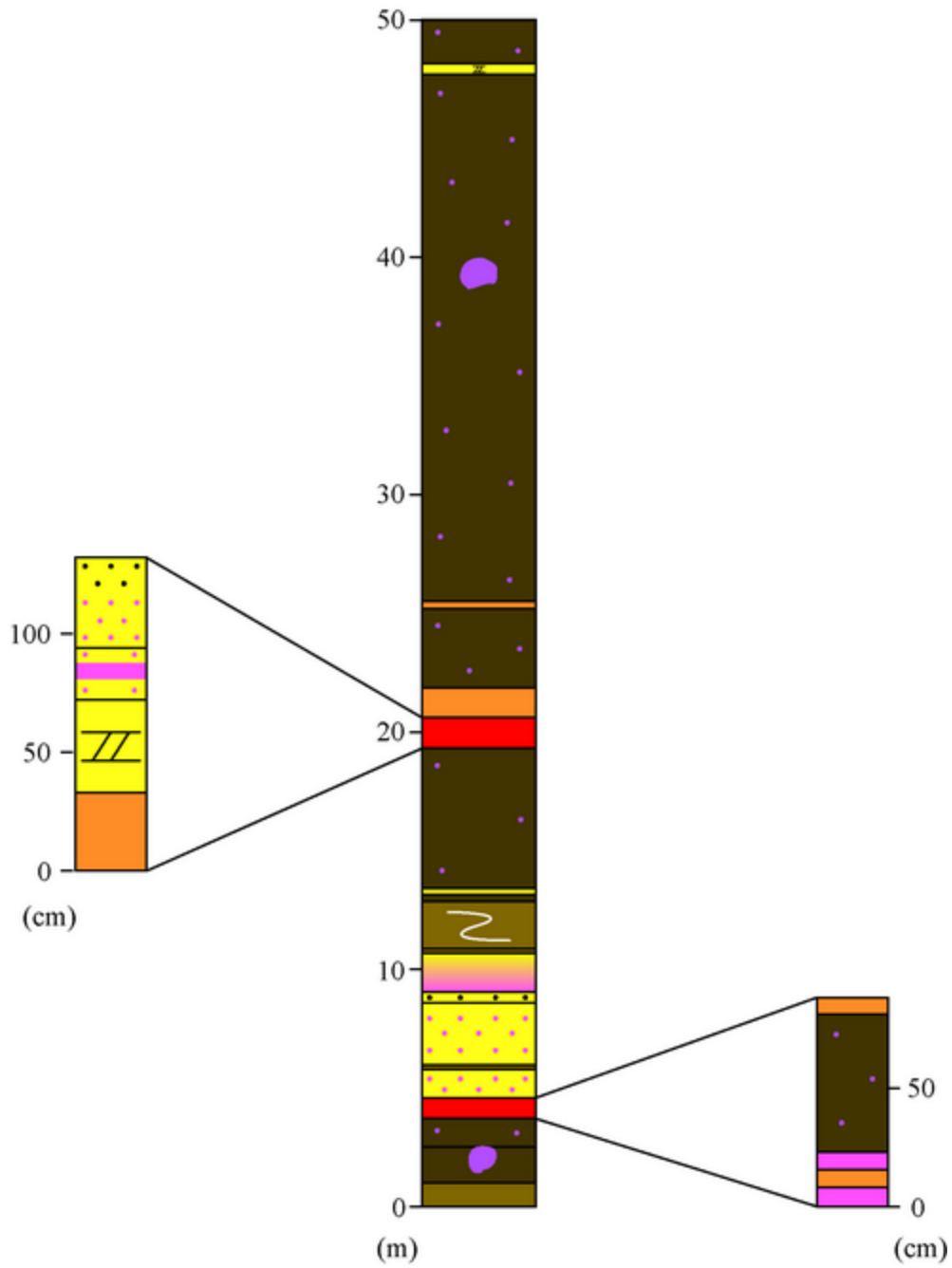




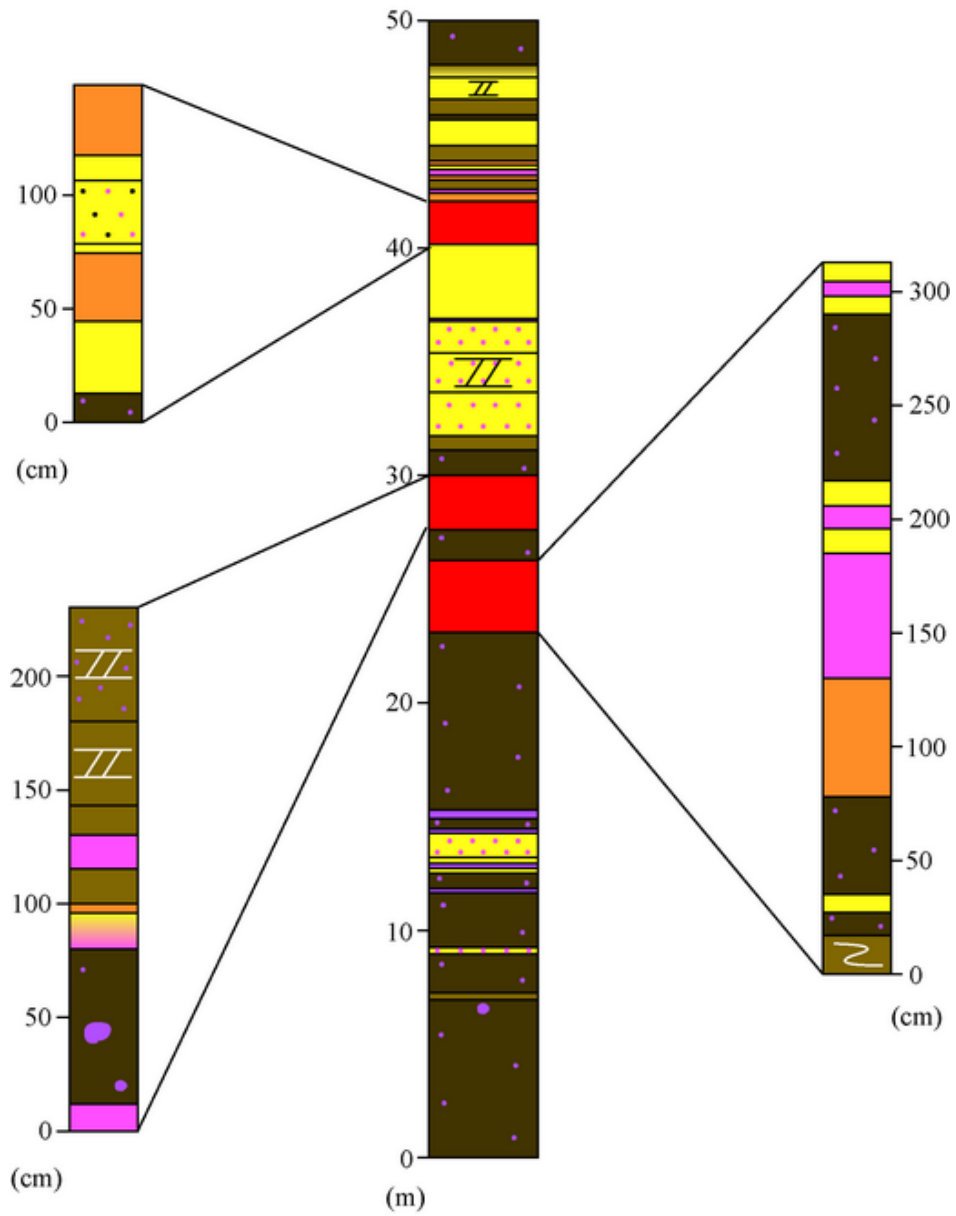
## Core - Gowganda, Lower, Hole 150-4 (b)



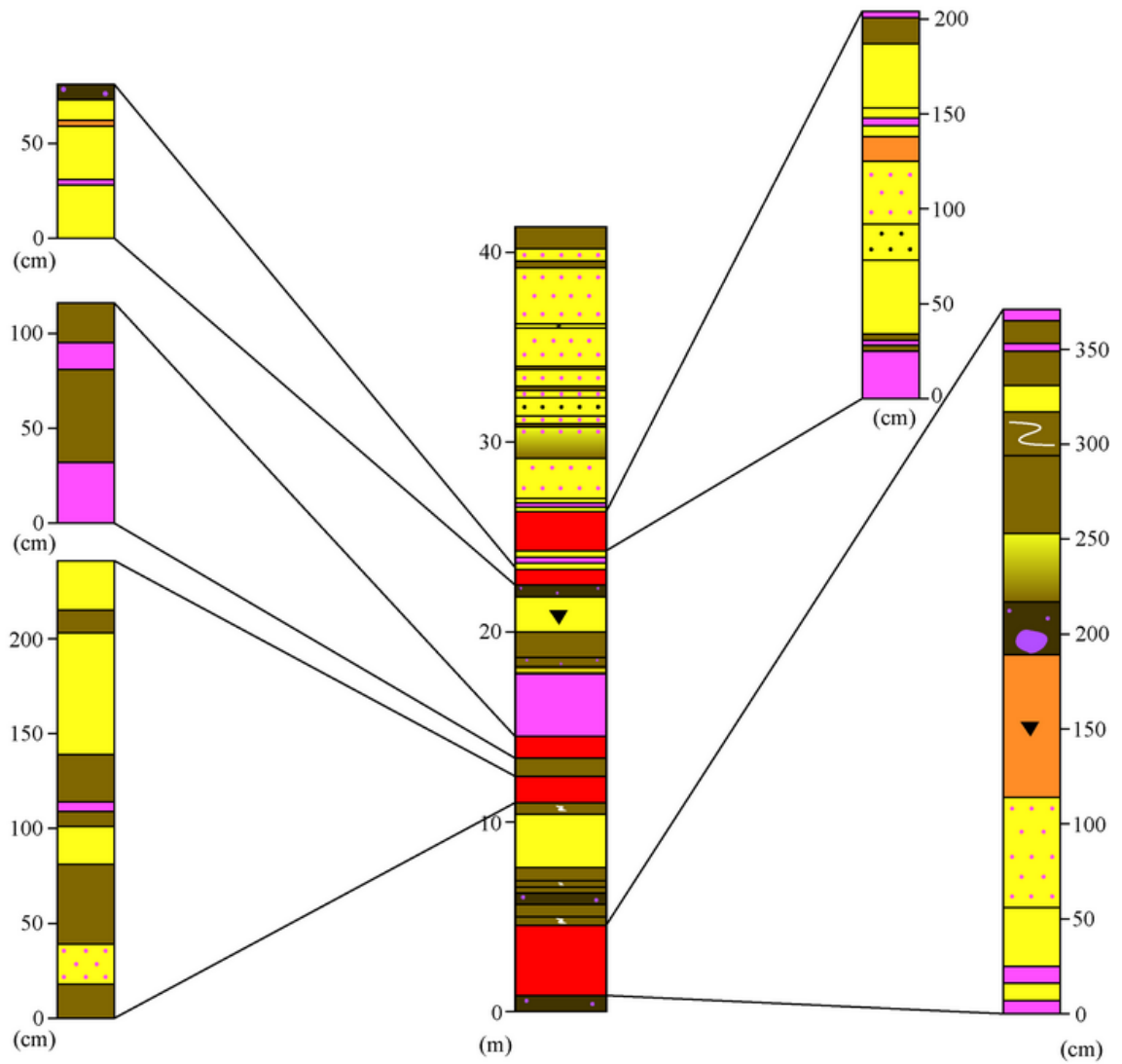
## Core - Gowganda, Lower, Hole 150-4 (c)



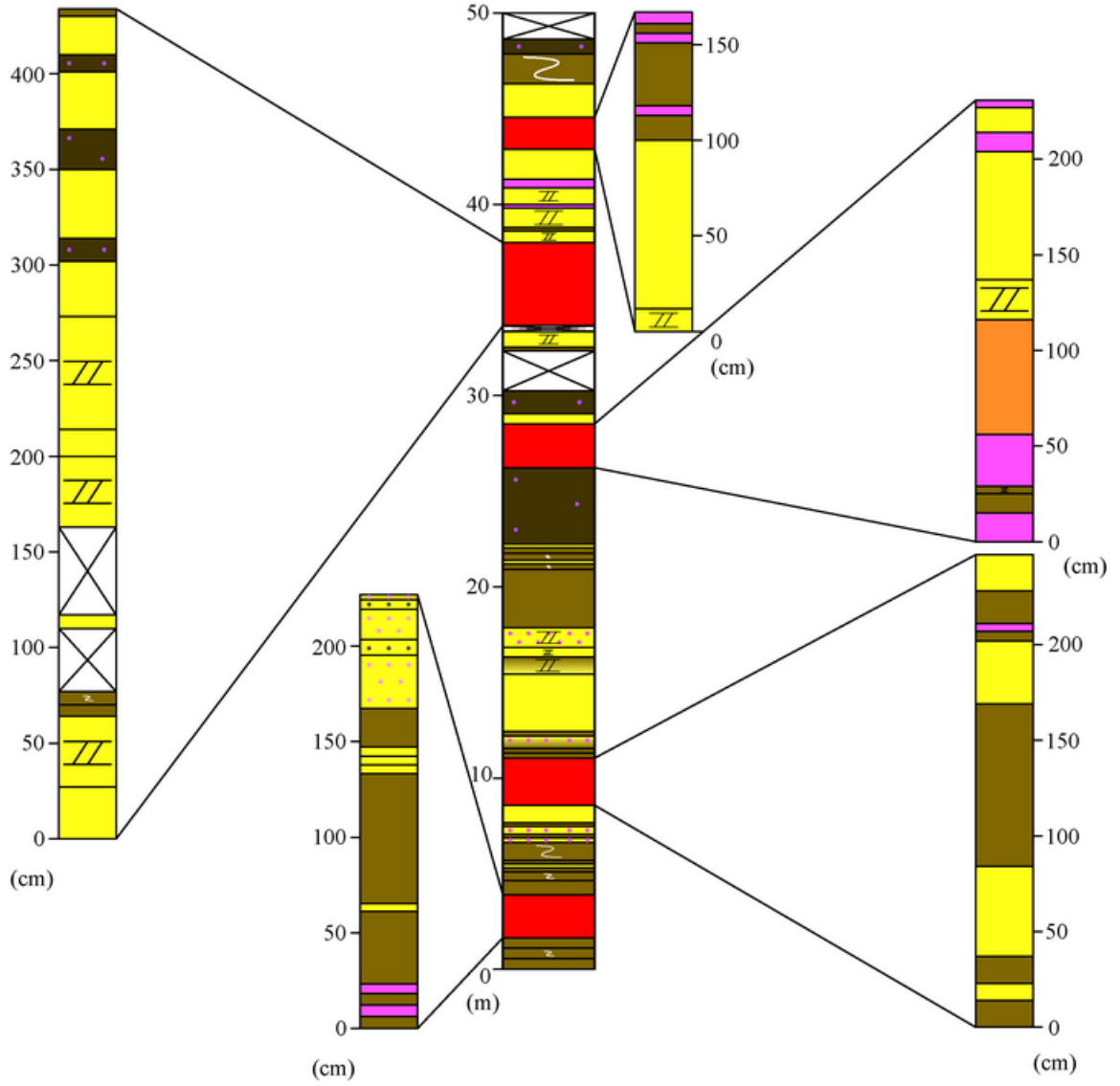
## Core - Gowganda, Lower, Hole 150-4 (d)



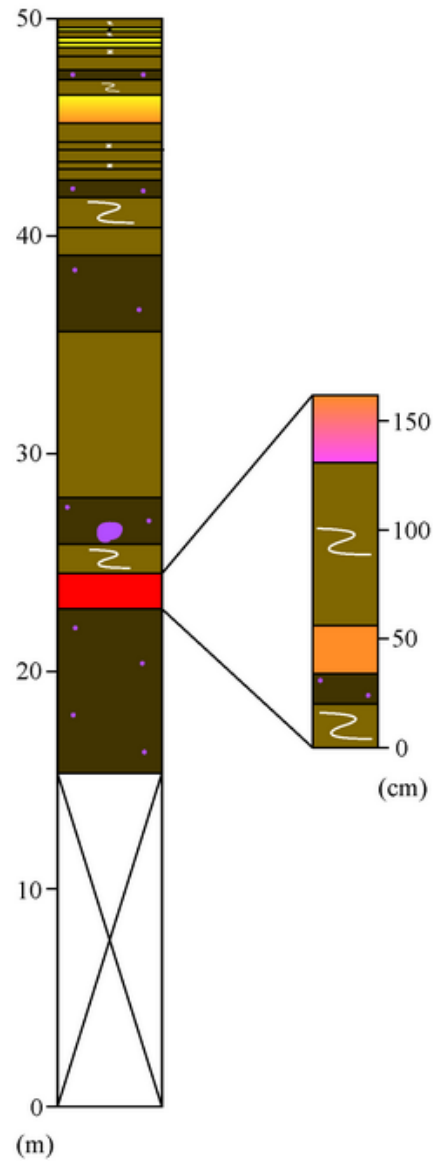
## Core - Gowganda, Lower, Hole 150-4 (e)



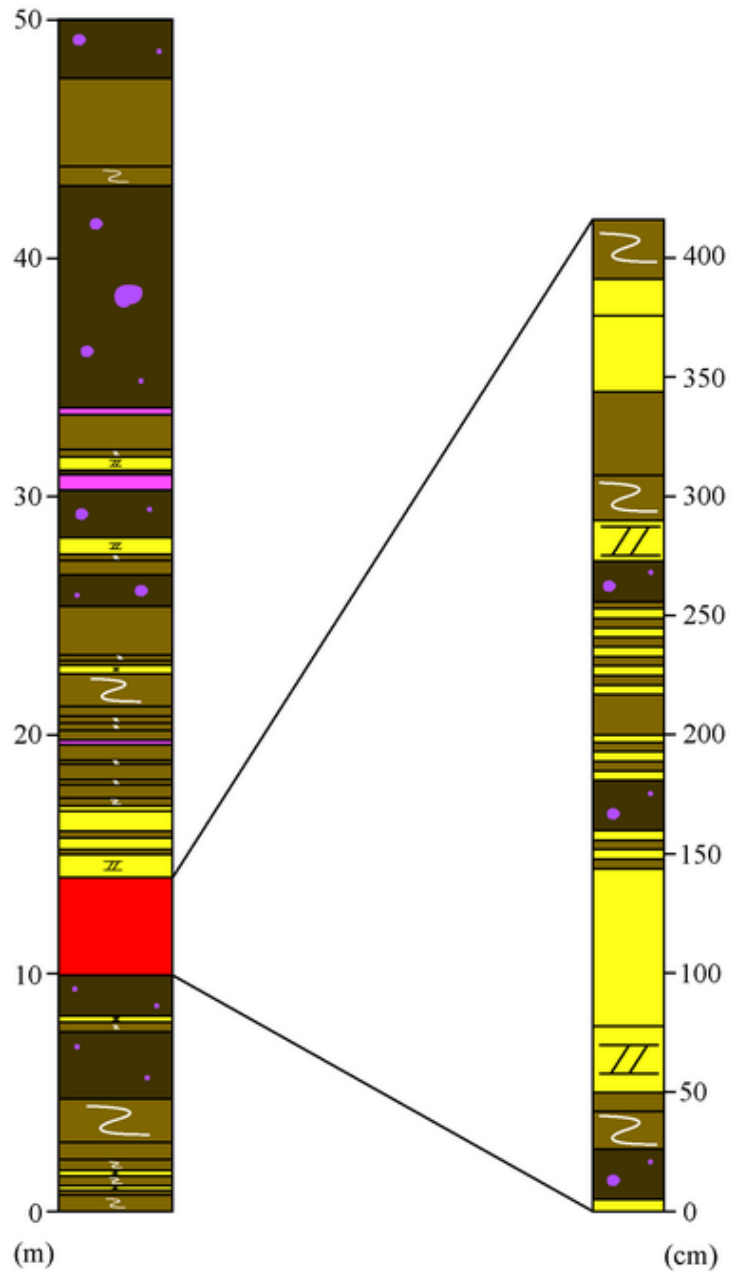
### Core - Gowganda, Lower, Hole 150-4 (f)



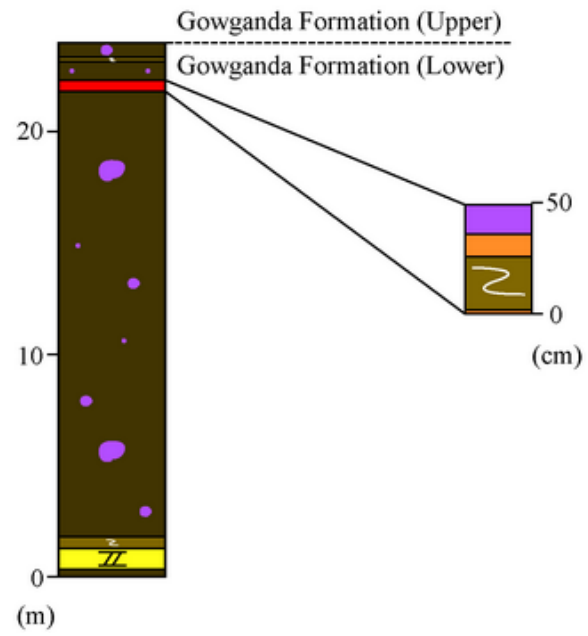
## Core - Gowganda, Lower, Hole 150-4 (g)



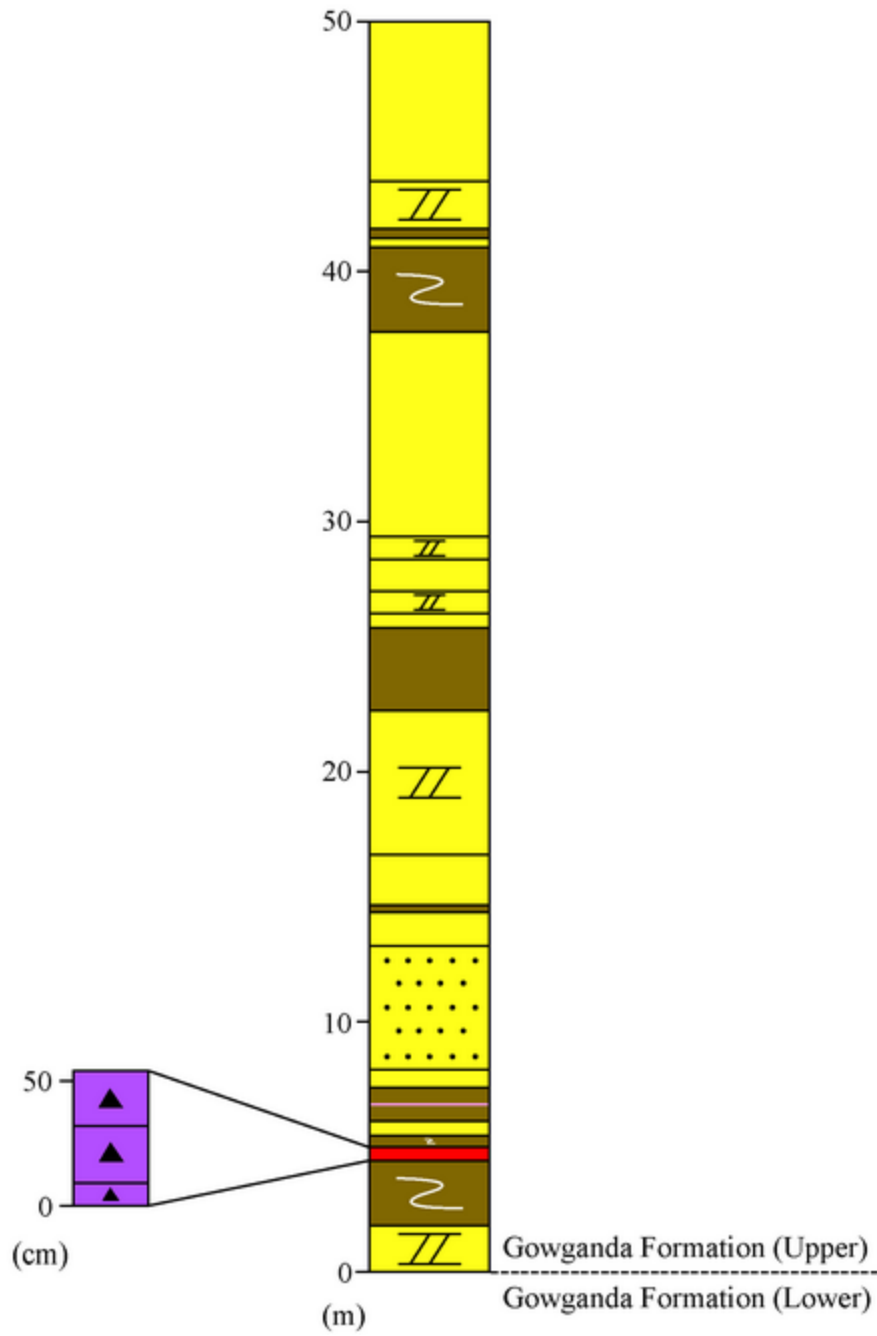
## Core - Gowganda, Lower, Hole 150-4 (h)



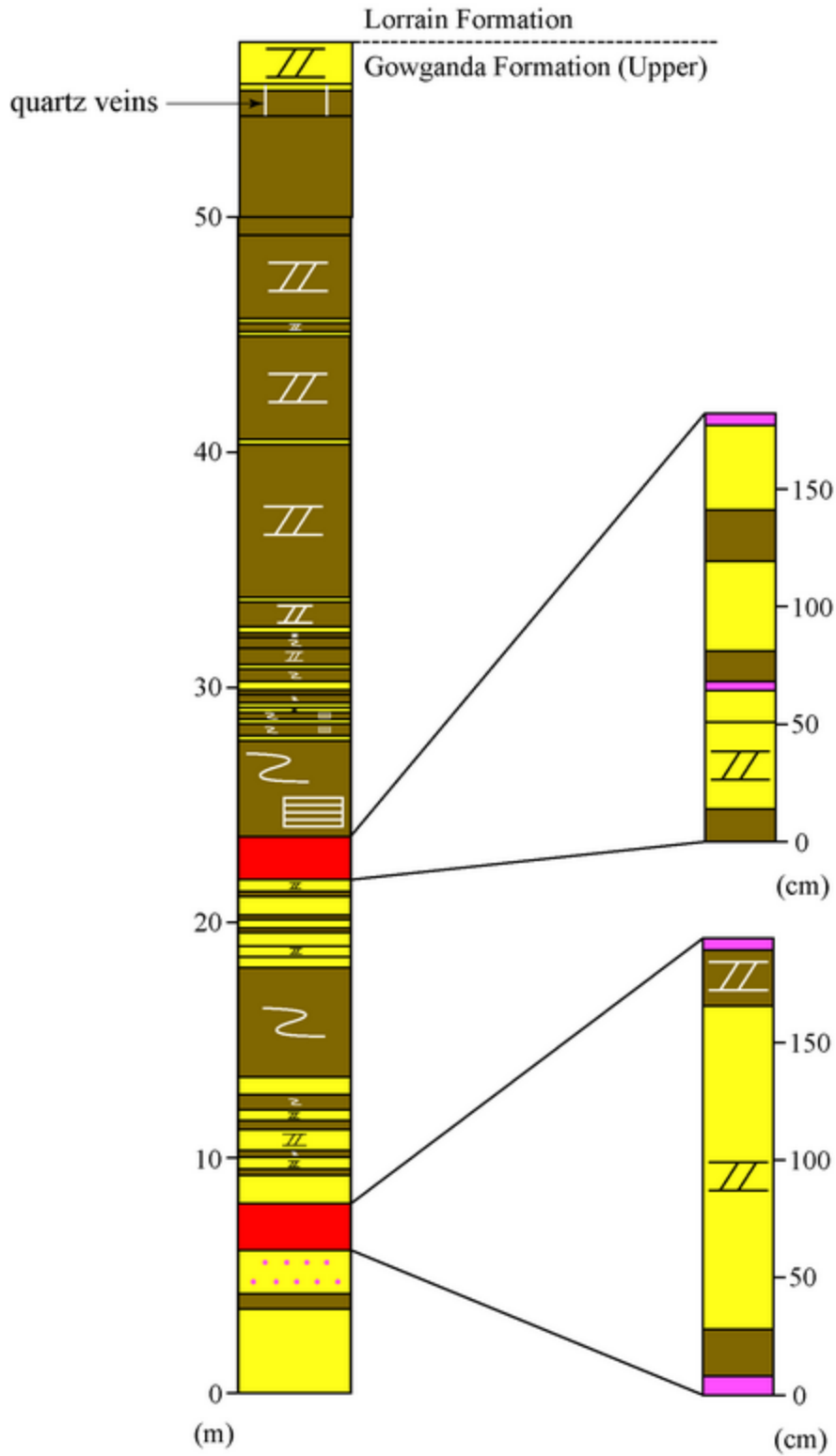
## Core - Gowganda, Lower, Hole 150-4 (i)



# Core - Gowganda, Upper, Hole 150-4 (a)



## Core - Gowganda, Upper, Hole 150-4 (b)



## Curriculum Vitae

**Name:** Timothy Howe

**Post-secondary  
Education and  
Degrees:** Wilfrid Laurier University  
Waterloo, Ontario, Canada  
1983-1987 B.Sc.

The University of Western Ontario  
London, Ontario, Canada  
2013-2015 M.Sc.

**Related Work  
Experience** Teaching Assistant  
The University of Western Ontario  
2013-2015

**Publications:**

Howe, T., Corcoran, P.L., Longstaffe, F.J., Webb, E., 2014. Investigating potential climatic cycles in glacially-influenced rhythmites of the upper Gowganda Formation. In: 2014 GSA Annual Meeting in Vancouver, British Columbia.